

Kuramoto model of synchronization: Equilibrium and nonequilibrium aspects

Shamik Gupta¹, Alessandro Campa², and Stefano Ruffo³

¹ Laboratoire de Physique Théorique et Modèles Statistiques (CNRS UMR 8626),
Université Paris-Sud, Orsay, France

² Complex Systems and Theoretical Physics Unit, Health and Technology Department,
Istituto Superiore di Sanità, and INFN Roma1, Gruppo Collegato Sanità, Viale Regina
Elena 299, 00161 Roma, Italy

³ Dipartimento di Fisica e Astronomia and CSDC, Università di Firenze, INFN and
CNISM, via G. Sansone, 1 50019 Sesto Fiorentino, Italy

E-mail:

shamikg1@gmail.com, alessandro.campa@iss.infn.it, stefano.ruffo@gmail.com

Abstract. The phenomenon of spontaneous synchronization, particularly within the framework of the Kuramoto model, has been a subject of intense research over the years. The model comprises oscillators with distributed natural frequencies interacting through a mean-field coupling, and serves as a paradigm to study synchronization. In this review, we put forward a general framework in which we discuss in a unified way known results with more recent developments obtained for a generalized Kuramoto model that includes inertial effects and noise. We describe the model from a different perspective, highlighting the long-range nature of the interaction between the oscillators, and emphasizing the equilibrium and out-of-equilibrium aspects of its dynamics from a statistical physics point of view. In this review, we first introduce the model and discuss both for the noiseless and noisy dynamics and for unimodal frequency distributions the synchronization transition that occurs in the stationary state. We then introduce the generalized model, and analyze its dynamics using tools from statistical mechanics. In particular, we discuss its synchronization phase diagram for unimodal frequency distributions. Next, we describe deviations from the mean-field setting of the Kuramoto model. To this end, we consider the generalized Kuramoto dynamics on a one-dimensional periodic lattice on the sites of which the oscillators reside and interact with one another with a coupling that decays as an inverse power-law of their separation along the lattice. For two specific cases, namely, in the absence of noise and inertia, and in the case when the natural frequencies are the same for all the oscillators, we discuss how the long-time transition to synchrony is governed by the dynamics of the mean-field mode (zero Fourier mode) of the spatial distribution of the oscillator phases.

PACS numbers: 05.45.Xt, 05.70.Fh, 05.70.Ln

Keywords: Stochastic particle dynamics (Theory), Stationary states, Phase diagrams (Theory)

Contents

1	Introduction	3
2	Kuramoto model of globally coupled oscillators	5
2.1	Synchronization transition	6
2.2	The noisy Kuramoto model	10
2.2.1	Linear stability analysis of the incoherent stationary state	11
3	Generalized Kuramoto model with inertia and noise	13
3.1	The model as a long-range interacting system	13
3.2	Previous studies	15
3.3	Dynamics in a reduced parameter space	16
3.4	Non-equilibrium first-order synchronization phase transition	17
3.5	Analysis in the continuum limit: The Kramers equation	21
3.5.1	Proof that the dynamics does not satisfy detailed balance unless $\sigma = 0$	22
3.5.2	Derivation of the Kramers equation	24
3.6	Stationary solutions of the Kramers equation	25
3.7	Linear stability analysis of the incoherent stationary state	27
3.7.1	Analysis of the eigenvalue equation	29
3.8	Comparison with numerical simulations	33
4	Dynamics of a lattice of oscillators interacting with a power-law coupling	37
4.1	The Kuramoto model with a power-law coupling between oscillators	39
4.1.1	Linear stability analysis of the mean-field incoherent stationary state	41
4.1.2	Numerical results	44
4.2	The noisy Kuramoto model with a power-law coupling and the same natural frequency for the oscillators	47
4.2.1	Linear stability analysis of the mean-field incoherent stationary state	49
4.2.2	Numerical results	50
4.2.3	Linear stability analysis of the mean-field synchronized stationary state	52
4.3	The inertial Kuramoto model with a power-law coupling and the same natural frequency for the oscillators	56
4.3.1	Linear stability analysis of the mean-field incoherent stationary state	58
4.3.2	Numerical results	59
5	Conclusions and perspectives	60
Appendix A: The noiseless Kuramoto model with inertia: Connection with electrical power distribution models		64

Appendix B: Simulation details	65
Appendix C: A fast numerical algorithm to compute the interaction term in the models with a power-law coupling	66
References	67

1. Introduction

A remarkable phenomenon quite ubiquitous in nature is that of collective synchronization, in which a large population of coupled oscillators spontaneously synchronizes to oscillate at a common frequency, despite each constituent having a different natural frequency of oscillation [1]. One witnesses such a spectacular cooperative effect in many physical and biological systems over length and time scales that span several orders of magnitude. Some common examples are metabolic synchrony in yeast cell suspensions [2], synchronized firings of cardiac pacemaker cells [3], flashing in unison by groups of fireflies [4], voltage oscillations at a common frequency in an array of current-biased Josephson junctions [5], phase synchronization in electrical power distribution networks [6–8], rhythmic applause [9], animal flocking behavior [10]; see [11] for a survey.

The Kuramoto model provides a simple theoretical framework to study how synchronization may emerge spontaneously in the dynamics of a many-body interacting system [12, 13]. The model comprises globally-coupled oscillators of distributed natural frequencies that are interacting via a mean-field coupling through the sine of their phase differences, with the phases following a first-order dynamics in time. Over the years, many aspects of the model, including applications cutting across disciplines, from physical and biological to even social modelling, have been considered in the literature [14, 15].

An early motivation behind studying the Kuramoto model was to explain the spectacular phenomenon of spontaneous synchronization among fireflies: In parts of south-east Asia, thousands of male fireflies gather in trees at night and flash on and off in unison. In this respect, focussing on fireflies of a particular species (the *Pteroptyx mallacae*), a study due to Ermentrout revealed that the approach to synchronization from an initially unsynchronized state is faster in the Kuramoto setting than in reality [16]. Ermentrout proposed a route to reconciliation by elevating the first-order dynamics of the Kuramoto model to the level of second-order dynamics. Including also a Gaussian noise term that accounts for the stochastic fluctuations of the natural frequencies in time [17], one arrives at a generalized Kuramoto model including inertia and noise, in which oscillator phases have a second-order dynamics in time [18–20]. One can prove that the resulting dynamics leads to a nonequilibrium stationary state (NESS) at long times [21].

Study of NESSs is an active area of research of modern day statistical mechanics [22]. Such states are characterized by a violation of detailed balance leading to a net non-zero

probability current around a closed loop in the configuration space. One of the primary challenges in this field is to formulate a tractable framework to analyze nonequilibrium systems on a common footing, similar to the one due to Gibbs and Boltzmann that has been established for equilibrium systems [23].

In a different context than that of coupled oscillators, the dynamics of the generalized Kuramoto model also describes a long-range interacting system of particles moving on a unit circle under the influence of a set of external drive in the form of a quenched external torque acting on the individual particles, in the presence of noise. With the noise, but without the external torques, the resulting model is the so-called Brownian mean-field (BMF) model [24, 25], introduced as a generalization of the celebrated Hamiltonian mean-field (HMF) model that serves as a prototype to study statics and dynamics of long-range interacting systems [26, 27]. In recent years, there has been a surge in interest in studies of systems with long-range interactions. In these systems, the inter-particle potential in d dimensions decays at large separation r as $r^{-\alpha}$, with $0 \leq \alpha \leq d$ [28, 29]. Examples are gravitational systems [30], plasmas [31], two-dimensional hydrodynamics [32], charged and dipolar systems [33], etc. Unlike systems with short-range interactions, long-range interacting systems are generically non-additive, implying that dividing the system into macroscopic subsystems and summing over their thermodynamic variables such as energy do not yield the corresponding variables of the whole system. Non-additivity leads to many significant thermodynamic and dynamical consequences, such as negative microcanonical specific heat, inequivalence of statistical ensembles, and others, which are unusual with short-range interactions [28].

In this review, starting with the first-order mean-field dynamics of the original Kuramoto model, we progressively modify the dynamics by including first the effects of a Gaussian noise, and then the consequences of an inertial term that makes the dynamics second order in time. In each case, we discuss the possible transitions to synchrony that the resulting stationary state exhibits. Here, we will explicitly consider a unimodal distribution of the natural frequencies. While the derivation of the phase diagram in the original model is based on an insightful self-consistent approach due to Kuramoto, inclusion of Gaussian noise allows to employ usual tools of statistical mechanics and explicitly study the evolution of the phase space distribution by using a Fokker-Planck approach. In both these cases, the transition between the unsynchronized and the synchronized phase turns out to be continuous or second order. We conveniently study the dynamics of the generalized Kuramoto model that includes the effects of both inertia and noise by introducing a reduced parameter space involving dimensionless moment of inertia, temperature, and width of the frequency distribution. We point out the relation of the model to the BMF model, thereby making references to the literature on long-range interacting systems. We give a rigorous proof that the system at long times settles into a NESS unless the width of the frequency distribution is zero when it has an equilibrium stationary state. We highlight that the generalized dynamics

exhibits a nonequilibrium first-order transition from a synchronized phase at low parameter values to an unsynchronized phase at high values. As a result, the system as a function of the transition parameters switches over in a discontinuous way from one phase to another, thereby mimicking an abrupt off-on switch. This may be contrasted to the case of no inertia when the transition is continuous. In proper limits, we discuss how one may recover the known continuous phase transitions in the Kuramoto model and in its noisy extension, and an equilibrium continuous transition in the BMF model. The present approach offers a complete and consistent picture of the phase diagram, unifying previous results with new ones in a common framework. In the last part of the review, we consider deviations from the mean-field setting of the Kuramoto model. To this end, we analyze the generalized Kuramoto dynamics on a one-dimensional periodic lattice on the sites of which the oscillators reside and interact with a coupling that decays as an inverse power-law of their separation along the lattice. We consider two specific cases of the dynamics, namely, in the absence of noise and inertia, and in the case when the natural frequencies are the same for all the oscillators (giving rise to the so-called α -HMF model). For the latter case, we consider both overdamped and underdamped dynamics. In particular, we discuss how the long-time transition to synchrony is governed by the dynamics of the mean-field mode (zero Fourier mode) of the spatial distribution of the oscillator phases. In this review, besides extensive numerical simulations, aspects of phase diagram are derived analytically by performing a linear stability analysis of the mean-field incoherent stationary state. Moreover, for the case of the overdamped dynamics of the generalized Kuramoto model on the lattice with the same natural frequency for all the oscillators, we present analytical results also on the linear stability analysis of the mean-field synchronized stationary state. We end the review with conclusions and perspectives.

2. Kuramoto model of globally coupled oscillators

We start with a derivation of the dynamics of the Kuramoto model by following Ref. [12]. Consider first a single Landau-Stuart oscillator. Its dynamics is given in terms of the complex variable Q as

$$\frac{dQ}{dt} = i\omega Q + (\alpha - \beta|Q|^2)Q, \quad (1)$$

with $\alpha, \beta, \omega \in \mathbb{R}$, and additionally, $\alpha, \beta > 0$. In Ref. [12], it is explained that the oscillator represented by Eq. (1) is a simple model for self-organized systems like, e.g., reacting chemical species. Writing Q in terms of its argument and modulus as $Q = \rho e^{i\theta}$ with $\rho, \theta \in \mathbb{R}$ and $\theta \in [-\pi, \pi]$, we see from equation (1) that θ rotates uniformly in time with angular frequency equal to the parameter ω , while ρ has a stable value $\rho_{\text{stable}} = \sqrt{\alpha/\beta}$, such that $d\rho/dt|_{\rho=\rho_{\text{stable}}} = 0$, $d\rho/dt|_{\rho<\rho_{\text{stable}}} > 0$, and $d\rho/dt|_{\rho>\rho_{\text{stable}}} < 0$. Then, setting $\rho = \rho_{\text{stable}}$ leads to self-sustained limit-cycle oscillations at frequency ω with amplitude ρ_{stable} ; the phase θ

varies as a function of time as

$$\frac{d\theta}{dt} = \omega. \quad (2)$$

Next, consider a population of N interacting Landau-Stuart oscillators with varying frequencies $\omega_1, \omega_2, \dots, \omega_N$ distributed according to a given probability distribution $g(\omega)$. The dynamics of the i th oscillator with angular frequency ω_i may be modelled as

$$\frac{dQ_i}{dt} = i\omega_i Q_i + (\alpha - \beta|Q_i|^2)Q_i + \sum_{j=1, j \neq i}^N K_{ij} Q_j, \quad (3)$$

where the real parameter $K_{ij} > 0$ describes the coupling between the i th and the j th oscillator. In deriving his model while starting from the dynamics (3), Kuramoto considers three simplifying premises, namely,

- (i) the limit of an infinite number of oscillators: $N \rightarrow \infty$,
- (ii) the coupling $K_{ij} \forall i, j$ scaling as $K_{ij} = K/N$ with K finite, implying thereby that every oscillator is coupled *weakly* and with equal strength to every other oscillator, and
- (iii) the limit $\alpha, \beta \rightarrow \infty$, while keeping α/β fixed and finite, and, moreover, $\omega_i \forall i$ being finite.

Writing $Q_i = \rho_i e^{i\theta_i}$, we see that because of the above assumptions, $\rho_i \forall i$ while starting from an initial value will relax over a time of $O(1/\beta)$ to its limit-cycle value equal to $\sqrt{\alpha/\beta}$. As a result, the long-time dynamics corresponds to self-sustained limit-cycle oscillations for each oscillator, which is described by the evolution equation

$$\frac{d\theta_i}{dt} = \omega_i + \frac{K}{N} \sum_{j=1}^N \sin(\theta_j - \theta_i). \quad (4)$$

Equation (4) is the governing dynamical equation of the Kuramoto model.

2.1. Synchronization transition

Most investigations of the Kuramoto model have been for a unimodal $g(\omega)$, i.e., one which is symmetric about the mean $\langle \omega \rangle$, and which decreases monotonically and continuously to zero with increasing $|\omega - \langle \omega \rangle|$. We will denote by σ the width of the distribution $g(\omega)$ (e.g., for a Gaussian distribution, σ is the standard deviation). As mentioned in the introduction, we will in this review consider specifically such frequency distributions. By going to a comoving frame rotating with frequency $\langle \omega \rangle$ with respect to the laboratory frame, one may from now on consider in the dynamics (4) the ω_i 's to have zero mean without loss of generality; we will implement this in the rest of the review.

In his early works, Kuramoto adduced a remarkable self-consistent analysis to predict the long-time stationary state of the dynamics (4). This analysis and its further generalizations

have established that the stationary state is characterized by one of two possible phases, depending on whether K is below or above a critical value K_c , given by [14, 15]

$$K_c = \frac{2}{\pi g(0)}. \quad (5)$$

The system for $K < K_c$ is in an unsynchronized or incoherent phase in which the oscillators exhibit independent oscillations, while for $K > K_c$ in a synchronized phase in which a macroscopic fraction of oscillators are in synchrony. On tuning K , a continuous phase transition occurs between the two phases. More precisely, the Kuramoto model being a dynamical system, one does not quite have a phase transition in the sense of thermodynamics, but rather a bifurcation for the order parameter, see below. For noisy dynamics, cases of which will be studied later in the review, a phase transition of course has its usual meaning as in thermodynamics. Here, by synchrony, we mean that in the limit $N \rightarrow \infty$, the oscillators have time-independent phases in the comoving frame, and have therefore phases that rotate uniformly in time with the same frequency $\langle \omega \rangle$ in the laboratory frame. The magnitude $r(t)$ and the phase $\psi(t)$ of the complex order parameter, defined as

$$\mathbf{r}(t) = r(t)e^{i\psi(t)} \equiv \frac{1}{N} \sum_{j=1}^N e^{i\theta_j(t)}, \quad (6)$$

measure the amount of synchronization and the average phase, respectively. For $K < K_c$, $r(t)$ while starting from any initial value relaxes at long times to zero, corresponding to an incoherent stationary state. On the other hand, for $K > K_c$, $r(t)$ has a non-zero stationary state value $r_{\text{st}}(K) \leq 1$ that increases continuously with K , and is such that $r_{\text{st}}(K \rightarrow K_c^+) = 0$. In the limit $K \rightarrow \infty$, all the oscillators are synchronized and at the same phase, so that $r_{\text{st}}(K \rightarrow \infty) = 1$. In terms of $r(t)$ and $\psi(t)$, the dynamics (4) reads

$$\frac{d\theta_i}{dt} = \omega_i + Kr \sin(\psi - \theta_i). \quad (7)$$

We now briefly recall a self-consistent analysis due to Kuramoto [14] that leads to equation (5). The starting point is to note that in the stationary state, the single-oscillator distribution $\rho(\theta, \omega, t)$, giving the fraction of oscillators with natural frequency ω that has phase θ at time t , converges to the time-independent form $\rho_{\text{st}}(\theta, \omega)$. Note that ρ satisfies $\rho(\theta, \omega, t) = \rho(\theta + 2\pi, \omega, t)$, and the normalization $\int_{-\pi}^{\pi} d\theta \rho(\theta, \omega, t) = 1 \forall \omega, t$. When synchronized, the average phase in the stationary state, ψ_{st} , will be a constant that may be set to zero by choosing properly the origin of the phase axes. The stationary value r_{st} of $r(t)$, on the other hand, satisfies

$$r_{\text{st}} = \int d\theta \int d\omega g(\omega) e^{i\theta} \rho_{\text{st}}(\theta, \omega). \quad (8)$$

Since r_{st} is real, the above equation implies that the imaginary part of the right hand side should vanish. As $g(\omega)$ is symmetric: $g(\omega) = g(-\omega)$, the vanishing of the imaginary part

is ensured if $\rho_{\text{st}}(-\theta, -\omega) = \rho_{\text{st}}(\theta, \omega)$. This is indeed the case, as we will see below. On the basis of the above discussion, one may rewrite equation (7) in the stationary state as

$$\frac{d\theta_i}{dt} = \omega_i - Kr_{\text{st}} \sin \theta_i. \quad (9)$$

The result (5) follows from a self-consistent equation derived by adopting the following strategy: At a fixed K , and for a given value of r_{st} , (i) obtain the stationary state distribution $\rho_{\text{st}}(\theta, \omega)$ implied by the dynamics (9), and (ii) require that the distribution when plugged into the right hand side of equation (8) reproduces the given value of r_{st} on the left hand side, thereby yielding the self-consistent equation; we now demonstrate this procedure. First, it follows from equation (9) that the dynamics of oscillators with $|\omega_i| \leq Kr_{\text{st}}$ approaches in time a stable fixed point defined implicitly by

$$\omega_i = Kr_{\text{st}} \sin \theta_i, \quad (10)$$

so that the i th oscillator in this group has the time-independent phase $\theta_i = \sin^{-1}[\omega_i/(Kr_{\text{st}})]$; $|\theta_i| \leq \pi/2$. This group of oscillators are thus “locked” or synchronized, and has the distribution

$$\rho_{\text{st}}(\theta, \omega) = Kr_{\text{st}} \cos \theta \delta(\omega - Kr_{\text{st}} \sin \theta) \Theta(\cos \theta); \quad |\omega| \leq Kr_{\text{st}}, \quad (11)$$

where $\Theta(\cdot)$ is the Heaviside step function. On the other hand, oscillators with $|\omega_i| \geq Kr_{\text{st}}$ have ever drifting time-dependent phases. However, to be consistent with the fact that we have a time-independent average phase, it is required that $\rho_{\text{st}}(\theta, \omega)$ for this group of “drifting” oscillators has the form

$$\rho_{\text{st}}(\theta, \omega) = \frac{C}{|\omega - Kr_{\text{st}} \sin \theta|}; \quad |\omega| > Kr_{\text{st}}; \quad (12)$$

this ensures that oscillators are more crowded at θ -values with lower local velocity $d\theta_i/dt$ than at values with higher local velocity. The constant C in equation (12) is fixed by the normalization condition $\int_{-\pi}^{\pi} d\theta \rho_{\text{st}}(\theta, \omega) = 1 \forall \omega$, yielding

$$C = \frac{1}{2\pi} \sqrt{\omega^2 - (Kr_{\text{st}})^2}. \quad (13)$$

We now require that the given value of r_{st} coincides with the one implied by the distributions in equations (11) and (12). Plugging the latter forms into equation (8), we get

$$\begin{aligned} r_{\text{st}} = & \int_{-\pi}^{\pi} d\theta \int_{|\omega| > Kr_{\text{st}}} d\omega g(\omega) e^{i\theta} \frac{C}{|\omega - Kr_{\text{st}} \sin \theta|} \\ & + \int_{-\pi/2}^{\pi/2} d\theta \int_{|\omega| \leq Kr_{\text{st}}} d\omega g(\omega) e^{i\theta} Kr_{\text{st}} \cos \theta \delta(\omega - Kr_{\text{st}} \sin \theta). \end{aligned} \quad (14)$$

The first integral on the right hand side vanishes due to the symmetry $g(\omega) = g(-\omega)$ combined with the property that $\rho_{\text{st}}(\theta + \pi, -\omega) = \rho_{\text{st}}(\theta, \omega)$ for the “drifting” oscillators, see

equation (12). The imaginary part of the second integral vanishes on using $g(\omega) = g(-\omega)$ and $\rho_{\text{st}}(-\theta, -\omega) = \rho_{\text{st}}(\theta, \omega)$ for the “locked” oscillators, see equation (11); the real part, after integration over ω , finally yields

$$r_{\text{st}} = Kr_{\text{st}} \int_{-\pi/2}^{\pi/2} d\theta \cos^2 \theta g(Kr_{\text{st}} \sin \theta), \quad (15)$$

which is the desired self-consistent equation. This equation has the trivial solution $r_{\text{st}} = 0$, valid for any value of K , corresponding to the incoherent phase with $\rho_{\text{st}}(\theta, \omega) = 1/(2\pi) \forall \theta, \omega$. There can however be another solution corresponding to $r_{\text{st}} \neq 0$ that satisfies

$$1 = K \int_{-\pi/2}^{\pi/2} d\theta \cos^2 \theta g(Kr_{\text{st}} \sin \theta). \quad (16)$$

This solution bifurcates continuously from the incoherent solution at the value $K = K_c$ given by equation (5) that follows from the above equation on taking the limit $r_{\text{st}} \rightarrow 0^+$. Since for a unimodal $g(\omega)$, one has a negative second derivative at $\omega = 0$, $g''(0) < 0$, one finds by expanding the integrand in equation (16) as a powers series in r_{st} that the bifurcation in this case is supercritical. As a matter of fact, it is not difficult to see that for a unimodal $g(\omega)$, a solution of equation (16) exists only for $K \geq K_c$. Indeed, the right hand side of equation (16) is equal to $K\pi g(0)/2$ for $r_{\text{st}} = 0$, while its partial derivative with respect to r_{st} , given by

$$K^2 \int_{-\pi/2}^{\pi/2} d\theta \cos^2 \theta \sin \theta g'(Kr_{\text{st}} \sin \theta), \quad (17)$$

is negative definite (here and henceforth, prime will denote derivative). On the other hand, for $r_{\text{st}} = 1$, the right hand side of equation (16) after the change of variable $K \sin \theta = u$ can be written as

$$\int_{-K}^K du \left(1 - \frac{u^2}{K^2}\right)^{\frac{1}{2}} g(u), \quad (18)$$

which is clearly smaller than 1, tending to 1 as $K \rightarrow \infty$. Finally, its derivative with respect to K is

$$\begin{aligned} & \int_{-\pi/2}^{\pi/2} d\theta \cos^2 \theta g(Kr_{\text{st}} \sin \theta) + Kr_{\text{st}} \int_{-\pi/2}^{\pi/2} d\theta \cos^2 \theta \sin \theta g'(Kr_{\text{st}} \sin \theta) \\ &= \int_{-\pi/2}^{\pi/2} d\theta \sin^2 \theta g(Kr_{\text{st}} \sin \theta), \end{aligned} \quad (19)$$

which is positive. These properties imply that a solution r_{st} of equation (16) exists for $K \geq K_c$, which equals 0 for $K = K_c$, and which increases with K and approaches unity as $K \rightarrow \infty$.

The linear stability of the incoherent solution, $\rho_{\text{st}}(\theta, \omega) = 1/(2\pi) \forall \theta, \omega$ [14], will be considered in Sec. 4.1, where it will appear as a special case of the Kuramoto model with non-mean-field long-range interactions. The stability analysis will establish that the incoherent state is neutrally stable below K_c and unstable above.

2.2. The noisy Kuramoto model

In order to account for stochastic fluctuations of the ω_i 's in time, the dynamics (4) with an additional Gaussian noise term $\eta_i(t)$ on the right hand side was studied by Sakaguchi [17]. The dynamical equations are

$$\frac{d\theta_i}{dt} = \omega_i + Kr \sin(\psi - \theta_i) + \eta_i(t), \quad (20)$$

where

$$\langle \eta_i(t) \rangle = 0, \quad \langle \eta_i(t) \eta_j(t') \rangle = 2D \delta_{ij} \delta(t - t'), \quad (21)$$

with the parameter D standing for the noise strength, while here and from now on, angular brackets will denote averaging with respect to noise realizations. In presence of $\eta_i(t)$, the continuous transition of the bare model is sustained, with K_c shifted to [17]

$$K_c(D) = 2 \left[\int_{-\infty}^{\infty} d\omega \frac{g(D\omega)}{\omega^2 + 1} \right]^{-1}. \quad (22)$$

On taking the limit $D \rightarrow 0$ in the above equation, one recovers the transition point (5) for the bare model. In the following, we briefly sketch the derivation of equation (22), following Ref. [17].

The starting point is to write down a Fokker-Planck equation for the time evolution of the distribution $\rho(\theta, \omega, t)$, which follows straightforwardly from the dynamics (20) as

$$\frac{\partial \rho}{\partial t} = -\frac{\partial}{\partial \theta} \left[\left(\omega + Kr \sin(\psi - \theta) \right) \rho \right] + D \frac{\partial^2 \rho}{\partial \theta^2}. \quad (23)$$

As before, in the stationary state, we set $\psi_{\text{st}} = 0$, and obtain from the above equation the result

$$\begin{aligned} \rho_{\text{st}}(\theta, \omega) = & \exp \left(\frac{-Kr_{\text{st}} + \omega\theta + Kr_{\text{st}} \cos \theta}{D} \right) \rho_{\text{st}}(0, \omega) \\ & \times \left[1 + \frac{(e^{-2\pi\omega/D} - 1) \int_0^\theta d\theta' e^{(-\omega\theta' - Kr_{\text{st}} \cos \theta')/D}}{\int_{-\pi}^\pi d\theta' e^{(-\omega\theta' - Kr_{\text{st}} \cos \theta')/D}} \right], \end{aligned} \quad (24)$$

where $\rho_{\text{st}}(0, \omega)$ is fixed by the normalization $\int_{-\pi}^\pi d\theta \rho_{\text{st}}(\theta, \omega) = 1 \forall \omega$. For $r_{\text{st}} = 0$ the above expression reduces to the incoherent state $\rho_{\text{st}}(\theta, \omega) = 1/(2\pi) \forall \theta, \omega$. Substituting equation (24) into equation (8), one obtains a self-consistent equation for r_{st} . As for the Kuramoto model, it has the trivial solution $r_{\text{st}} = 0$, corresponding to the incoherent state. In finding the other solution, one observes that the imaginary part of the right hand side of equation (8) is zero due to the symmetry $g(\omega) = g(-\omega)$ together with the property $\rho_{\text{st}}(-\theta, -\omega) = \rho_{\text{st}}(\theta, \omega)$, see equation (24); thus, only the real part contributes. Expanding the resulting equation in powers of Kr_{st}/D , and taking the limit $r_{\text{st}} \rightarrow 0^+$ [17] yield the critical coupling strength $K_c(D)$ given by equation (22).

2.2.1. *Linear stability analysis of the incoherent stationary state* The stability analysis of the incoherent state $\rho_{\text{st}}(\theta, \omega) = 1/(2\pi) \forall \theta, \omega$ is performed by studying the linearized Fokker-Planck equation obtained from equation (23) after expanding $\rho(\theta, \omega, t)$ as

$$\rho(\theta, \omega, t) = \frac{1}{2\pi} + \delta\rho(\theta, \omega, t); \quad |\delta\rho| \ll 1. \quad (25)$$

Writing explicitly the expression for r , the resulting linear equation is

$$\begin{aligned} \frac{\partial}{\partial t} \delta\rho(\theta, \omega, t) &= -\omega \frac{\partial}{\partial \theta} \delta\rho(\theta, \omega, t) + D \frac{\partial^2}{\partial \theta^2} \delta\rho(\theta, \omega, t) \\ &+ \frac{K}{2\pi} \int_{-\pi}^{\pi} d\theta' \int d\omega' g(\omega') \cos(\theta' - \theta) \delta\rho(\theta', \omega', t). \end{aligned} \quad (26)$$

With the Fourier expansion

$$\delta\rho(\theta, \omega, t) = \sum_{k=-\infty}^{+\infty} \widehat{\delta\rho}_k(\omega, t) e^{ik\theta}, \quad (27)$$

equation (26) gives

$$\frac{\partial}{\partial t} \widehat{\delta\rho}_k(\omega, t) = -ik\omega \widehat{\delta\rho}_k(\omega, t) - Dk^2 \widehat{\delta\rho}_k(\omega, t) + \frac{K}{2} (\delta_{k,1} + \delta_{k,-1}) \int d\omega' g(\omega') \widehat{\delta\rho}_k(\omega', t). \quad (28)$$

For $k \neq \pm 1$, the integral term vanishes, and we have

$$\frac{\partial}{\partial t} \widehat{\delta\rho}_k(\omega, t) = -ik\omega \widehat{\delta\rho}_k(\omega, t) - Dk^2 \widehat{\delta\rho}_k(\omega, t), \quad (29)$$

so that with ω varying in the support of $g(\omega)$, one has a continuous spectrum of stable modes that decay exponentially in time with rate Dk^2 . For $k = \pm 1$, after posing

$$\widehat{\delta\rho}_{\pm 1}(\omega, t) = \widetilde{\delta\rho}_{\pm 1}(\omega, \lambda) e^{\lambda t}, \quad (30)$$

we have

$$[\lambda \pm i\omega + D] \widetilde{\delta\rho}_{\pm 1}(\omega, \lambda) = \frac{K}{2} \int d\omega' g(\omega') \widetilde{\delta\rho}_{\pm 1}(\omega', \lambda). \quad (31)$$

This equation also admits a continuous spectrum of stable modes, given by $\lambda = \mp i\omega_0 - D$ for each ω_0 in the support of $g(\omega)$. The modes, normalized so that the right hand side of equation (31) is equal to 1, are given by

$$\widetilde{\delta\rho}_{\pm 1}(\omega, \mp i\omega_0 - D) = \mp i\mathcal{P} \frac{1}{\omega - \omega_0} + c_{\pm 1}(\omega_0) \delta(\omega - \omega_0), \quad (32)$$

with

$$c_{\pm 1}(\omega_0) g(\omega_0) = \frac{2}{K} \pm i\mathcal{P} \int d\omega \frac{g(\omega)}{\omega - \omega_0}, \quad (33)$$

where \mathcal{P} denotes the principal value. However, unlike for $k \neq \pm 1$, there is also a discrete spectrum for $\lambda \pm i\omega + D \neq 0$. From equation (31), we have

$$\widetilde{\delta\rho}_{\pm 1}(\omega, \lambda) = \frac{K}{2(\lambda \pm i\omega + D)} \int d\omega' \widetilde{\delta\rho}_{\pm 1}(\omega', \lambda) g(\omega'). \quad (34)$$

In order to have a non-trivial solution of the above equation, the integral on the right hand side must not vanish. We can impose that this integral is equal to 1, since equation (31) is linear. We then obtain the dispersion relation

$$\frac{K}{2} \int_{-\infty}^{+\infty} d\omega \frac{g(\omega)}{\lambda \pm i\omega + D} = 1. \quad (35)$$

Decomposing λ into real and imaginary parts, $\lambda = \lambda_r + i\lambda_i$, we obtain from equation (35) that

$$\frac{K}{2} \int_{-\infty}^{+\infty} d\omega g(\omega) \frac{\lambda_r + D}{(\lambda_r + D)^2 + (\lambda_i \pm \omega)^2} = 1, \quad (36)$$

$$\frac{K}{2} \int_{-\infty}^{+\infty} d\omega g(\omega) \frac{\lambda_i \pm \omega}{(\lambda_r + D)^2 + (\lambda_i \pm \omega)^2} = 0. \quad (37)$$

With the change of variable $\lambda_i \pm \omega = x$, the integral in the second equation can be transformed to

$$\int_0^{+\infty} dx [g(\pm x \mp \lambda_i) - g(\mp x \mp \lambda_i)] \frac{x}{(\lambda_r + D)^2 + x^2}. \quad (38)$$

One may check that for unimodal $g(\omega)$, the above expression can be equal to 0 only for $\lambda_i = 0$. So equation (36) becomes

$$\frac{K}{2} \int_{-\infty}^{+\infty} d\omega g(\omega) \frac{\lambda + D}{(\lambda + D)^2 + \omega^2} = 1, \quad (39)$$

with λ real. This equation shows that only solutions $\lambda > -D$ are possible; when such a solution is not present, there is no discrete spectrum, and the incoherent state is stable. However, stability holds also when there is a solution $\lambda < 0$, since we have seen that all the eigenvalues of the continuous spectrum have a negative real part. The change of variable $\omega = (\lambda + D)y$ transforms equation (39) to

$$\frac{K}{2} \int_{-\infty}^{+\infty} dy g[(\lambda + D)y] \frac{1}{1 + y^2} = 1. \quad (40)$$

The left hand side tends to 0 as $\lambda \rightarrow \infty$, while its derivative with respect to λ is

$$\frac{K}{2} \int_{-\infty}^{+\infty} dy g'[(\lambda + D)y] \frac{y}{1 + y^2}, \quad (41)$$

which is negative. Therefore, a solution for λ exists only when the value of the left hand side of equation (40) for $\lambda = -D$ is larger than 1. In particular, we have stability when this solution is negative; the threshold for stability is thus given by

$$\frac{K}{2} \int_{-\infty}^{+\infty} dy g(Dy) \frac{1}{1 + y^2} = 1, \quad (42)$$

that gives the critical value (22).

3. Generalized Kuramoto model with inertia and noise

In the generalized dynamics, an additional dynamical variable, namely, angular velocity, is assigned to each oscillator, thereby elevating the first-order dynamics of the Kuramoto model to the level of second-order dynamics; the equations of motion are [18–20]:

$$\frac{d\theta_i}{dt} = v_i, \tag{43}$$

$$m \frac{dv_i}{dt} = -\gamma v_i + \tilde{K} r \sin(\psi - \theta_i) + \gamma \omega_i + \tilde{\eta}_i(t).$$

Here, v_i is the angular velocity of the i th oscillator, m is the moment of inertia of the oscillators, γ is the friction constant, \tilde{K} is the strength of the coupling between the oscillators, while $\tilde{\eta}_i(t)$ is a Gaussian noise with

$$\langle \tilde{\eta}_i(t) \rangle = 0, \quad \langle \tilde{\eta}_i(t) \tilde{\eta}_j(t') \rangle = 2\tilde{D} \delta_{ij} \delta(t - t'). \tag{44}$$

In the limit of overdamped motion ($m \rightarrow 0$ at a fixed $\gamma \neq 0$), the dynamics (43) reduces to

$$\gamma \frac{d\theta_i}{dt} = \tilde{K} r \sin(\psi - \theta_i) + \gamma \omega_i + \tilde{\eta}_i(t). \tag{45}$$

Then, defining $K \equiv \tilde{K}/\gamma$ and $\eta_i(t) \equiv \tilde{\eta}_i(t)/\gamma$ so that $D = \tilde{D}/\gamma^2$, the dynamics (45) for $D = 0$ becomes that of the Kuramoto model, equation (4), and for $D \neq 0$ that of its noisy version, the dynamics (20).

In Appendix A, we illustrate how the dynamics (43) without the noise term, studied in [34], arises in a completely different context, namely, in electrical power distribution networks comprising synchronous generators (representing power plants) and motors (representing customers) [6, 7]; the dynamics arises in the approximation in which every node of the network is connected to every other.

3.1. The model as a long-range interacting system

We now discuss that in a different context than that of coupled oscillators, the dynamics (43) describes a long-range interacting system of particles moving on a unit circle, with each particle acted upon by a quenched external torque $\tilde{\omega}_i \equiv \gamma \omega_i$.

Much recent exploration of the static and dynamic properties of long-range interacting systems has been pursued within the framework of an analytically tractable prototypical model called the Hamiltonian mean-field (HMF) model [26, 27]. The model comprises N particles of mass m moving on a unit circle and interacting through a long-range interparticle potential that is of the mean-field type: every particle is coupled to every other with equal strength. This system can also be seen as a set of XY -rotators that reside on a lattice and interact through ferromagnetic coupling. The structure and dimensionality of the lattice need not be specified, since the coupling between each pair of rotators is

the same (mean-field system). Since the configuration of an XY -rotator is defined by a single angle variable, one might also view the rotators as spin vectors. However, one should be aware that this identification is not completely correct. This is because the dynamics of spins is defined differently, through Poisson brackets, or, equivalently, through the derivative of the Hamiltonian with respect to the spins, that yields the effective magnetic field acting on the individual spins. On the other hand, the XY -rotators are more correctly identified with particles confined to a circle, with angle and angular momentum as canonically conjugate variables, and with the dynamics generated by the Hamilton equations for these variables [35]. Apart from academic interest, the model provides a tractable reference to study physical systems like gravitational sheet models [36] and the free-electron laser [37].

The Hamiltonian of the HMF model is [27]

$$H = \sum_{i=1}^N \frac{p_i^2}{2m} + \frac{\tilde{K}}{2N} \sum_{i,j=1}^N [1 - \cos(\theta_i - \theta_j)], \quad (46)$$

where $\theta_i \in [-\pi, \pi]$ gives the position of the i th particle on the circle, while $p_i = mv_i$ is its conjugated angular momentum, with v_i being the angular velocity. The time evolution of the system within a microcanonical ensemble follows the deterministic Hamilton equations of motion given by

$$\frac{d\theta_i}{dt} = v_i, \quad (47)$$

$$m \frac{dv_i}{dt} = \tilde{K} r \sin(\psi - \theta_i).$$

Here, the quantities r and ψ are as defined in equation (6). The dynamics conserves the total energy and momentum. Under the evolution (47), the system at long times settles into an equilibrium stationary state in which, depending on the energy density $\epsilon = H/N$, the system could be in one of two possible phases. Namely, for ϵ smaller than a critical value $\epsilon_c = 3\tilde{K}/4$, the system is in a clustered phase in which the particles are close together on the circle, while for energies larger than ϵ_c , the particles are uniformly distributed on the circle, characterizing a homogeneous phase [28]. A continuous phase transition between the two phases is effectively characterized by the quantity $r(t)$ defined in equation (6), that in the present context may be interpreted as the specific magnetization of the system. The phase transition may be interpreted as one from a high-energy paramagnetic phase (similar to the incoherent phase in the setting of coupled oscillators) to a low-energy ferromagnetic phase (similar to the synchronized phase).

One may generalize the microcanonical dynamics (47) to include the effect of an interaction with an external heat bath at temperature T . The resulting Brownian mean-field (BMF) model has thus a canonical ensemble dynamics given by [24, 25].

$$\frac{d\theta_i}{dt} = v_i,$$

(48)

$$m \frac{dv_i}{dt} = -\gamma v_i + \tilde{K} r \sin(\psi - \theta_i) + \tilde{\eta}_i(t),$$

where $\tilde{\eta}_i(t)$ is defined in equation (44). A fluctuation-dissipation relation expresses the strength \tilde{D} of the noise in terms of the temperature T and the friction constant γ as

$$\tilde{D} = \gamma k_B T. \quad (49)$$

We will set the Boltzmann constant k_B to unity in the rest of the paper. The canonical dynamics (48) also leads to a long-time equilibrium stationary state in which a generic configuration C with energy $E(C)$ occurs with the usual Gibbs-Boltzmann weight: $P_{\text{eq}}(C) \propto e^{-E(C)/T}$. The phase transition in the HMF model within the microcanonical ensemble occurs within the canonical ensemble on tuning the temperature across the critical value $T_c = \tilde{K}/2$. This latter critical value may be derived very simply by following standard procedure [28]. Due to full rotational $O(2)$ symmetry, we may take the direction along which particles cluster to be along x without loss of generality. Then, the x -component of the magnetization r , namely, $r_x = r \cos \psi$, satisfies in equilibrium the equation

$$r_x = \frac{\int_{-\pi}^{\pi} d\theta \cos \theta e^{\tilde{K}(r_x/T) \cos \theta}}{\int_{-\pi}^{\pi} d\theta e^{\tilde{K}(r_x/T) \cos \theta}}. \quad (50)$$

Close to the critical point ($T \rightarrow T_c$), expanding the above equation to leading order in r_x , we get

$$r_x \left(2\pi - \frac{\tilde{K}}{T} \int_{-\pi}^{\pi} d\theta \cos^2 \theta \right) = 0. \quad (51)$$

With $r_x \neq 0$, we get the critical temperature as $T_c = \tilde{K}/2$.

Let us now envisage the following situation: A set of quenched external torques $\{\tilde{\omega}_i \equiv \gamma \omega_i\}$ acts on each of the particles, thereby pumping energy into the system. In this case, the second equation in the canonical dynamics (48) has an additional term $\tilde{\omega}_i$ on the right hand side. The resulting dynamics becomes exactly identical to the dynamics (43) of the generalized Kuramoto model.

3.2. Previous studies

Introducing inertia alone into the Kuramoto dynamics (equation (43) without the noise term) has significant consequences. Tanaka *et al.* showed, mainly on the basis of numerical simulations, that finite large inertia leads to the synchronization transition becoming of first order, occurring in an abrupt way on tuning K [34]. Analysis of the dynamics (43) in the continuum limit, based on a suitable Fokker-Planck-like equation, was pursued in Refs. [18,20]. It was shown that for a Lorentzian $g(\omega)$, either larger inertia or larger frequency spread (measured in terms of the width of the Lorentzian $g(\omega)$) makes the system harder to synchronize, leading to an incoherent stationary state.

3.3. Dynamics in a reduced parameter space

We start our analysis of the dynamics (43) by noting that the effect of σ may be made explicit by replacing ω_i in the second equation by $\sigma\omega_i$. We thus consider from now on the dynamics (43) with the substitution $\omega_i \rightarrow \sigma\omega_i$. In the resulting model, $g(\omega)$ therefore has zero mean and unit width. Also, we will consider in the dynamics (43) the parameter \tilde{D} to have the scaling (49).

For $m \neq 0$, using dimensionless quantities

$$\bar{t} \equiv t\sqrt{\tilde{K}/m}, \quad (52)$$

$$\bar{v}_i \equiv v_i\sqrt{m/\tilde{K}}, \quad (53)$$

$$1/\sqrt{\bar{m}} \equiv \gamma/\sqrt{\tilde{K}m}, \quad (54)$$

$$\bar{\sigma} \equiv \gamma\sigma/\tilde{K}, \quad (55)$$

$$\bar{T} \equiv T/\tilde{K}, \quad (56)$$

$$\bar{\eta}_i(\bar{t}) \equiv \tilde{\eta}_i(t)/\tilde{K}, \quad (57)$$

the equations of motion become

$$\frac{d\theta_i}{d\bar{t}} = \bar{v}_i, \quad (58)$$

$$\frac{d\bar{v}_i}{d\bar{t}} = -\frac{1}{\sqrt{\bar{m}}}\bar{v}_i + r \sin(\psi - \theta_i) + \bar{\sigma}\omega_i + \bar{\eta}_i(\bar{t}),$$

where

$$\langle \bar{\eta}_i(\bar{t})\bar{\eta}_j(\bar{t}') \rangle = 2(\bar{T}/\sqrt{\bar{m}})\delta_{ij}\delta(\bar{t} - \bar{t}'). \quad (59)$$

For $m = 0$, using dimensionless time

$$\bar{t} \equiv t(\tilde{K}/\gamma), \quad (60)$$

and with $\bar{\sigma}$ and \bar{T} defined as above, the dynamics becomes the overdamped motion

$$\frac{d\theta_i}{d\bar{t}} = r \sin(\psi - \theta_i) + \bar{\sigma}\omega_i + \bar{\eta}_i(\bar{t}), \quad (61)$$

where

$$\langle \bar{\eta}_i(\bar{t})\bar{\eta}_j(\bar{t}') \rangle = 2\bar{T}\delta_{ij}\delta(\bar{t} - \bar{t}'). \quad (62)$$

We have thus reduced the dynamics (43) involving five parameters, $m, \gamma, \tilde{K}, \sigma, T$, to the dynamics (58) (or (61) in the overdamped limit) that involves only three dimensionless parameters, $\bar{m}, \bar{T}, \bar{\sigma}$. From now on, we consider the dynamics in this reduced parameter space, dropping overbars for simplicity of notation.

With $\sigma = 0$ (i.e. $g(\omega) = \delta(\omega)$ [18], [20]), the dynamics (58) is that of the BMF model with an equilibrium stationary state. For other $g(\omega)$, the dynamics (58) violates detailed

balance, leading to a nonequilibrium stationary state (NESS) [21]. In section 3.5.1, we give a rigorous proof of this statement.

3.4. Non-equilibrium first-order synchronization phase transition

In this section, we report on a very interesting non-equilibrium phase transition that occurs in the stationary state of the dynamics (58). As discussed above, the three relevant parameters of the dynamics are m, T, σ . In this three-dimensional space of parameters, let us first locate the phase transitions in the Kuramoto model and in its noisy extension, discussed in section 2.

- The phase transition of the Kuramoto dynamics ($m = T = 0, \sigma \neq 0$) corresponds now to a continuous transition from a low- σ synchronized to a high- σ incoherent phase across the critical point $\sigma_c(m = 0, T = 0) = \pi g(0)/2$.
- Extending the Kuramoto dynamics to $T \neq 0$, the above mentioned critical point becomes a second-order critical line on the (T, σ) -plane, given by solving $2 = \int_{-\infty}^{\infty} d\omega g(\omega)[T/(T^2 + \omega^2 \sigma_c^2(m = 0, T))]$.
- The transition in the BMF dynamics ($m, T \neq 0, \sigma = 0$) corresponds now to a continuous transition occurring at the critical temperature $T_c = 1/2$.

The complete phase diagram is shown schematically in Fig. 1(a), where the thick red second-order critical lines denote the continuous transitions mentioned above. On the other hand, for m, σ, T all non-zero, we demonstrate below that the synchronization transition becomes first order, occurring across the shaded blue transition surface. This surface is bounded by the second-order critical lines on the (T, σ) and (m, T) planes, and by a first-order transition line on the (m, σ) -plane. Let us remark that all phase transitions for $\sigma \neq 0$ are in NESSs, and are interpreted to be of dynamical origin, accounted for by stability considerations of stationary solutions of equations (for example, the Kramers equation discussed below) for temporal evolution of phase space distributions. More rigorously, to qualify as thermodynamics phases, one needs to show that the different phases extremize a free energy-like quantity (e.g., a large deviation functional [38]). Such a demonstration in this nonequilibrium scenario is a daunting task, while for $\sigma = 0$, the phases have actually been shown to minimize the equilibrium free energy [28].

In order to demonstrate the first-order nature of the transition, we performed N -body simulations for a representative $g(\omega)$, i.e., the Gaussian given by equation (89). For given m and T , we prepared an initial state with all oscillators at $\theta = 0$ and frequencies v_i 's sampled from a Gaussian distribution with zero mean and standard deviation $\propto T$. We then let the system equilibrate at $\sigma = 0$, and subsequently increase σ adiabatically to high values and back in a cycle. The simulations involved integrations of the $2N$ coupled equations of motion (58), see Appendix B for details. Figure 2 shows the behavior of r for several m 's at a fixed T less than the BMF transition point $T_c = 1/2$, where one may observe

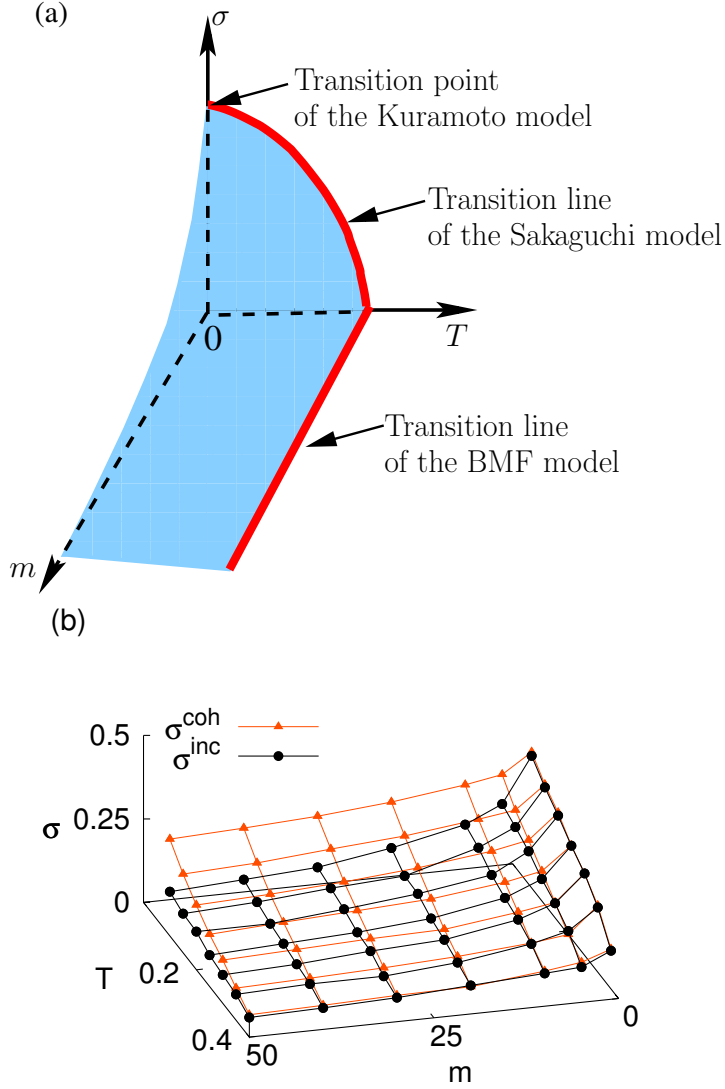


Figure 1. (a) The figure shows the schematic phase diagram of model (58) in terms of dimensionless moment of inertia m , temperature T , and width of the frequency distribution σ . Here, the shaded blue surface is a first-order transition surface, while the thick red lines are second-order critical lines. The system is synchronized inside the region bounded by the surface, and is incoherent outside. The transitions of known models are also marked in the figure. The blue surface in (a) is bounded from above and below by the dynamical stability thresholds $\sigma^{\text{coh}}(m, T)$ and $\sigma^{\text{inc}}(m, T)$ of respectively the synchronized and the incoherent phase, which are estimated in N -body simulations from hysteresis plots (see Fig. 2 for an example); the surfaces $\sigma^{\text{coh}}(m, T)$ and $\sigma^{\text{inc}}(m, T)$ for $N = 500$ in the case of a Gaussian $g(\omega)$ with zero mean and unit width are shown in panel (b).

sharp jumps and hysteresis behavior expected of a first-order transition. With decrease of m , the jump in r becomes less sharp, and the hysteresis loop area decreases, both features

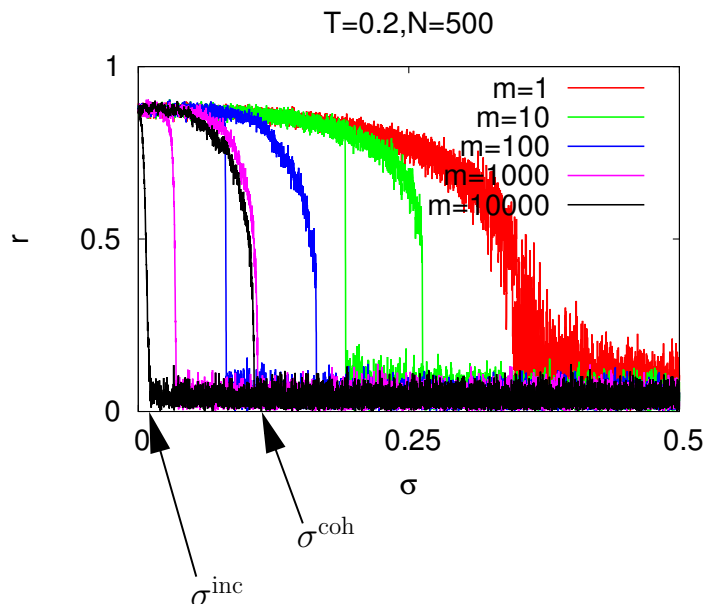


Figure 2. For the model (58), the figure shows r vs. adiabatically tuned σ for different m values at $T = 0.2 < T_c = 1/2$, showing also the stability thresholds, $\sigma^{\text{inc}}(m, T)$ and $\sigma^{\text{coh}}(m, T)$, for $m = 10000$. The data are obtained from simulations with $N = 500$. For a given m , the branch of the plot to the right (left) corresponds to σ increasing (decreasing); for $m = 1$, the two branches almost overlap. The data are for the Gaussian $g(\omega)$ given by equation (89).

being consistent with the transition becoming second-order-like as $m \rightarrow 0$, see Fig. 1(a). For $m = 10000$, we mark in Fig. 2 the approximate stability thresholds for the incoherent and the synchronized phase, denoted respectively by $\sigma^{\text{inc}}(m, T)$ and $\sigma^{\text{coh}}(m, T)$. The actual phase transition point $\sigma_c(m, T)$ lies in between the two thresholds. Let us note from the figure that both the thresholds decrease and approach zero with the increase of m . A qualitatively similar behavior is observed for a Lorentzian $g(\omega)$, see Fig. 3. Figure 4 shows hysteresis plots for a Gaussian $g(\omega)$ at a fixed m and for several values of $T \leq T_c$, where one observes that with T approaching T_c , the hysteresis loop area decreases, jumps in r become less sharp and occur between smaller and smaller values that approach zero. Moreover, the r value at $\sigma = 0$ decreases as T increases towards T_c , reaching zero at T_c . Disappearance of the hysteresis loop with increase of T similar to that in Fig. 4 was reported in Ref. [19]. Our findings suggest that the thresholds $\sigma^{\text{inc}}(m, T)$ and $\sigma^{\text{coh}}(m, T)$ coincide on the second-order critical lines, as expected, and moreover, they asymptotically come close together and approach zero as $m \rightarrow \infty$ at a fixed T . For given m and T , and for σ in between $\sigma^{\text{inc}}(m, T)$ and $\sigma^{\text{coh}}(m, T)$, Fig. 5(a) for r as a function of time in the stationary state shows bistability, whereby the system switches back and forth between incoherent ($r \approx 0$) and synchronized ($r > 0$) states. The distribution $P(r)$ depicted in Figure 5(b) is bimodal with a peak around either $r \approx 0$

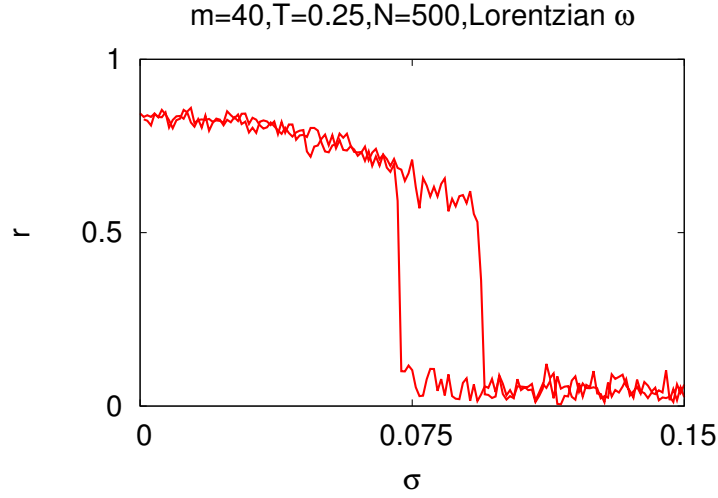


Figure 3. For the model (58), the figure shows r vs. adiabatically tuned σ at $m = 40, T = 0.25$. The data are obtained from simulations with $N = 500$. The branch of the plot to the right (left) corresponds to σ increasing (decreasing). The data are for a Lorentzian $g(\omega)$ with zero mean and unit width.

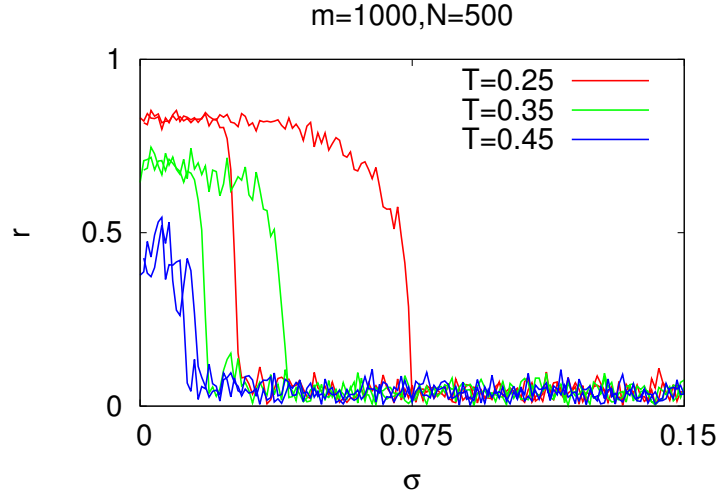


Figure 4. For the model (58), the figure shows r vs. adiabatically tuned σ for different temperatures $T \leq T_c = 1/2$ at a fixed moment of inertia $m = 1000$. The data are obtained from simulations with $N = 500$. For a given T , the branch of the plot to the right (left) corresponds to σ increasing (decreasing); for $T \geq 0.45$, the two branches almost overlap. The data are for the Gaussian $g(\omega)$ given by equation (89).

or $r > 0$ as σ varies between $\sigma^{\text{inc}}(m, T)$ and $\sigma^{\text{coh}}(m, T)$. Figure 5 lends further credence to the phase transition being first order.

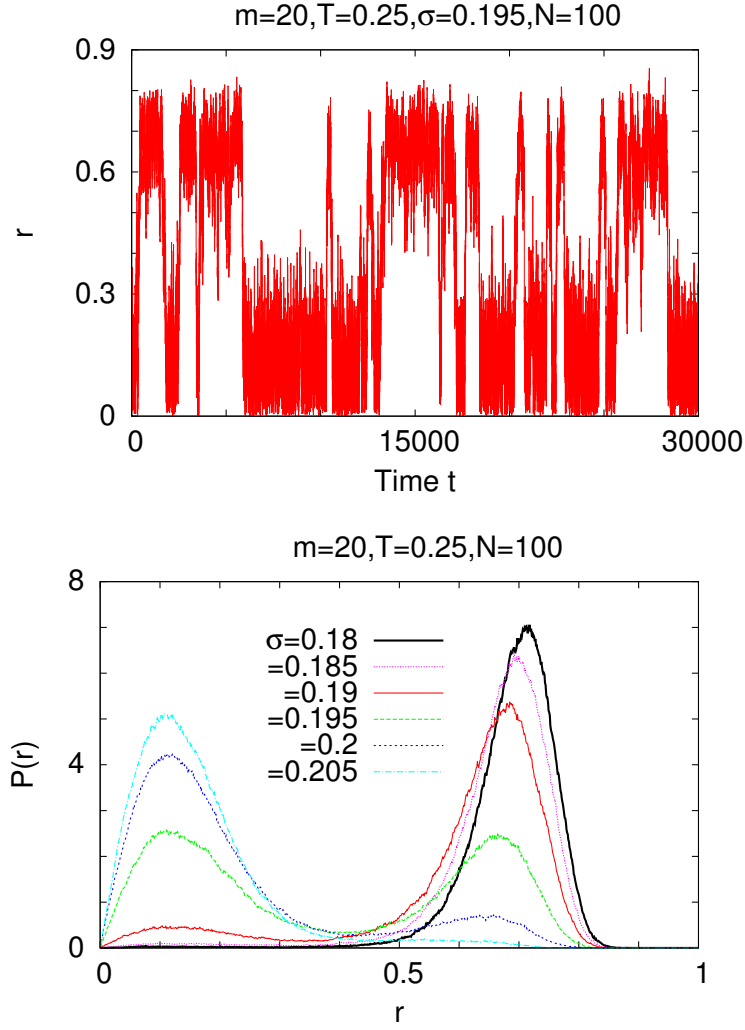


Figure 5. For the dynamics (58) at $m = 20, T = 0.25, N = 100$, and the Gaussian $g(\omega)$ given by equation (89), (a) shows at $\sigma = 0.195$, the numerically estimated first-order phase transition point, r vs. time in the stationary state, while (b) shows the distribution $P(r)$ at several σ 's around 0.195. The data are obtained from simulations with $N = 100$.

3.5. Analysis in the continuum limit: The Kramers equation

We now turn to an analytical characterization of the dynamics (58) in the continuum limit $N \rightarrow \infty$. To this end, we define the single-oscillator distribution $f(\theta, v, \omega, t)$ that gives at time t and for each ω the fraction of oscillators with phase θ and angular velocity v . The distribution is 2π -periodic in θ , and obeys the normalization

$$\int_{-\pi}^{\pi} d\theta \int_{-\infty}^{\infty} dv f(\theta, v, \omega, t) = 1, \quad (63)$$

while evolving following the Kramers equation [20, 21]

$$\frac{\partial f}{\partial t} = -v \frac{\partial f}{\partial \theta} + \frac{\partial}{\partial v} \left(\frac{v}{\sqrt{m}} - \sigma \omega - r \sin(\psi - \theta) \right) f + \frac{T}{\sqrt{m}} \frac{\partial^2 f}{\partial v^2}, \quad (64)$$

where

$$r e^{i\psi} = \int d\theta dv d\omega g(\omega) e^{i\theta} f(\theta, v, \omega, t). \quad (65)$$

Let us briefly sketch the derivation of equation (64), while the details may be found in Ref. [21]. We will along the way also indicate how one may prove rigorously that the dynamics (58) does not satisfy detailed balance unless $\sigma = 0$. For simplicity of presentation, we first consider the case of a discrete bimodal $g(\omega)$, and then in the end extend our discussion to a general $g(\omega)$. Then, consider a given realization of $g(\omega)$ in which there are N_1 oscillators with frequencies ω_1 and N_2 oscillators with frequencies ω_2 , where $N_1 + N_2 = N$. Let us then define the N -oscillator distribution function $f_N(\theta_1, v_1, \dots, \theta_{N_1}, v_{N_1}, \theta_{N_1+1}, v_{N_1+1}, \dots, \theta_N, v_N, t)$ as the probability density at time t to observe the system around the values $\{\theta_i, v_i\}_{1 \leq i \leq N}$. In the following, we use the shorthand notations $z_i \equiv (\theta_i, v_i)$ and $\mathbf{z} = (z_1, z_2, \dots, z_N)$. Note that f_N satisfies the normalization

$$\int \left(\prod_{i=1}^N dz_i \right) f_N(\mathbf{z}, t) = 1. \quad (66)$$

The distribution f_N evolves in time according to the following Fokker-Planck equation that may be derived straightforwardly from the equations of motion (58):

$$\begin{aligned} \frac{\partial f_N}{\partial t} = & - \sum_{i=1}^N \left[v_i \frac{\partial f_N}{\partial \theta_i} - \frac{1}{\sqrt{m}} \frac{\partial (v_i f_N)}{\partial v_i} \right] - \sigma \sum_{j=1}^N \left(\Omega^T \right)_j \frac{\partial f_N}{\partial v_j} + \frac{T}{\sqrt{m}} \sum_{i=1}^N \frac{\partial^2 f_N}{\partial v_i^2} \\ & - \frac{1}{2N} \sum_{i,j=1}^N \sin(\theta_j - \theta_i) \left[\frac{\partial f_N}{\partial v_i} - \frac{\partial f_N}{\partial v_j} \right], \end{aligned} \quad (67)$$

where the $N \times 1$ column vector Ω has its first N_1 entries equal to ω_1 and the following N_2 entries equal to ω_2 , and where the superscript T denotes matrix transpose operation:

$$\Omega^T \equiv [\omega_1 \ \omega_1 \ \dots \ \omega_1 \ \omega_2 \ \dots \ \omega_2]. \quad (68)$$

3.5.1. Proof that the dynamics does not satisfy detailed balance unless $\sigma = 0$ Let us rewrite the Fokker-Planck equation (67) as

$$\frac{\partial f_N(\mathbf{x})}{\partial t} = - \sum_{i=1}^{2N} \frac{\partial [A_i(\mathbf{x}) f_N(\mathbf{x})]}{\partial x_i} + \frac{1}{2} \sum_{i,j=1}^{2N} \frac{\partial^2 [B_{i,j}(\mathbf{x}) f_N(\mathbf{x})]}{\partial x_i \partial x_j}, \quad (69)$$

where

$$x_i = \begin{cases} \theta_i; & i = 1, 2, \dots, N, \\ v_{i-N}; & i = N + 1, \dots, 2N, \end{cases} \quad (70)$$

and

$$\mathbf{x} = \{x_i\}_{1 \leq i \leq 2N}. \quad (71)$$

Here, the drift vector $A_i(\mathbf{x})$ is given by

$$A_i(\mathbf{x}) = \begin{cases} v_i; i = 1, 2, \dots, N, \\ -\frac{1}{\sqrt{m}}v_{i-N} + \frac{1}{N} \sum_{j=1}^N \sin(\theta_j - \theta_{i-N}) + \sigma \left(\Omega^T \right)_{i-N}; \\ i = N + 1, \dots, 2N, \end{cases} \quad (72)$$

while the diffusion matrix $B_{i,j}(\mathbf{x})$ is

$$B_{i,j}(\mathbf{x}) = \begin{cases} \frac{2T}{\sqrt{m}} \delta_{ij}; i, j > N, \\ 0, \text{ Otherwise.} \end{cases} \quad (73)$$

The dynamics described by the Fokker-Planck equation of the form (69) satisfies detailed balance if and only if the following conditions are satisfied [39]:

$$\epsilon_i \epsilon_j B_{i,j}(\epsilon \mathbf{x}) = B_{i,j}(\mathbf{x}), \quad (74)$$

$$\epsilon_i A_i(\epsilon \mathbf{x}) f_N^s(\mathbf{x}) = -A_i(\mathbf{x}) f_N^s(\mathbf{x}) + \sum_{j=1}^{2N} \frac{\partial [B_{i,j}(\mathbf{x}) f_N^s(\mathbf{x})]}{\partial x_j}, \quad (75)$$

where $f_N^s(\mathbf{x})$ is the stationary solution of equation (69). Here, $\epsilon_i = \pm 1$ denotes the parity with respect to time reversal of the variables x_i 's: Under time reversal, we have $x_i \rightarrow \epsilon_i x_i$, where $\epsilon_i = -1$ (respectively, $+1$) depending on whether x_i is odd (respectively, even) under time reversal. For example, θ_i 's are even, while v_i 's are odd.

Using equation (73), the condition (74) is trivially satisfied, while to check the condition given by (75), we formally solve this equation for $f_N^s(\mathbf{x})$ and check if the solution solves equation (69) in the stationary state. From equation (75), we see that for $i = 1, 2, \dots, N$, the condition reduces to

$$\epsilon_i A_i(\epsilon \mathbf{x}) f_N^s(\mathbf{x}) = -A_i(\mathbf{x}) f_N^s(\mathbf{x}). \quad (76)$$

The above equation, using equation (72), is obviously satisfied. For $i = N + 1, \dots, 2N$, we have

$$v_k f_N^s(\mathbf{x}) = -\frac{T \partial f_N^s(\mathbf{x})}{\partial v_k}; k = i - N, \quad (77)$$

solving which we get

$$f_N^s(\mathbf{x}) \propto d(\theta_1, \theta_2, \dots, \theta_N) \exp \left[-\frac{1}{2T} \sum_{k=1}^N v_k^2 \right], \quad (78)$$

where $d(\theta_1, \theta_2, \dots, \theta_N)$ is a function to be determined. Substituting the distribution (78) into equation (69) and requiring that it is a stationary solution implies that σ has to be equal to zero, while

$$d(\theta_1, \theta_2, \dots, \theta_N) = \exp \left(-\frac{1}{2NT} \sum_{i,j=1}^N \left[1 - \cos(\theta_i - \theta_j) \right] \right). \quad (79)$$

Thus, for $\sigma = 0$, when the dynamics reduces to that of the BMF model, we get the stationary solution as

$$f_{N,\sigma=0}^s(\mathbf{z}) \propto \exp \left[-\frac{H}{T} \right]. \quad (80)$$

where H is the Hamiltonian (46) (expressed in terms of dimensionless variables introduced above). The lack of detailed balance for $\sigma \neq 0$ obviously extends to any distribution $g(\omega)$.

3.5.2. Derivation of the Kramers equation The starting point is to define the reduced distribution function f_{s_1,s_2} , with $s_1 = 0, 1, 2, \dots, N_1$ and $s_2 = 0, 1, 2, \dots, N_2$ as [40]

$$\begin{aligned} & f_{s_1,s_2}(z_1, z_2, \dots, z_{s_1}, z_{N_1+1}, \dots, z_{N_1+s_2}, t) \\ &= \frac{N_1!}{(N_1 - s_1)!N_1^{s_1}} \frac{N_2!}{(N_2 - s_2)!N_2^{s_2}} \int dz_{s_1+1} \dots dz_{N_1} dz_{N_1+s_2+1} \dots dz_N f_N(z, t) \end{aligned} \quad (81)$$

Note that the following normalizations hold for the single-oscillator distribution functions:

$$\int dz_1 f_{1,0}(z_1, t) = 1, \text{ and } \int dz_{N_1+1} f_{0,1}(z_{N_1+1}, t) = 1. \quad (82)$$

Assuming that

- (i) f_N is symmetric with respect to permutations of dynamical variables within the same group of oscillators, and
- (ii) f_N , together with the derivatives $\partial f_N / \partial v_i \forall i$, vanish on the boundaries of the phase space,

and then using equation (67) in equation (81), one obtains the Bogoliubov-Born-Green-Kirkwood-Yvon (BBGKY) hierarchy equations for the dynamics (58) (for details, see [21]).

In particular, the first equations of the hierarchy are

$$\begin{aligned} & \frac{\partial f_{1,0}(\theta, v, t)}{\partial t} + \frac{v \partial f_{1,0}(\theta, v, t)}{\partial \theta} - \frac{1}{\sqrt{m}} \frac{\partial}{\partial v} (v f_{1,0}(\theta, v, t)) \\ &+ \sigma \omega_1 \frac{\partial f_{1,0}(\theta, v, t)}{\partial v} - \frac{T}{\sqrt{m}} \frac{\partial^2 f_{1,0}(\theta, v, t)}{\partial v^2} \\ &= -\frac{N_1}{N} \int d\theta' dv' \sin(\theta' - \theta) \frac{\partial f_{2,0}(\theta, v, \theta', v', t)}{\partial v} \\ &- \frac{N_2}{N} \int d\theta' dv' \sin(\theta' - \theta) \frac{\partial f_{1,1}(\theta, v, \theta', v', t)}{\partial v}, \end{aligned} \quad (83)$$

and a similar equation for $f_{0,1}(\theta, v, t)$. In the limit $N \rightarrow \infty$, writing

$$g(\omega) = \left[\frac{N_1}{N} \delta(\omega - \omega_1) + \frac{N_2}{N} \delta(\omega - \omega_2) \right], \quad (84)$$

one can express equation (83) in terms of $g(\omega)$.

In order to generalize the above treatment to the case of a continuous $g(\omega)$, note for this case that the single-oscillator distribution function is $f(\theta, v, \omega, t)$. The first equation of the hierarchy is then

$$\begin{aligned} & \frac{\partial f(\theta, v, \omega, t)}{\partial t} + \frac{v \partial f(\theta, v, \omega, t)}{\partial \theta} - \frac{1}{\sqrt{m}} \frac{\partial}{\partial v} (v f(\theta, v, \omega, t)) \\ & + \sigma \omega \frac{\partial f(\theta, v, \omega, t)}{\partial v} - \frac{T}{\sqrt{m}} \frac{\partial^2 f(\theta, v, \omega, t)}{\partial v^2} \\ & = - \int d\omega' \int d\theta' dv' g(\omega') \sin(\theta' - \theta) \frac{\partial f(\theta, v, \theta', v', \omega, \omega', t)}{\partial v}. \end{aligned} \quad (85)$$

In the continuum limit $N \rightarrow \infty$, one may neglect oscillator-oscillator correlations, and approximate $f(\theta, v, \theta', v', \omega, \omega', t)$ as

$$\begin{aligned} f(\theta, v, \theta', v', \omega, \omega', t) & = f(\theta, v, \omega, t) f(\theta', v', \omega', t) \\ & + \text{corrections subdominant in } N, \end{aligned} \quad (86)$$

so that equation (85) reduces to the Kramers equation (64).

3.6. Stationary solutions of the Kramers equation

The stationary solutions of equation (64) are obtained by setting the left hand side to zero. For $\sigma = 0$, the stationary solution is

$$f_{\text{st}}(\theta, v) \propto \exp[-(v^2/2 - r_{\text{st}} \cos \theta)/T], \quad (87)$$

that corresponds to canonical equilibrium, with r_{st} determined self-consistently [25], see equation (50). For $\sigma \neq 0$, the incoherent stationary state is [20]

$$f_{\text{st}}^{\text{inc}}(\theta, v, \omega) = 1/((2\pi)^{3/2} \sqrt{T}) \exp[-(v - \sigma \omega \sqrt{m})^2/(2T)]. \quad (88)$$

In the class of unimodal frequency distributions, let us consider a representative $g(\omega)$, namely, a Gaussian:

$$g(\omega) = \frac{1}{\sqrt{2\pi}} \exp[-\omega^2/2]. \quad (89)$$

We then have for the marginal angular velocity distribution

$$\begin{aligned} P_{\text{st}}^{\text{inc}}(v) & = \int_{-\infty}^{\infty} d\omega g(\omega) \int_{-\pi}^{\pi} d\theta f_{\text{st}}^{\text{inc}}(\theta, v, \omega) \\ & = \sqrt{\frac{1}{2\pi T (1 + \sigma^2 m/T)}} \exp\left[-\frac{v^2}{2T(1 + \sigma^2 m/T)}\right], \end{aligned} \quad (90)$$

and the marginal angle distribution

$$P_{\text{st}}^{\text{inc}}(\theta) = \frac{1}{2\pi} \int_{-\infty}^{\infty} d\omega g(\omega) \int_{-\infty}^{\infty} dv f_{\text{st}}^{\text{inc}}(\theta, v, \omega) = \frac{1}{2\pi}, \quad (91)$$

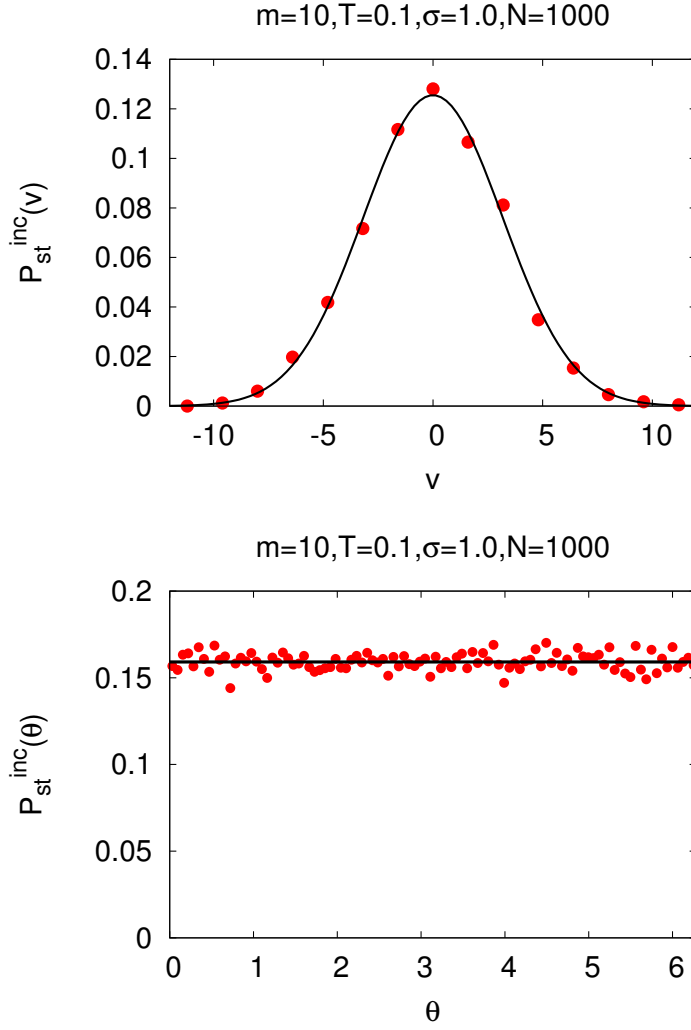


Figure 6. For the dynamics (58), here we show the marginal distributions, $P_{st}^{inc}(v)$ and $P_{st}^{inc}(\theta)$, corresponding to the incoherent phase for $m = 10, T = 0.1, \sigma = 1.0$. The points denoting simulation data are for $N = 1000$ for one fixed realization of the ω_i 's sampled from the Gaussian distribution (89), while the continuous lines denote theoretical results (90) and (91).

both correctly normalized to unity. In Figs. 6 and 7, we compare our theoretical predictions, (90) and (91), with numerical simulation results.

The existence of the synchronized stationary state is borne out by our simulation results in Fig. 7, although its analytical form is not known.

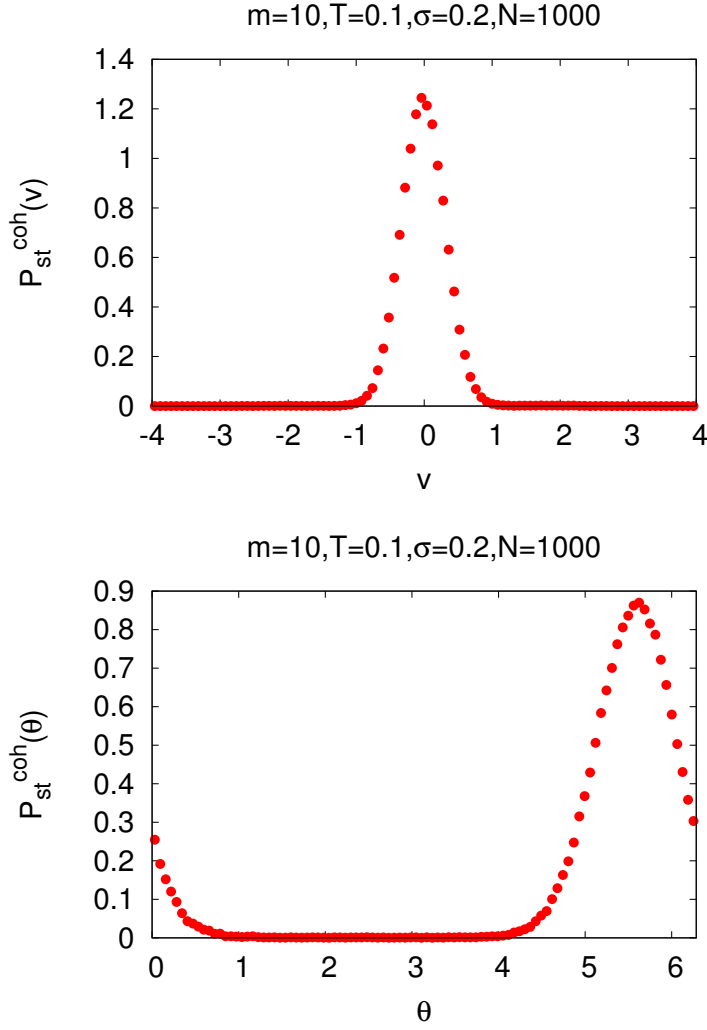


Figure 7. For the dynamics (58), the figure shows the marginal distributions, $P_{\text{st}}^{\text{coh}}(v)$ and $P_{\text{st}}^{\text{coh}}(\theta)$, corresponding to the synchronized phase for $m = 10, T = 0.1, \sigma = 0.2$. The points denoting simulation data are for $N = 1000$ for one fixed realization of the ω_i 's sampled from the Gaussian distribution (89).

3.7. Linear stability analysis of the incoherent stationary state

We now discuss about the linear stability analysis of the incoherent state (88); a similar analysis for the BMF model is discussed in Ref. [41]. Following Ref. [20], we linearize equation (64) about the state by expanding f as

$$f(\theta, v, \omega, t) = f_{\text{st}}^{\text{inc}}(\theta, v, \omega) + e^{\lambda t} \delta f(\theta, v, \omega), \quad (92)$$

where $\delta f \ll 1$ satisfies the linearized Kramers equation:

$$\lambda \delta f + v \frac{\partial \delta f}{\partial \theta} - \frac{\partial}{\partial v} \left(\frac{v}{\sqrt{m}} - \sigma \omega \right) \delta f - \frac{T}{\sqrt{m}} \frac{\partial^2 \delta f}{\partial v^2}$$

$$= -\frac{\partial f_{\text{st}}^{\text{inc}}}{\partial v} \int_{-\pi}^{\pi} \int_{-\infty}^{\infty} \int_{-\infty}^{\infty} d\phi dv d\omega g(\omega) \delta f(\phi, v, \omega) \sin(\phi - \theta). \quad (93)$$

Since f and $f_{\text{st}}^{\text{inc}}$ are normalized, we have

$$\int_{-\pi}^{\pi} \int_{-\infty}^{\infty} d\theta dv \delta f(\theta, v, \omega) = 0. \quad (94)$$

Substituting

$$\delta f(\theta, v, \omega) = \sum_{n=-\infty}^{\infty} b_n(v, \omega, \lambda) e^{in\theta} \quad (95)$$

in equation (93), one gets

$$\begin{aligned} & \frac{d^2 b_n}{dv^2} + \frac{1}{T} (v - \sigma\omega\sqrt{m}) \frac{db_n}{dv} + \frac{1}{T} (1 - \lambda\sqrt{m} - inv\sqrt{m}) b_n \\ &= \frac{\sqrt{m}}{T} \frac{\partial f_{\text{st}}^{\text{inc}}}{\partial v} \pi (i\delta_{n,1} - i\delta_{n,-1}) \langle 1, b_n \rangle, \end{aligned} \quad (96)$$

where one has the scalar product

$$\langle \varphi, \psi \rangle \equiv \int_{-\infty}^{\infty} \int_{-\infty}^{\infty} dv d\omega g(\omega) \varphi^*(v, \omega) \psi(v, \omega), \quad (97)$$

with $*$ denoting complex conjugation. Since δf is real, one has $b_{-n} = b_n^*$, while equation (94) implies that $b_0 = 0$. We can then restrict to consider only $n \geq 0$. Next, equation (96) is transformed into a nonhomogeneous parabolic cylinder equation by the transformations

$$b_n(v, \omega, \lambda) = \exp \left[-\frac{(v - \sigma\omega\sqrt{m})^2}{4T} \right] \beta_n(z, \omega, \lambda), \quad (98)$$

$$z = \frac{1}{\sqrt{T}} (v - \sigma\omega\sqrt{m} + 2nT\sqrt{m}i), \quad (99)$$

which when substituted into equation (96) yield

$$\begin{aligned} & \frac{d^2 \beta_n}{dz^2} + \left[\frac{1}{2} - \frac{z^2}{4} - \sqrt{m}(\lambda + in\sigma\omega\sqrt{m} + n^2T\sqrt{m}) \right] \beta_n \\ &= i\pi\sqrt{m} \frac{\partial f_{\text{st}}^{\text{inc}}}{\partial v} e^{\frac{1}{4}(z-2i\sqrt{m}T)^2} \langle 1, e^{-\frac{1}{4}(z-2i\sqrt{m}T)^2} \beta_1 \rangle \delta_{n,1}. \end{aligned} \quad (100)$$

For $n \neq 1$, the right hand side of the above equation is zero, yielding the eigenvalues

$$\lambda_{p,n}(\omega) = -\frac{p}{\sqrt{m}} - n^2T\sqrt{m} - in\sigma\omega\sqrt{m}, \quad p = 0, 1, 2, \dots, \quad (101)$$

and the corresponding eigenfunctions

$$\beta_{p,n}(z, \omega, \lambda_{p,n}) = D_p(z) = 2^{-\frac{p}{2}} e^{-\frac{z^2}{4}} H_p\left(\frac{z}{\sqrt{2}}\right), \quad (102)$$

that do not depend on n and ω ; here, $D_p(z)$ and $H_p(x)$ are respectively the parabolic cylinder function and the Hermite polynomial of degree p [42]. The eigenvalues $\lambda_{p,n}(\omega)$ form a continuous spectrum. All of them have negative real parts, thus leading to linear stability

of the incoherent state (88), for $n = 2, 3, \dots$ and $p = 0, 1, 2, \dots$. For $n = 0$ the eigenvalues have also negative real parts unless those with $p = 0$, that have a vanishing real part. They would correspond to neutrally stable modes; however, the modes with $n = 0$ have zero amplitude due to the normalization condition (94).

For $n = 1$, solving (96) gives

$$\beta_1(z, \omega, \lambda) = -i\pi \langle 1, e^{-(\frac{z}{2} - i\sqrt{mT})^2} \beta_1 \rangle \times \sum_{p=0}^{\infty} \frac{\int_{-\infty}^{\infty} dz_1 e^{(\frac{z_1}{2} - i\sqrt{mT})^2} D_p[f_{\text{st}}^{\text{inc}}]'}{\sqrt{2\pi} p! \left(\frac{p}{\sqrt{m}} + \lambda + i\sigma\omega\sqrt{m} + T\sqrt{m} \right)} D_p(z), \quad (103)$$

where

$$[f_{\text{st}}^{\text{inc}}(v)]' = \left. \frac{\partial f_{\text{st}}^{\text{inc}}}{\partial v} \right|_{v=\sigma\omega\sqrt{m} - i2T\sqrt{m} + \sqrt{T}z} = -\frac{(z - 2i\sqrt{mT})}{(2\pi)^{\frac{3}{2}} T} e^{-\frac{1}{2}(z - 2i\sqrt{mT})^2}, \quad (104)$$

Using the above expression to compute $\langle 1, e^{-(\frac{z}{2} - i\sqrt{mT})^2} \beta_1 \rangle$, one obtains from the resulting self-consistent equation the following eigenvalue equation for λ [20]:

$$\frac{e^{mT}}{2T} \sum_{p=0}^{\infty} \frac{(-mT)^p (1 + \frac{p}{mT})}{p!} \int_{-\infty}^{\infty} \frac{g(\omega) d\omega}{1 + \frac{p}{mT} + i\frac{\sigma\omega}{T} + \frac{\lambda}{T\sqrt{m}}} = 1. \quad (105)$$

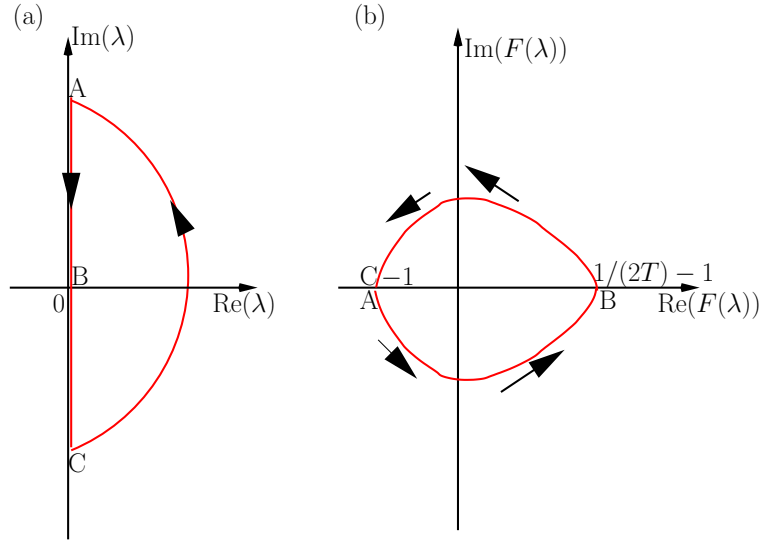


Figure 8. The loop in the complex F -plane, (b), corresponding to the loop in the complex λ -plane, (a), as determined by the function $F(\lambda)$ in equation (106).

3.7.1. Analysis of the eigenvalue equation A detailed analysis of the eigenvalue equation (105), carried out in Ref. [21], shows that the equation admits at most one solution for λ

with a positive real part, and when the solution exists, it is necessarily real. We now briefly sketch the analysis. We rewrite equation (105) as

$$F(\lambda; m, T, \sigma) = \frac{e^{mT}}{2T} \sum_{p=0}^{\infty} \frac{(-mT)^p (p+mT)}{p!} \int d\omega \frac{g(\omega)}{mT+p+\sqrt{m}\lambda+i\sigma m\omega} - 1 = 0. \quad (106)$$

where $g(\omega)$ is unimodal. The incoherent state (88) is unstable if there is a λ with a positive real part that satisfies the above eigenvalue equation.

We first look for possible pure imaginary solutions $\lambda = i\mu$. Separating equation (106) into real and imaginary parts, we have

$$\begin{aligned} & \text{Re}[F(i\mu; m, T, \sigma)] \\ &= \frac{e^{mT}}{2T} \sum_{p=0}^{\infty} \frac{(-mT)^p}{p!} \int d\omega g(\omega) \frac{(p+mT)^2}{(p+mT)^2 + (m\sigma\omega + \sqrt{m}\mu)^2} - 1 = 0, \end{aligned} \quad (107)$$

$$\begin{aligned} & \text{Im}[F(i\mu; m, T, \sigma)] \\ &= -\frac{e^{mT}}{2T} \sum_{p=0}^{\infty} \frac{(-mT)^p}{p!} \int d\omega g(\omega) \frac{(p+mT)(m\sigma\omega + \sqrt{m}\mu)}{(p+mT)^2 + (m\sigma\omega + \sqrt{m}\mu)^2} = 0. \end{aligned} \quad (108)$$

In the second equation above, making the change of variables $m\sigma\omega + \sqrt{m}\mu = m\sigma x$, and exploiting the parity in x of the sum, we get

$$\begin{aligned} \text{Im}[F(i\mu; m, T, \sigma)] &= -\frac{e^{mT}}{2T} m\sigma \int_0^{\infty} dx \left\{ \left[g\left(x - \frac{\mu}{\sqrt{m}\sigma}\right) - g\left(-x - \frac{\mu}{\sqrt{m}\sigma}\right) \right] \right. \\ &\quad \left. \times x \sum_{p=0}^{\infty} \frac{(-mT)^p}{p!} \frac{p+mT}{(p+mT)^2 + m^2\sigma^2 x^2} \right\} = 0. \end{aligned} \quad (109)$$

It is possible to show that the sum on the right-hand side is positive definite for any finite σ , while for our class of unimodal $g(\omega)$'s, the term within the square brackets is positive (respectively, negative) definite for $\mu > 0$ (respectively, for $\mu < 0$). Therefore, the last equation is never satisfied for $\mu \neq 0$, implying thereby that the eigenvalue equation (106) does not admit pure imaginary solutions (the proof holds also for the particular case $g(\omega) = \delta(\omega)$). This analysis also proves that there can be at most one solution of equation (106) with positive real part. In fact, let us consider, in the complex λ -plane, the loop $A - B - C - A$ depicted in Fig. 8(a), with A and C representing $\text{Im}\lambda \rightarrow \pm\infty$, respectively, and the radius of the arc $C - A$ going to ∞ . Due to the sign properties of $\text{Im}[F(i\mu; m, T, \sigma)]$ just described, we obtain in the complex- $F(\lambda)$ plane the loop qualitatively represented in Fig. 8(b). While the point $F = -1$ is obtained when λ is at the points A and C , the point B is determined by the value of $F(0)$ given by

$$F(0; m, T, \sigma) = \frac{e^{mT}}{2T} \sum_{p=0}^{\infty} \frac{(-mT)^p}{p!} \int d\omega g(\omega) \frac{(p+mT)^2}{(p+mT)^2 + (m\sigma\omega)^2} - 1. \quad (110)$$

From a well-known theorem of complex analysis [43], we therefore conclude that for $F(0; m, T, \sigma) > 0$, there is one and only one solution of the eigenvalue equation with positive real part and no solution for $F(0; m, T, \sigma) < 0$. When the single solution with positive real part exists, it is necessarily real, since a complex solution would imply the presence of its complex conjugate. For $\sigma = 0$, one has $F(0; m, T, 0) = 1/(2T) - 1$. For $\sigma > 0$, the value of $F(0; m, T, \sigma)$ depends on the distribution function $g(\omega)$. It is possible to prove that the value is always smaller than $1/(2T) - 1$; this is reasonable since if the incoherent state is stable for $\sigma = 0$, which happens when $T > 1/2$, it is *a fortiori* stable for $\sigma > 0$.

The surface delimiting the region of instability of the incoherent state (88) in the (m, T, σ) phase space is implicitly given by equation (110) that may be solved to obtain the stability threshold $\sigma^{\text{inc}} = \sigma^{\text{inc}}(m, T)$. It is reasonable to expect on physical grounds that the threshold is a single-valued function, and that for any given value of m , it is a decreasing function of T for $0 \leq T \leq 1/2$, reaching 0 for $T = 1/2$. These facts may be proved analytically for the class of unimodal distributions functions $g(\omega)$ considered in this work. Also, one can prove for any $g(\omega)$ that $\sigma^{\text{inc}}(m, T)$ approaches 0 as $m \rightarrow \infty$, by using the integral representation

$$\begin{aligned} & \sum_{p=0}^{\infty} \frac{(-mT)^p}{p!} \frac{(p+mT)^2}{(p+a)^2 + (m\sigma\omega)^2} \\ &= e^{-mT} - (m\sigma\omega) \int_0^{\infty} dt \exp[-mT(t+e^{-t})] \sin(m\sigma\omega t). \end{aligned} \quad (111)$$

For $\sigma > 0$, as $m \rightarrow \infty$, the term with the integral in the right-hand side of the last equation tends to e^{-mT} , so that equation (110) gives $F(0; m \rightarrow \infty, T > 0, \sigma > 0) = -1$. Combined with the fact that $F(0; m, T, 0) = 1/(2T) - 1$, we get $\sigma^{\text{inc}}(m \rightarrow \infty, 0 \leq T \leq 1/2) = 0$. Turning to a representative Gaussian case, equation (89), and using the subscript g to distinguish results for this case, equation (111) gives

$$F_g(0; m, T, \sigma) = \frac{1}{2T} - 1 - \frac{1}{2T} \int_0^{\infty} dy y e^{-\frac{y^2}{2}} \exp \left[mT \left(1 - \frac{y}{m\sigma} - e^{-\frac{y}{m\sigma}} \right) \right] \quad (112)$$

The equation $F_g(0; m, T, \sigma) = 0$ defines implicitly the function $\sigma^{\text{inc}}(m, T)$. We can show that this is a single-valued function with the properties $\partial\sigma^{\text{inc}}/\partial m < 0$ and $\partial\sigma^{\text{inc}}/\partial T < 0$. We have

$$\begin{aligned} \frac{\partial}{\partial m} F_g(0; m, T, \sigma) &= -\frac{1}{2} \int_0^{\infty} dy y e^{-\frac{y^2}{2}} \\ &\quad \times \left(1 - e^{-\frac{y}{m\sigma}} - \frac{y}{m\sigma} e^{-\frac{y}{m\sigma}} \right) \exp \left[mT \left(1 - \frac{y}{m\sigma} - e^{-\frac{y}{m\sigma}} \right) \right] \end{aligned} \quad (113)$$

which is negative as $1 - e^{-x} - xe^{-x}$ is positive for $x > 0$. From the implicit function theorems, we then derive that $\partial\sigma^{\text{inc}}/\partial m < 0$. On the other hand, we have

$$\begin{aligned} \frac{\partial}{\partial \sigma} F_g(0; m, T, \sigma) &= -\frac{1}{2\sigma^2} \int_0^{\infty} dy y^2 e^{-\frac{y^2}{2}} \left(1 - e^{-\frac{y}{m\sigma}} \right) \\ &\quad \times \exp \left[mT \left(1 - \frac{y}{m\sigma} - e^{-\frac{y}{m\sigma}} \right) \right], \end{aligned} \quad (114)$$

which is clearly negative. Since we are considering $T > 0$, multiplying equation (112) by $2T$ gives

$$2TF_g(0; m, T, \sigma) = 1 - 2T - \int_0^\infty dy y e^{-\frac{y^2}{2}} \exp \left[mT \left(1 - \frac{y}{m\sigma} - e^{-\frac{y}{m\sigma}} \right) \right]. \quad (115)$$

Considering the integral on the right-hand side, since $1 - x - e^{-x}$ is negative for $x > 0$, the T -derivative of the integral is negative, while its second T derivative is positive. Then the right-hand side of equation (115) for $T > 0$ can be zero for at most one value of T . Furthermore, since for fixed y and m the value of $y/(m\sigma)$ decreases if σ increases, the T value for which $F_g(0; m, T, \sigma) = 0$ decreases for increasing σ at fixed m . This concludes the proof. Furthermore, for what we have seen before, $\sigma^{\text{inc}}(m, 1/2) = 0$ and $\lim_{m \rightarrow \infty} \sigma^{\text{inc}}(m, T) = 0$ for $0 \leq T \leq 1/2$.

It is evident from the above analysis that the proof is not restricted to the Gaussian case, but works equally well for any $g(\omega)$ such that

$$\beta \int dx g(x) x \sin(\beta x), \quad (116)$$

is positive for any β . However, on physical grounds, we are led to assume that the same conclusions hold for any even single-humped $g(\omega)$.

We conclude on the basis of the above analysis that $\lambda = 0$ at the point of neutral stability, so that equation (105) gives $\sigma^{\text{inc}}(m, T)$ to be satisfying

$$\frac{2T}{e^{mT}} = \sum_{p=0}^{\infty} \frac{(-mT)^p (1 + \frac{p}{mT})^2}{p!} \int_{-\infty}^{\infty} \frac{g(\omega) d\omega}{(1 + \frac{p}{mT})^2 + \frac{(\sigma^{\text{inc}})^2 \omega^2}{T^2}}. \quad (117)$$

In the (m, T, σ) space, the above equation defines the stability surface $\sigma^{\text{inc}}(m, T)$. There will similarly be the stability surface $\sigma^{\text{coh}}(m, T)$. The two surfaces coincide on the critical lines on the (T, σ) and (m, T) planes where the transition becomes continuous; outside these planes, the surfaces enclose the first-order transition surface $\sigma_c(m, T)$ i.e., $\sigma^{\text{coh}}(m, T) > \sigma_c(m, T) > \sigma^{\text{inc}}(m, T)$. Let us show by taking limits that the surface $\sigma^{\text{inc}}(m, T)$ meets the critical lines on the (T, σ) and (m, T) planes, and also obtain its intersection with the (m, σ) -plane. On considering $m \rightarrow 0$ at a fixed T , only the $p = 0$ term in the sum in equation (117) contributes, so that one has

$$\lim_{m \rightarrow 0, T \text{ fixed}} \sigma^{\text{inc}}(m, T) = \sigma_c(m = 0, T), \quad (118)$$

with the implicit expression of $\sigma_c(m = 0, T)$ given earlier. Similarly, one has

$$\lim_{T \rightarrow T_c^-, m \text{ fixed}} \sigma^{\text{inc}}(m, T) = 0. \quad (119)$$

When $T \rightarrow 0$ at a fixed m , we get

$$\sigma_{\text{noiseless}}^{\text{inc}}(m) \equiv \lim_{T \rightarrow 0, m \text{ fixed}} \sigma^{\text{inc}}(m, T), \quad (120)$$

with

$$1 = \frac{\pi g(0)}{2\sigma_{\text{noiseless}}^{\text{inc}}} - \frac{m}{2} \int_{-\infty}^{\infty} d\omega \frac{g(\omega)}{1 + m^2(\sigma_{\text{noiseless}}^{\text{inc}})^2 \omega^2}. \quad (121)$$

For the representative case of the Gaussian $g(\omega)$, equation (89), we get from equation (117) that

$$1 = \frac{e^{mT} \sqrt{\pi}}{2\sqrt{2}\sigma^{\text{inc}}} \sum_{p=0}^{\infty} \frac{(-mT)^p (1 + \frac{p}{mT})}{p! e^{-\frac{T^2(1+p/mT)^2}{2(\sigma^{\text{inc}})^2}}} \text{Erfc} \left[\frac{T(1 + \frac{p}{mT})}{\sigma^{\text{inc}} \sqrt{2}} \right], \quad (122)$$

where $\text{Erfc}(x)$ is the complementary error function: $\text{Erfc}(x) = \frac{2}{\sqrt{\pi}} \int_x^{\infty} dt e^{-t^2}$.

3.8. Comparison with numerical simulations

Choosing $m = 20$, and $T = 0.25$, equation (122) gives $\sigma^{\text{inc}}(m, T) \approx 0.10076$. Then, starting with the incoherent state (88) at a given σ and evolving under the dynamics (58), our theoretical continuum-limit analysis predicts that the order parameter r for $\sigma < \sigma^{\text{inc}}$ relaxes at long times from its value equal to 0 to its stationary state value corresponding to the synchronized phase. For $\sigma > \sigma^{\text{inc}}(m, T)$, on the other hand, r remains zero for all times.

In this subsection, we compare the above continuum-limit theoretical predictions with N -body simulations. A phenomenological picture of viewing dynamically a phase transition is to model the dynamics as dissipative relaxation of the order parameter towards the minimum of a phenomenological Landau free-energy landscape [44]. For a first-order phase transition, we draw in Fig. 9 the corresponding schematic free energy landscapes $F(r)$ vs. r for fixed m and T at different σ values. Note that for non-zero σ , one should instead be drawing landscapes of the large deviation functional; here, we assume that the landscape picture of phase transitions will also hold in that case. The landscapes in Fig. 9 explain the occurrence of flips in r shown in Fig. 5(a): the flips correspond to dynamics at σ values close to σ_c at which the system switches back and forth between the two almost-stable synchronized and incoherent states, thereby leading to the bistability in Fig. 5(a).

In order to check our theoretical estimate of $\sigma^{\text{inc}}(m, T)$ for the Gaussian $g(\omega)$, equation (89), we perform the following experiment. For a given large value of N , we prepare for the dynamics (58) a realization of an initial state that is incoherent, by sampling the ω_i 's independently for each i from the distribution (89), and then sampling the θ_i 's and v_i 's according to the distribution (88). We let the system evolve according to the dynamics (58), and monitor the evolution of the quantity r in time. For $m = 20, T = 0.25$, we choose four values of σ , two below and two above $\sigma^{\text{inc}}(m, T) \approx 0.10076$. Figures 10(i)-(iv) show the results for 20 different realizations of the initial state for three values of N .

In Fig. 10(i) for σ below $\sigma^{\text{inc}}(m, T)$, we see that the system while starting from the unstable incoherent state at this value of σ settles down in time into the globally stable synchronized state; this is consistent with the corresponding schematic landscape in Fig.

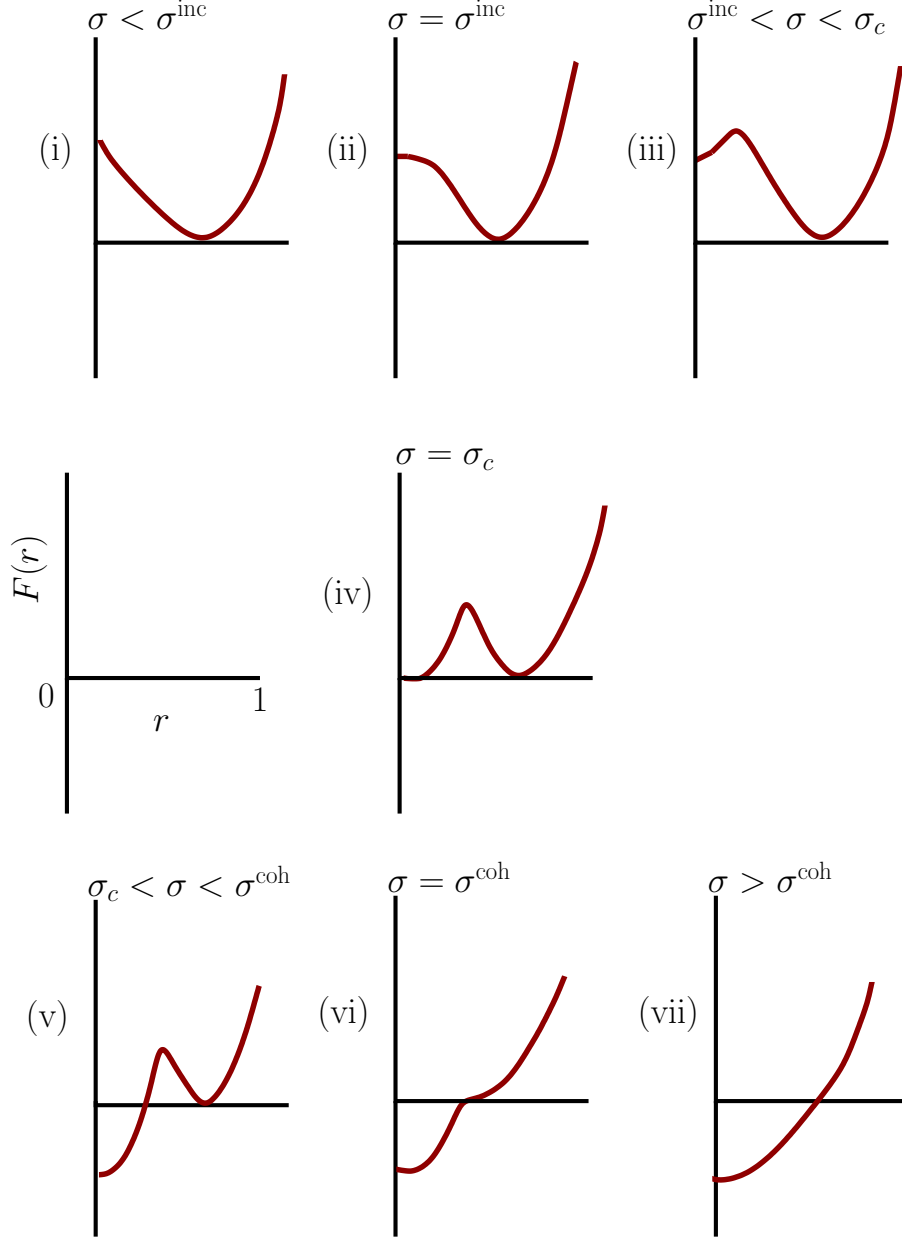


Figure 9. (Color online) Considering the model (58), we show here schematic Landau free energy $F(r)$ vs. r for first-order transitions at fixed m and T while varying σ . Panels (i) and (vii) correspond to the synchronized and incoherent phase being at the global minimum. In panel (iii) (respectively, (v)), the synchronized (respectively, incoherent) phase is at the global minimum, while the incoherent (respectively, synchronized) phase is at a local minimum, hence, metastable. Panel (iv) corresponds to the first-order transition point, with the two phases coexisting at two minima of equal heights.

9(a). The relaxation of r occurs exponentially fast in time according to $e^{\lambda t}$ for $\sigma < \sigma^{\text{inc}}(m, T)$, where the growth rate λ may be obtained from equation (105) after substituting equation

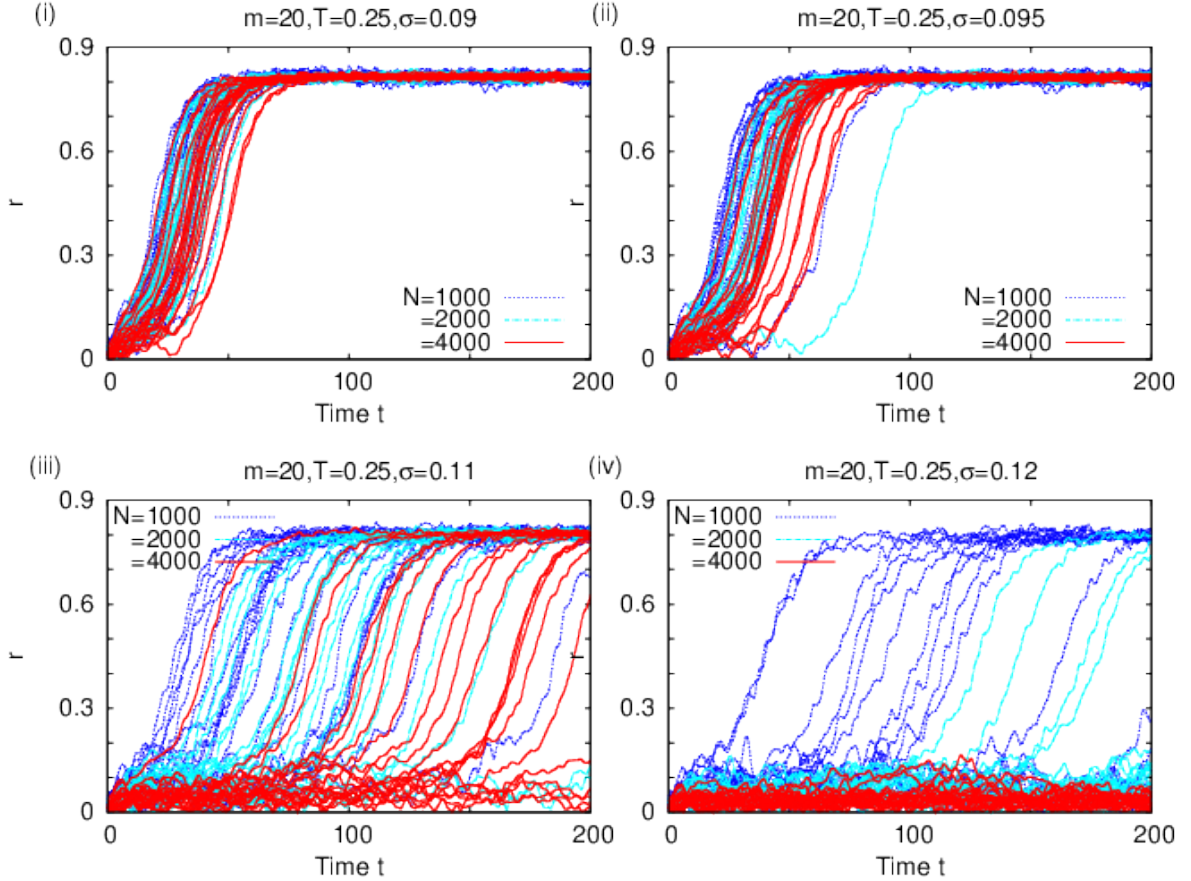


Figure 10. For the dynamics (58), panels (i)-(iv) show r vs. time at $m = 20, T = 0.25$ for four values of σ , two below ((i): $\sigma = 0.09$, (ii): $\sigma = 0.095$), and two above ((iii): $\sigma = 0.11$, (iv): $\sigma = 0.12$) the theoretical threshold $\sigma^{\text{inc}}(m, T) \approx 0.10076$. The data are obtained from simulations for the Gaussian $g(\omega)$ given by equation (89).

(89) for $g(\omega)$. Figure 11 shows that the theoretical growth rates are in excellent agreement with numerical estimates.

Figure 10(ii) for σ larger than in (i) but below $\sigma^{\text{inc}}(m, T)$ shows that similar to (i), the system relaxes at long times to the synchronized state for all realizations. Some realizations for short times stay in the initial incoherent state due to finite- N effects not captured by our continuum limit theory. For $\sigma > \sigma^{\text{inc}}(m, T)$, the landscape in Fig. 9(iii) implies that the system, while at long times should relax to the globally stable synchronized state, remain trapped for finite times in the metastable incoherent state. This is clearly borne out by Fig. 10(iii) in which one may observe that most realizations relax to synchronized states. With increase of N , the number of realizations staying close to the initial incoherent state for a finite time increases. Figure 12 shows that in fact the fraction η of realizations relaxing to synchronized state decreases exponentially with increasing N for large N . This fraction in

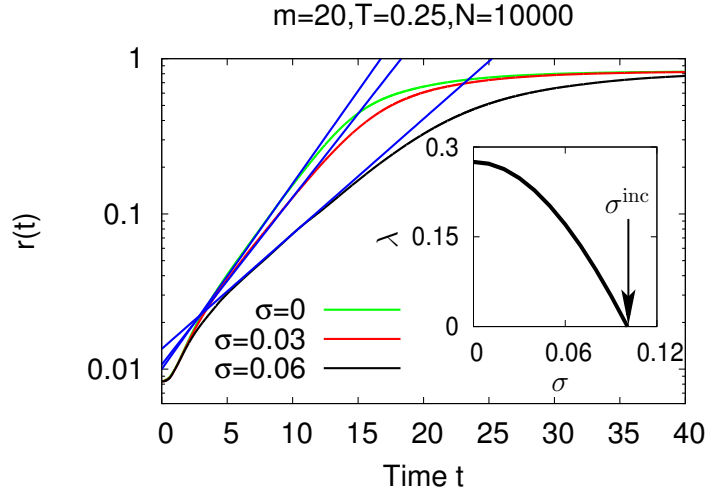


Figure 11. Considering the dynamics (58), we show here exponentially fast relaxation $\sim e^{\lambda t}$ of r from its initial incoherent state value to its final synchronized state value for $\sigma < \sigma^{\text{inc}}(m, T) \approx 0.10076$ for the Gaussian $g(\omega)$ given by equation (89), and for $m = 20, T = 0.25, N = 10^4$; the blue solid lines stand for exponential growth with rates λ obtained from equation (105) by using equation (89) for $g(\omega)$. The inset shows theoretical λ as a function of σ for the same m and T values; in particular, λ hits zero at the stability threshold $\sigma^{\text{inc}}(m, T)$. The data are obtained from simulations with $N = 10000$ for the Gaussian $g(\omega)$ given by equation (89).

numerical simulations is taken to be the fraction of realizations that cross $r = 0.5$ during evolution in the given fixed time of observation. This exponential decrease of η with N implies that for the fixed time of observation and in the limit $N \rightarrow \infty$, all realizations remain close to the incoherent state and none relax to the synchronized state. This is consistent with our interpretation of $\sigma^{\text{inc}}(m, T)$ as the stability threshold above which the incoherent state (88) is linearly stable. In order to explain physically the exponential decrease of η with N , let us recall a classical result due to Kramers concerning the relaxation time out of a metastable state under the stochastic dynamics of a single particle on a potential landscape. In the weak-noise limit, this time is an exponential in the ratio of the potential energy barrier to come out of the metastable state to the strength of the noise responsible for the escape [45]. For a mean-field system, considering the dynamics of the order parameter on a free energy landscape, the escape time out of a metastable state obeys Kramers formula with the value of the potential energy barrier replaced by N times the free-energy barrier [46]. This then explains the finding in Fig. 12.

Figure 10(iv) for σ larger than $\sigma^{\text{inc}}(m, T)$ than in (iii) shows that with respect to (iii), more realizations stay close to the initial incoherent state for longer times. This is easily explained as due to a larger barrier separating the incoherent from the synchronized state.

Based on our discussions above, we conclude that our theoretical predictions are

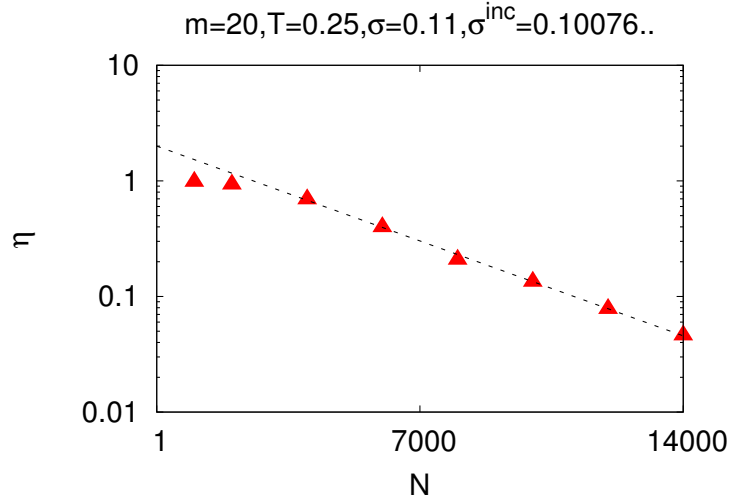


Figure 12. For the dynamics (58) with $m = 20, T = 0.25, \sigma = 0.11$, the figure shows the fraction η of realizations of initial incoherent state relaxing to synchronized state within the fixed time of observation $t = 200$, for a value of σ above $\sigma^{\text{inc}}(m, T)$, for which the incoherent phase is linearly stable in the continuum limit. The figure shows that η for large N decreases exponentially fast with increase of N . The data are obtained from N -body simulations for the Gaussian $g(\omega)$ given by equation (89).

corroborated by our simulation results. Note that the simulation results suggest that the stability threshold of the incoherent state is between $\sigma = 0.095$ and $\sigma = 0.11$, and indeed the theoretical estimate ≈ 0.10076 is in that range.

4. Dynamics of a lattice of oscillators interacting with a power-law coupling

So far we have studied purely mean-field models, namely, where the coupling between each pair of oscillators is exactly the same. There are clearly situations where this scenario is not realistic. In this section, we will consider models in which the coupling between oscillators decays as an inverse power-law of the distance between them, i.e., the coupling K of equation (4) is substituted by

$$K_{ij} = \frac{K_0}{|\mathbf{r}_i - \mathbf{r}_j|^\alpha}, \quad (123)$$

with K_0 a constant, $\alpha \geq 0$, and where \mathbf{r}_i is the position vector in the d -dimensional space of the i th oscillator. We immediately realize that this setting requires the definition of a lattice on the sites of which the oscillators reside. This definition was not necessary for the mean-field models.

Once the notion of distance has been introduced, we see that a mean-field model is recovered if the parameter α is set equal to 0 so that K_{ij} does not decay with the distance.

Thus, mean-field models are the extreme case of long-range interacting systems. As discussed in the introduction, a long-range interaction is realized when the parameter α is not larger than the embedding dimension d . This definition applies not only to lattice systems, as those considered in this review, but also to systems of particles described by ordinary Cartesian coordinates in d -dimensional space [28].

The analytical study of systems with power-law interactions is inherently more difficult than that of mean-field systems. In the latter, the interaction among the oscillators can be represented in a convenient form that is not easily attainable in the former. To exemplify this concept, let us consider the passage from equation (4) to equation (7), where use has been made of equation (6) defining the order parameter r ; we see that each oscillator is subject to the mean field generated by all the other oscillators, and that this mean field is simply expressed in terms of the order parameter. We have seen in the preceding sections that the analytical treatment obtains the equilibrium and out-of-equilibrium behavior from the self-consistency between the order parameter and the mean field. This simple association between a mean field and an order parameter is no more possible in general in systems with power-law interactions. Still, the possibility to study the thermodynamic and dynamic behaviour of such systems by using only the single-particle distribution function, as will be explained later in this section, allows to derive self-consistent relations determining the stationary states of the system. It is not within the scope of this review to offer a complete description of the tools employed in the study of systems with power-law interactions. However, before considering the Kuramoto model with a power-law coupling, we would now like to give a physical argument that supports the existence of similarities between mean-field systems and systems with power-law interactions.

A convenient approach to understand the differences between short and long-range systems, and at the same time the similarities between mean-field systems and long-range systems with power-law interactions, is to grasp the physical meaning of the term that in the first equation of the BBGKY hierarchy couples the one-particle distribution function to the two-particle distribution function. The argument does not depend on the presence of dissipation and noise, but only on this coupling term (e.g., the right hand side of equation (83)) that behaves differently in short and long-range systems. As we have seen in the analysis following that equation, if we write $f_2(x, x', t) = f_1(x, t)f_1(x', t) + g_2(x, x', t)$, where $x \equiv (\theta, v)$ and $x' \equiv (\theta', v')$, then the first term on the right hand side gives rise to the mean-field term that leads, e.g., in our case, to the Kramers equation (64). On the other hand, the term g_2 , whose contribution we neglected in deriving the Kramers equation, takes into account the two-particle correlation. In principle, both the terms describe the variation of $f(x, t)$ as determined by the behavior of particles within the range of interaction around θ . In short-range systems, f_1 is practically uniform within the interaction range, and therefore, the correlation term g_2 is considerably larger than the mean-field term. In long-range systems, either with a mean-field or with a power-law interaction, the interaction range spans the

whole system. Since in this case the correlation g_2 decays quite rapidly with inter-particle separation, the mean-field term is dominant. For the evaluation of the relative weight of the mean-field term and the correlation term g_2 in different classes of systems, see, e.g., the excellent book of Balescu [47].

Although both exhibiting the peculiar features of long-range systems, mean-field ($\alpha = 0$) systems and systems with weakly decaying interactions ($0 < \alpha \leq d$) can differ in several aspects. In fact, the presence of a topological structure in the latter can induce features that do not occur in the former. For example, in the equilibrium magnetized phase of a mean-field spin system, the average magnetization is uniform, i.e., it is the same for every spin. On the other hand, in a spin system with power-law interactions and with free boundary conditions, the equilibrium magnetization will be larger away from boundaries and smaller near the boundaries; here, uniformity of the equilibrium state is recovered by adopting periodic boundary conditions, that we will actually use in the analysis of this section. However, the uniformity of an equilibrium state, either magnetized or non-magnetized, does not prevent an out-of-equilibrium behavior in which the underlying lattice structure does play a role.

Summarizing, it is meaningful to study the generalization of the type of models studied in the previous sections, in which the mean-field interaction is replaced by a slowly-decaying long-range interaction. We will not consider the most general case, i.e., the case of interacting oscillators with inertia and noise and driven by quenched torques. Instead, we will study several particular cases. In all of them, the interaction between the oscillators will be through coupling constants of the form (123). Besides, we will be concerned with one-dimensional lattices with periodic boundary conditions.

The first subsection will be devoted to an extension of the Kuramoto model obtained by the above-mentioned modification of the coupling constants. Thus, it is a model of overdamped oscillators driven by quenched external torques in the absence of noise. In the second and third subsections, we will consider two different versions of the model without the quenched torques.

4.1. The Kuramoto model with a power-law coupling between oscillators

Let us consider a one-dimensional periodic lattice of N sites labelled by the index $i = 1, 2, \dots, N$, and with lattice constant equal to a . With a proper choice of the origin, the coordinate of the i th site is $x_i = ia$. On each site resides an oscillator, with the dynamics of the i th oscillator governed by the evolution equation [48, 49]

$$\frac{d\theta_i}{dt} = \omega_i + \frac{K}{\tilde{N}} \sum_{j=1}^N \frac{\sin(\theta_j - \theta_i)}{|x_j - x_i|^\alpha}, \quad (124)$$

where the exponent α lies in the range $0 \leq \alpha < 1$. Since we adopt periodic boundary conditions, the distance $|x_j - x_i|$ between the i th and j th sites is not unambiguously defined.

In equation (124), we adopt the closest distance convention:

$$|x_j - x_i|_c \equiv \min(|x_j - x_i|, Na - |x_j - x_i|). \quad (125)$$

The factor \tilde{N} in equation (124), which in the mean-field case ($\alpha = 0$) becomes the normalizing factor N in the equations of motion (see equation 4), is given by

$$\tilde{N} \equiv \sum_{j=1}^N \frac{1}{|x_j - x_i|_c^\alpha}. \quad (126)$$

In the last expression, we take $|x_j - x_i|_c = a$ for $i = j$. While this choice is irrelevant for the equation of motion (124), it allows to include in the summation in equation (126) the term with $j = i$, thereby making \tilde{N} non-diverging. Note that the right hand side of equation (126) is independent of i due to the closest distance convention.

The introduction of a lattice on the sites of which the oscillators reside, and of a coupling that depends on the distance between the oscillators, has two important consequences on the analytical treatment of the system. The first is that it is no more possible to define a global order parameter, similar to r in equation (6), that can be used to rewrite the equations of motion in an equivalent form (compare, e.g., equations (4) and (7)). The second consequence has also a conceptual relevance. Let us consider those oscillators with the same value of the natural frequency ω , say, $\omega = \omega^*$ (since we will be eventually interested in the limit $N \rightarrow \infty$, we may imagine in this limit to have a fraction of oscillators with the same frequency $\omega = \omega^*$, or, more precisely, with ω within a given small range around ω^*). One realizes that the equation of motion (124) is not invariant under permutations of the phase of these oscillators as the latter could be identified by the lattice sites they are occupying, contrary to what happens for the mean-field case $\alpha = 0$. Therefore, at variance with the latter case, it is not possible to define the distribution function $\rho(\theta, \omega, t)$ giving, among the oscillators characterized by ω , their density at phase value θ at time t . This fact is rooted in the impossibility, due to the lack of invariance with respect to permutations, to define the usual reduced distribution functions as in, e.g., equation (81). A bit of thought allows to understand that the very same feature explains also the first consequence mentioned above.

We thus arrive at the conclusion that the only possibility to use distribution functions for analysis is to define for any given ω a distribution function for each of the lattice sites. In the limit $N \rightarrow \infty$, this means that we have to consider the situation in which, together with this limit, the lattice constant a approaches 0, keeping the product Na constant that without loss of generality can be fixed equal to 1. This procedure defines the continuum limit, implementing which we can define the one-particle distribution function $\rho(\theta, \omega, s, t)$, where $s \in [0, 1]$ is a continuous variable obtained by considering $s_j \equiv j/N$ in the continuum limit. Since the lattice constant a approaches 0, one has in each infinitesimal range ds a continuum of oscillators such that $\rho(\theta, \omega, s, t)g(\omega)d\omega ds d\theta$ is the fraction of oscillators located between s and $s + ds$, with natural frequency between ω and $\omega + d\omega$, and having at time t

the phase between θ and $\theta + d\theta$. The function $\rho(\theta, \omega, s, t)$ is non-negative, 2π periodic in θ , and obeys the normalization

$$\int_{-\pi}^{\pi} d\theta \rho(\theta, \omega, s, t) = 1 \quad \forall \omega, s. \quad (127)$$

In the continuum limit, we can rewrite the equation of motion (124) as

$$\frac{\partial \theta(\omega, s, t)}{\partial t} = \omega + \frac{K}{B(\alpha)} \int d\omega' \int_0^1 ds' \int_{-\pi}^{\pi} d\theta' \frac{\sin(\theta' - \theta)}{|s' - s|_c^\alpha} \rho(\theta', \omega', s', t) g(\omega'), \quad (128)$$

where now θ is labelled by the position s and the natural frequency ω . The normalizing factor $B(\alpha)$ is given by

$$B(\alpha) = \int_{-\frac{1}{2}}^{\frac{1}{2}} ds \frac{1}{|s|^\alpha}. \quad (129)$$

Since $\alpha < 1$, the integral on the right hand side is finite, and equals $2^\alpha/(1 - \alpha)$. The closest distance convention now reads

$$|s' - s|_c = \min(|s' - s|, 1 - |s' - s|), \quad (130)$$

that allowed us to write the denominator in the integrand of equation (129) without the subscript c .

From the equation of motion (128), one derives analogously to the mean-field case a Fokker-Planck equation for the distribution $\rho(\theta, \omega, s, t)$. Actually, since in the present case there is no noise in the dynamics, the equations of motion are deterministic, and the Fokker-Planck equation is nothing but the continuity equation expressing the conservation for each s and ω of the number of oscillators. We have

$$\begin{aligned} \frac{\partial \rho(\theta, \omega, s, t)}{\partial t} &= -\frac{\partial}{\partial \theta} \left[\left(\frac{\partial \theta(\omega, s, t)}{\partial t} \right) \rho(\theta, \omega, s, t) \right] \\ &= -\frac{\partial}{\partial \theta} \left\{ \left[\omega + \frac{K}{B(\alpha)} \int d\omega' \int_0^1 ds' \int_{-\pi}^{\pi} d\theta' \frac{\sin(\theta' - \theta)}{|s' - s|_c^\alpha} \rho(\theta', \omega', s', t) g(\omega') \right] \rho(\theta, \omega, s, t) \right\}. \end{aligned} \quad (131)$$

We note that an initial distribution that is s -independent remains so under the evolution (131). Of course, one should check the stability of such a conservation with respect to s -dependent perturbations. In the following, we will analyze the dynamical stability of the particular s -independent (therefore, mean-field) stationary solution that represents the unsynchronized or the incoherent state, i.e.,

$$\rho_0(\theta, \omega, s, t) = \frac{1}{2\pi}. \quad (132)$$

4.1.1. Linear stability analysis of the mean-field incoherent stationary state To study the linear stability of the incoherent state (132), we expand ρ_0 as

$$\rho(\theta, \omega, s, t) = \frac{1}{2\pi} + \delta\rho(\theta, \omega, s, t); \quad |\delta\rho| \ll 1. \quad (133)$$

Inserting the above expansion into the continuity equation (131), and keeping only the first order terms in $\delta\rho$, we obtain the linearized equation

$$\begin{aligned} \frac{\partial\delta\rho(\theta, \omega, s, t)}{\partial t} &= -\omega\frac{\partial\delta\rho(\theta, \omega, s, t)}{\partial\theta} \\ &+ \frac{K}{2\pi B(\alpha)} \int d\omega' \int_0^1 ds' \int_0^{2\pi} d\theta' \frac{\cos(\theta' - \theta)}{|s' - s|_c^\alpha} \delta\rho(\theta', \omega', s', t)g(\omega'). \end{aligned} \quad (134)$$

To solve the above equation for $\delta\rho$, let us perform its Fourier expansion in θ as

$$\delta\rho(\theta, \omega, s, t) = \sum_{k=-\infty}^{+\infty} \widehat{\delta\rho}_k(\omega, s, t)e^{ik\theta}. \quad (135)$$

Substitution in equation (134) gives

$$\begin{aligned} \frac{\partial\widehat{\delta\rho}_k(\omega, s, t)}{\partial t} &= -ik\omega\widehat{\delta\rho}_k(\omega, s, t) \\ &+ \frac{K}{2B(\alpha)} (\delta_{k,1} + \delta_{k,-1}) \int d\omega' \int_0^1 ds' \frac{\widehat{\delta\rho}_k(\omega', s', t)}{|s' - s|_c^\alpha} g(\omega'). \end{aligned} \quad (136)$$

For $k \neq \pm 1$, the second term on the right hand side of equation (136) is zero, and solving the resulting equation gives

$$\widehat{\delta\rho}_k(\omega, s, t) = \widehat{\delta\rho}_k(\omega, s, 0)e^{-ik\omega t}; \quad k \neq \pm 1. \quad (137)$$

These solutions correspond to the neutrally stable Fourier modes; there are an infinity of such modes for each ω belonging to the support of $g(\omega)$. The eigenfunction corresponding to any particular value of ω , say, $\omega = \omega_0$, is

$$\widehat{\delta\rho}_{k,\omega_0}(\omega, s, 0) = \delta(\omega - \omega_0)c(s), \quad (138)$$

where $c(s)$ is an arbitrary function of s . On the other hand, equation (136) for $k = \pm 1$ gives

$$\frac{\partial\widehat{\delta\rho}_{\pm 1}(\omega, s, t)}{\partial t} = \mp i\omega\widehat{\delta\rho}_{\pm 1}(\omega, s, t) + \frac{K}{2B(\alpha)} \int d\omega' \int_0^1 ds' \frac{\widehat{\delta\rho}_{\pm 1}(\omega', s', t)}{|s' - s|_c^\alpha} g(\omega'). \quad (139)$$

This equation is best solved by performing a further Fourier expansion, this time in s space:

$$\widehat{\delta\rho}_{\pm 1}(\omega, s, t) = \sum_{n=-\infty}^{+\infty} \overline{\delta\rho}_{\pm 1,n}(\omega, t)e^{2\pi ins}. \quad (140)$$

Substituting in equation (139), we obtain

$$\frac{\partial\overline{\delta\rho}_{\pm 1,n}(\omega, t)}{\partial t} = \mp i\omega\overline{\delta\rho}_{\pm 1,n}(\omega, t) + \frac{K\Lambda_n(\alpha)}{2B(\alpha)} \int d\omega' \overline{\delta\rho}_{\pm 1,n}(\omega', t)g(\omega'), \quad (141)$$

where $\Lambda_n(\alpha)$ is given by

$$\Lambda_n(\alpha) = \int_{-\frac{1}{2}}^{\frac{1}{2}} ds \frac{e^{2\pi ins}}{|s|^\alpha} = \int_{-\frac{1}{2}}^{\frac{1}{2}} ds \frac{\cos(2\pi ns)}{|s|^\alpha}. \quad (142)$$

Clearly $\Lambda_{-n}(\alpha) = \Lambda_n(\alpha)$; we can therefore restrict to consider $n \geq 0$. It is also evident that $\Lambda_0(\alpha) = B(\alpha) > \Lambda_n(\alpha)$ for $n > 0$. Let us first consider the mean-field case $\alpha = 0$. In that case, $\Lambda_0(0) = 1$ and $\Lambda_n(0) = 0$ for $n > 0$. Therefore, in the mean-field case, all modes $n \neq 0$ are neutrally stable, and we have to study equation (141) only for $n = 0$. For $\alpha > 0$, all values of n have to be considered. It is not difficult to prove that $\Lambda_n(\alpha) > 0$, that $\lim_{n \rightarrow \infty} \Lambda_n(\alpha) = 0$, and that for given n , one has $\Lambda_n(\alpha)$ as an increasing function of α . One may check numerically that $\Lambda_n(\alpha)$ is a decreasing function of $|n|$ for any α , see Ref. [49]. In the following, it is understood that for $\alpha = 0$, only the case $n = 0$ has to be considered.

We look for solutions of equation (141) of the form

$$\bar{\delta\rho}_{\pm 1,n}(\omega, t) = \tilde{\delta\rho}_{\pm 1,n}(\omega, \lambda_n) e^{\lambda_n t}. \quad (143)$$

Substituting in equation (141) gives

$$(\lambda_n \pm i\omega) \tilde{\delta\rho}_{\pm 1,n}(\omega, \lambda_n) = \frac{K\Lambda_n(\alpha)}{2B(\alpha)} \int d\omega' \tilde{\delta\rho}_{\pm 1,n}(\omega', \lambda_n) g(\omega'). \quad (144)$$

Hence, we have a continuous spectrum given by $\lambda_n = \mp i\omega_0$ for each ω_0 in the support of $g(\omega)$. In this case, the neutrally stable modes, normalized so that the right hand side of equation (144) is equal to 1, are given by

$$\tilde{\delta\rho}_{\pm 1,n}(\omega, \mp i\omega_0) = \mp i\mathcal{P} \frac{1}{\omega - \omega_0} + c_{\pm 1,n}(\omega_0) \delta(\omega - \omega_0), \quad (145)$$

with

$$c_{\pm 1,n}(\omega_0) g(\omega_0) = \frac{2B(\alpha)}{K\Lambda_n(\alpha)} \pm i\mathcal{P} \int d\omega \frac{g(\omega)}{\omega - \omega_0}, \quad (146)$$

where \mathcal{P} denotes the principal value. We are interested in the discrete spectrum, obtained for $\lambda_n \pm i\omega \neq 0$. From equation (144), we then have

$$\tilde{\delta\rho}_{\pm 1,n}(\omega, \lambda_n) = \frac{K\Lambda_n(\alpha)}{2(\lambda_n \pm i\omega)B(\alpha)} \int d\omega' \tilde{\delta\rho}_{\pm 1,n}(\omega', \lambda_n) g(\omega'), \quad (147)$$

which implies that in order to have a non-trivial solution, the integral on the right hand side should not vanish. We can exploit the linearity of equation (144) to impose that the integral is equal to 1. From the last equation, we then obtain the dispersion relation

$$\frac{K\Lambda_n(\alpha)}{2B(\alpha)} \int_{-\infty}^{+\infty} d\omega \frac{g(\omega)}{\lambda_n \pm i\omega} = 1. \quad (148)$$

For the class of distributions $g(\omega)$ being considered in this review, that is, for a unimodal $g(\omega)$ with a single maximum at $\omega = 0$ and symmetric, $g(\omega) = g(-\omega)$, we now prove that the last equation can have at most one solution for λ_n , which is necessarily real. Note that when there is no solution for λ_n , only the trivial vanishing perturbation $\tilde{\delta\rho}_{\pm 1,n}(\omega, \lambda_n) = 0$ satisfies equation (147). Decomposing λ_n into real and imaginary parts, $\lambda_n = \lambda_{nr} + i\lambda_{ni}$, we

obtain from equation (148)

$$\frac{K\Lambda_n(\alpha)}{2B(\alpha)} \int_{-\infty}^{+\infty} d\omega g(\omega) \frac{\lambda_{nr}}{\lambda_{nr}^2 + (\lambda_{ni} \pm \omega)^2} = 1, \quad (149)$$

$$\frac{K\Lambda_n(\alpha)}{2B(\alpha)} \int_{-\infty}^{+\infty} d\omega g(\omega) \frac{\lambda_{ni} \pm \omega}{\lambda_{nr}^2 + (\lambda_{ni} \pm \omega)^2} = 0. \quad (150)$$

Proceeding as for equation (37) and exploiting the fact that $g(\omega)$ is even, the second equation implies that $\lambda_{ni} = 0$. We are therefore left with the equation

$$\frac{K\Lambda_n(\alpha)}{2B(\alpha)} \int_{-\infty}^{+\infty} d\omega g(\omega) \frac{\lambda_n}{\lambda_n^2 + \omega^2} = 1, \quad (151)$$

where now it is understood that λ_n is real. This equation implies that only positive solutions are possible. With the change of variable $\omega = \lambda_n y$, we have

$$\frac{K\Lambda_n(\alpha)}{2B(\alpha)} \int_{-\infty}^{+\infty} dy g(\lambda_n y) \frac{1}{1 + y^2} = 1. \quad (152)$$

By taking the derivative with respect to λ_n , one immediately finds that the left hand side decreases with increasing positive λ_n , and that it tends to 0 as $\lambda_n \rightarrow \infty$. Therefore, there is one and only one solution that exists only when the value of the left hand side for $\lambda_n = 0$ is larger than one, i.e., when

$$\frac{K\Lambda_n(\alpha)}{2B(\alpha)} \pi g(0) \geq 1. \quad (153)$$

We finally obtain the following threshold above which the mode $\tilde{\delta\rho}_{\pm 1, n}$ is unstable:

$$K_c^{(n)} = \frac{2B(\alpha)}{\pi g(0)\Lambda_n(\alpha)}. \quad (154)$$

The final outcome of the stability analysis is that the incoherent state (132) is either neutrally stable or unstable. This is analogous to what happens in the original Kuramoto model [14], that is included in our analysis for $\alpha = 0$. Since $\Lambda_n(\alpha)$ is a decreasing function of n , we have that $K_c^{(n)}$ is an increasing function of n . Then, the incoherent state is neutrally stable for

$$K \leq K_c^{(0)} = \frac{2}{\pi g(0)}, \quad (155)$$

and is unstable otherwise. We note that the critical value for $n = 0$ does not depend on α , and the instability threshold is therefore the same as that for the original mean-field ($\alpha = 0$) Kuramoto model, see equation (5).

4.1.2. Numerical results The analysis above implies that increasing progressively the value of K , more and more modes destabilize. For example, if $K_c^{(p)} < K < K_c^{(p+1)}$, then we have $p + 1$ unstable modes, corresponding to $n = 0, 1, \dots, p$. According to equation (143), each of these modes has an exponential growth with rate given by the corresponding λ_n .

To check our analytical predictions with simulations, we choose a Gaussian $g(\omega)$:

$$g(\omega) = \frac{1}{\sqrt{2\pi}} e^{-\frac{\omega^2}{2}}. \quad (156)$$

In this case, we can express the integral in equation (151) with the help of the complementary error function. In fact, using

$$\int_{-\infty}^{+\infty} dx \frac{e^{-b^2 x^2}}{x^2 + a^2} = \frac{\pi}{a} e^{a^2 b^2} \operatorname{Erfc}(ab), \quad (157)$$

we can rewrite equation (151) as

$$\frac{K\Lambda_n(\alpha)}{2B(\alpha)} \sqrt{\frac{\pi}{2}} e^{\frac{\lambda_n^2}{2}} \operatorname{Erfc}\left(\frac{\lambda_n}{\sqrt{2}}\right) = \frac{K}{K_c^{(n)}} e^{\frac{\lambda_n^2}{2}} \operatorname{Erfc}\left(\frac{\lambda_n}{\sqrt{2}}\right) = 1, \quad (158)$$

where we have also used the definition of the thresholds (154), which for the Gaussian $g(\omega)$ becomes

$$K_c^{(n)} = \frac{2\sqrt{2}B(\alpha)}{\sqrt{\pi}\Lambda_n(\alpha)}. \quad (159)$$

The simulations are performed by integrating the equations of motion (124), taking N oscillators on a lattice of length N with periodic boundary conditions and lattice constant $a = 1$. Although the equations of motion imply a computation time at every step of integration that scales as N^2 (there is a sum over N terms for each of the N oscillators), it is possible to employ an integration algorithm that scales as $N \ln N$. In Appendix C, we show how this is achieved by exploiting standard fast Fourier transform routines. The observables evaluated in simulations are the discrete quantities corresponding to the density perturbations in equation (140), namely,

$$r_n(t) = \frac{1}{N} \left| \sum_{j=1}^N e^{i(\theta_j + 2\pi j n/N)} \right|; \quad n = 0, 1, 2, \dots \quad (160)$$

The initial conditions of the simulations are obtained by extracting independently the phases of the oscillators from a uniform distribution in the range $[0, 2\pi]$; this reproduces the incoherent state (132). The frequencies ω_i 's are extracted independently from the Gaussian distribution (156). In this initial state, the observables r_n are equal to 0 (only approximately, due to finite-size effects). According to the theoretical analysis, depending on the value of K employed, the quantities $r_n(t)$ should behave in the following way. For $K < K_c^{(0)}$, all r_n should remain close to 0, while for $K_c^{(p)} < K < K_c^{(p+1)}$, the observables r_n with $n \geq p+1$ should remain close to 0 and those with $n = 0, 1, \dots, p$ should grow exponentially in time (at least as long as the linear approximation of the continuity equation is valid) at a rate equal to the corresponding eigenvalue λ_n .

We present here some results for $\alpha = 0.5$, referring the reader to Ref. [49] for further and more complete results. In Fig. 13, we report the time evolution of $r_0(t)$, $r_1(t)$, $r_2(t)$ and $r_3(t)$ for a simulation run in which the initial condition has been chosen as explained

above. The simulation has been performed for a system of $N = 2^{14}$ oscillators, and with $K = 15$. From equation (159), one finds that this value of K lies in between $K_c^{(11)}$ and $K_c^{(12)}$. Therefore, in particular, the observables plotted in Fig. 13 should all increase exponentially in time. This is confirmed by the numerical results shown in the figure.

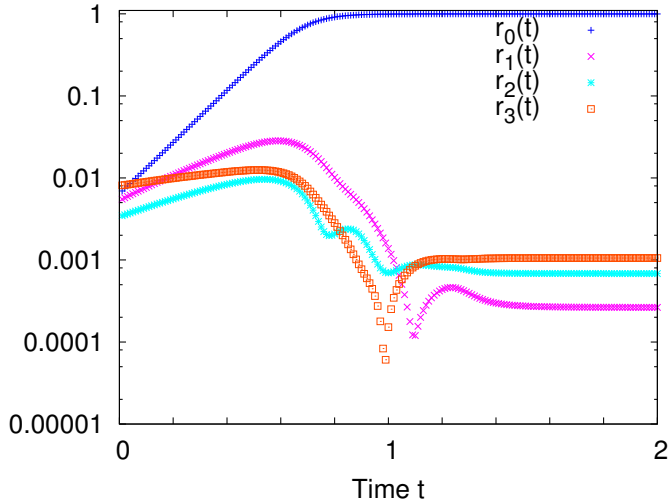


Figure 13. For the model (124), the figure shows the time evolution of the observables $r_0(t), r_1(t), r_2(t)$, and $r_3(t)$ while starting with an initial incoherent state $\{\theta_i(0), \omega_i(0); i = 1, 2, \dots, N\}$ prepared by extracting the θ_i 's uniformly in $[-\pi, \pi]$, while the ω_i 's have been chosen from a Gaussian distribution with zero mean and unit variance, equation (156). Here, $N = 2^{14}$, $\alpha = 0.5$, and $K = 15$. Using equation (159), one then has $K_c^{(0)} \approx 1.59577$, $K_c^{(1)} \approx 4.26696$, $K_c^{(2)} \approx 6.53664$, $K_c^{(3)} \approx 7.71516$. Thus, in particular, the Fourier modes $n = 0, 1, 2, 3$ are all linearly unstable. Consequently, $r_0(t), r_1(t), r_2(t)$, and $r_3(t)$ for short times show an exponential growth in time from their initial values at $t = 0$.

To have a comparison between the numerical and the theoretical rates of the initial exponential growth of the unstable modes, we plot in Fig. 14 the time evolution of $r_0(t)$ and $r_1(t)$ for the same values of α and K as in Fig. 13, namely, $\alpha = 0.5$ and $K = 15$. In the plots are shown results of 10 different simulation runs, corresponding to 10 different realizations of the incoherent initial condition. The exponential growth rates of $r_0(t)$ and $r_1(t)$ are compared with their theoretical values λ_0 and λ_1 computed from equation (158). The agreement is clearly good. We note that for few realizations, the numerical growth rate for $r_1(t)$ deviates from λ_1 , see Fig. 14(b), arguably due to finite-size effects. The plots also suggest that the system settles down to a stationary state in which r_0 assumes a value very close to 1, while r_1 takes a negligible value compatible with 0, considering the finite-size effects. In Fig. 13, we see that the same happens for r_2 and r_3 . We therefore conclude that the long-time dynamics is dominated by the mean-field mode. In particular, the final state is fully synchronized, where the synchronization refers to oscillators residing on all lattice sites.

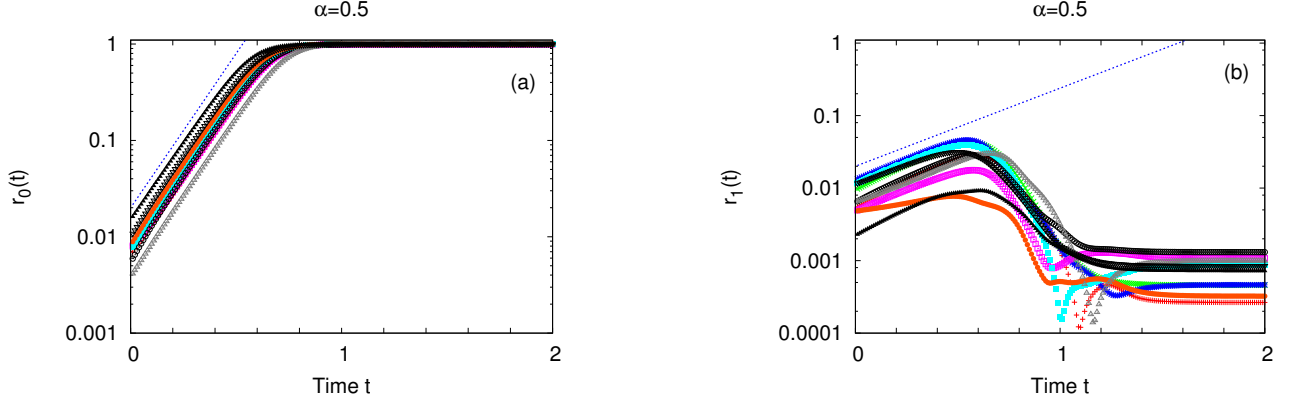


Figure 14. For the model (124), the figure shows the time evolution of the observables $r_0(t)$ (panel (a)) and $r_1(t)$ (panel (b)) for 10 different realizations of the initial state $\{\theta_i(0), \omega_i(0); i = 1, 2, \dots, N\}$. As in Fig. 13, we present here simulations for $K = 15$ at $\alpha = 0.5$. Similarly, each initial state has been obtained by extracting the θ_i 's uniformly in in $[-\pi, \pi]$, while the ω_i 's have been extracted from a Gaussian distribution with zero mean and unit variance, equation (156). Thus, each initial state is the incoherent one. Since the Fourier modes 0 and 1 are linearly unstable, $r_0(t)$ and $r_1(t)$ grow in time from their initial values. The dotted blue line in each plot shows the exponential growth with the rates λ_0 and λ_1 given implicitly by equation (158). The data in the plots are obtained from numerical simulations with $N = 2^{14}$.

4.2. The noisy Kuramoto model with a power-law coupling and the same natural frequency for the oscillators

We now turn our attention to the case when all the oscillators have the same natural frequency, say, $\langle \omega \rangle$. As discussed in section 2, one can scale out $\langle \omega \rangle$ from the equations of motion by going to a comoving frame rotating uniformly with frequency $\langle \omega \rangle$ with respect to the laboratory frame. Thus, we are effectively considering the dynamics without the presence of quenched torques. We will first study an overdamped model with noise [50–52]. Namely, the model obtained from the one studied in section 4.1 by adding Gaussian noise terms to the equations of motion, but excluding the frequency terms. Later, we will focus on the underdamped model with noise.

Let us then begin with the equation of motion for the i th oscillator:

$$\frac{d\theta_i}{dt} = \frac{K}{\tilde{N}} \sum_{j=1}^N \frac{\sin(\theta_j - \theta_i)}{|x_j - x_i|_c^\alpha} + \eta_i(t), \quad (161)$$

where $\eta_i(t)$ is a Gaussian white noise:

$$\langle \eta_i(t) \rangle = 0, \quad (162)$$

$$\langle \eta_i(t) \eta_j(t') \rangle = 2T \delta_{ij} \delta(t - t'). \quad (163)$$

The equation of motion (161) describes the overdamped dynamics of the so-called α -HMF

model [50, 51], within a canonical ensemble (see equation (217) below).

The definition of \tilde{N} and the closest distance convention are the same as in section 4.1, and so is the procedure to obtain the continuum limit ($N \rightarrow \infty, a \rightarrow 0$, keeping the product Na constant at unity, where a stands for the lattice constant). To discuss this limit, we introduce the variable $s \in [0, 1]$, obtained as the continuum limit of $s_j = j/N$. However, contrary to section 4.1, the one-particle distribution function will now not depend on the frequency. Here, we introduce the one-particle distribution function $\rho(\theta, s, t)$, defined such that the quantity $\rho(\theta, s, t)dsd\theta$ represents the fraction of oscillators located between s and $s + ds$ that at time t has their phase between θ and $\theta + d\theta$. The normalization is

$$\int_{-\pi}^{\pi} d\theta \rho(\theta, s, t) = 1 \quad \forall s. \quad (164)$$

In the continuum limit, the equation of motion takes the form

$$\frac{\partial \rho(s, t)}{\partial t} = \frac{K}{B(\alpha)} \int_0^1 ds' \int_{-\pi}^{\pi} d\theta' \frac{\sin(\theta' - \theta)}{|s' - s|_c^\alpha} \rho(\theta', s', t) + \eta(s, t), \quad (165)$$

where the normalizing factor $B(\alpha)$ and the closest distance convention $|s' - s|_c$ are given in equations (129) and (130), respectively. The statistical properties of the noise become

$$\langle \eta(s, t) \rangle = 0, \quad (166)$$

$$\langle \eta(s, t) \eta(s', t') \rangle = 2T \delta(s - s') \delta(t - t'). \quad (167)$$

The Fokker-Planck equation governing the evolution of $\rho(\theta, s, t)$ is

$$\begin{aligned} & \frac{\partial \rho(\theta, s, t)}{\partial t} \\ &= -\frac{K}{B(\alpha)} \frac{\partial}{\partial \theta} \left\{ \left[\int_0^1 ds' \int_{-\pi}^{\pi} d\theta' \frac{\sin(\theta' - \theta)}{|s' - s|_c^\alpha} \rho(\theta', s', t) \right] \rho(\theta, s, t) \right\} + T \frac{\partial^2 \rho(\theta, s, t)}{\partial \theta^2}. \end{aligned} \quad (168)$$

The generic stationary solution $\rho_0(\theta, s)$ of the Fokker-Planck equation (168) is obtained by setting the left hand side to zero, yielding

$$\rho_0(\theta, s) = A(s) \exp \left[\frac{K}{TB(\alpha)} \int_0^1 ds' \int_{-\pi}^{\pi} d\theta' \frac{\cos(\theta' - \theta)}{|s' - s|_c^\alpha} \rho_0(\theta', s) \right], \quad (169)$$

where the constants $A(s)$ for every s are determined by the normalization condition (164). There are also consistency relations to be satisfied, as we now show. Let us denote by $m_x(s)$ and $m_y(s)$ the two components of the local magnetization:

$$m_x(s) \equiv \int_{-\pi}^{\pi} d\theta \cos \theta \rho_0(\theta, s), \quad (170)$$

$$m_y(s) \equiv \int_{-\pi}^{\pi} d\theta \sin \theta \rho_0(\theta, s). \quad (171)$$

From the definition of the modified Bessel function of the first kind of order n ,

$$I_n(x) = \frac{1}{2\pi} \int_{-\pi}^{\pi} d\theta \cos(n\theta) e^{x \cos \theta}, \quad (172)$$

and denoting

$$\widehat{m}_x^{(\alpha)}(s) = \int_0^1 ds' \frac{m_x(s')}{|s' - s|_c^\alpha}, \quad (173)$$

$$\widehat{m}_y^{(\alpha)}(s) = \int_0^1 ds' \frac{m_y(s')}{|s' - s|_c^\alpha}, \quad (174)$$

one obtains for the normalization constant the equation

$$A(s) = \left[2\pi I_0 \left(\frac{K}{TB(\alpha)} \sqrt{\left[\widehat{m}_x^{(\alpha)}(s) \right]^2 + \left[\widehat{m}_y^{(\alpha)}(s) \right]^2} \right) \right]^{-1}, \quad (175)$$

together with the self-consistency relations

$$\sqrt{m_x^2(s) + m_y^2(s)} = \frac{I_1}{I_0} \left(\frac{K}{TB(\alpha)} \sqrt{\left[\widehat{m}_x^{(\alpha)}(s) \right]^2 + \left[\widehat{m}_y^{(\alpha)}(s) \right]^2} \right). \quad (176)$$

We note for later use that if we choose an s -independent stationary distribution $\rho_0(\theta)$, then $A(s)$, $m_x(s)$ and $m_y(s)$ are also s -independent, with $\widehat{m}_{x,y}^{(\alpha)} = B(\alpha)m_{x,y}$.

4.2.1. Linear stability analysis of the mean-field incoherent stationary state Let us now consider the s -independent (that is, the mean-field) incoherent state, obtained when $m_x(s) = m_y(s) = 0$, i.e.,

$$\rho_0(\theta) = \frac{1}{2\pi}. \quad (177)$$

As before, its linear stability can be analyzed by posing

$$\rho(\theta, s, t) = \frac{1}{2\pi} + \delta\rho(\theta, s, t); \quad |\delta\rho| \ll 1, \quad (178)$$

and studying the linearized Fokker-Planck equation for $\delta\rho(\theta, s, t)$:

$$\frac{\partial \delta\rho(\theta, s, t)}{\partial t} = \frac{K}{2\pi B(\alpha)} \int_0^1 ds' \int_{-\pi}^{\pi} d\theta' \frac{\cos(\theta' - \theta)}{|s' - s|_c^\alpha} \delta\rho(\theta', s', t) + T \frac{\partial^2 \delta\rho(\theta, s, t)}{\partial \theta^2}. \quad (179)$$

The procedure for stability analysis is the same as that adopted in the preceding subsection. We first perform a Fourier expansion in θ :

$$\delta\rho(\theta, s, t) = \sum_{k=-\infty}^{+\infty} \widehat{\delta\rho}_k(s, t) e^{ik\theta}, \quad (180)$$

which when used in equation (179) gives

$$\frac{\partial \widehat{\delta\rho}_k(s, t)}{\partial t} = \frac{K}{2B(\alpha)} (\delta_{k,1} + \delta_{k,-1}) \int_0^1 ds' \frac{\widehat{\delta\rho}_k(s', t)}{|s' - s|_c^\alpha} - k^2 T \widehat{\delta\rho}_k(s, t). \quad (181)$$

For $k \neq \pm 1$, the first term on the right hand side of equation (181) vanishes, and we have

$$\widehat{\delta\rho}_k(s, t) = \widehat{\delta\rho}_k(s, 0) e^{-k^2 T t}; \quad k \neq \pm 1; \quad (182)$$

these are perturbations that decay exponentially in time, and thus correspond to stable modes. The equation for $k = \pm 1$,

$$\frac{\partial \widehat{\delta\rho}_{\pm 1}(s, t)}{\partial t} = \frac{K}{2B(\alpha)} \int_0^1 ds' \frac{\widehat{\delta\rho}_{\pm 1}(s', t)}{|s' - s|^\alpha} - T \widehat{\delta\rho}_{\pm 1}(s, t), \quad (183)$$

is studied by performing a further Fourier expansion in s -space:

$$\widehat{\delta\rho}_{\pm 1}(s, t) = \sum_{n=-\infty}^{+\infty} \overline{\delta\rho}_{\pm 1, n}(t) e^{2\pi i n s}. \quad (184)$$

Substituting in equation (183), we obtain

$$\frac{\partial \overline{\delta\rho}_{\pm 1, n}(t)}{\partial t} = \frac{K \Lambda_n(\alpha)}{2B(\alpha)} \overline{\delta\rho}_{\pm 1, n}(t) - T \overline{\delta\rho}_{\pm 1}(t), \quad (185)$$

where $\Lambda_n(\alpha)$ is given by equation (142). We therefore have

$$\overline{\delta\rho}_{\pm 1, n}(t) = \exp \left[\left(\frac{K \Lambda_n(\alpha)}{2B(\alpha)} - T \right) t \right] \overline{\delta\rho}_{\pm 1, n}(0). \quad (186)$$

For a fixed K , this expression determines the value of the temperature for which the mode $\overline{\delta\rho}_{\pm 1, n}$ is stable. Precisely, the mode $\overline{\delta\rho}_{\pm 1, n}$ decays exponentially in time and is therefore stable for $T > \frac{K \Lambda_n(\alpha)}{2B(\alpha)}$, while it is unstable, growing exponentially in time, for $T < \frac{K \Lambda_n(\alpha)}{2B(\alpha)}$. Therefore, the critical temperature for the neutral stability of $\overline{\delta\rho}_{\pm 1, n}$ is

$$T_{c, n} = \frac{K \Lambda_n(\alpha)}{2B(\alpha)}. \quad (187)$$

Since, as previously explained, $\Lambda_{-n}(\alpha) = \Lambda_n(\alpha)$, and $\Lambda_n(\alpha)$ is a decreasing function of $|n|$, we have $T_{c, -n} = T_{c, n}$, and

$$\frac{K}{2} = T_{c, 0} > T_{c, 1} > T_{c, 2} > T_{c, 3} > \dots \quad (188)$$

We note in particular that for $\alpha = 0$, we have $T_{c, n} = 0$ for $n > 0$, so that the modes $\overline{\delta\rho}_{\pm 1, n}$ for $|n| > 0$ never destabilize.

4.2.2. Numerical results In the following, we take $K = 1$ without loss of generality (with a rescaling of the time unit, it is always possible to reduce to such a case). From the analysis presented above, we see that for $T > 1/2$, the incoherent state is stable. Decreasing the temperature, the first perturbation mode to destabilize will be $\overline{\delta\rho}_{\pm 1, 0}$, which happens at $T = 1/2$. Decreasing further the temperature, the modes $\overline{\delta\rho}_{\pm 1, n}$ with $|n| > 0$ will progressively destabilize.

We now discuss the results of simulations of the equation of motion (161) for a system with $N = 2^{14}$ oscillators with $\alpha = 0.5$. The effect of the stochastic noise has been taken into account with the same method as that described in Appendix B, equation (B.3) for the case of systems with inertia. We have studied the observables $r_n(t)$ defined in equation

(160). In Fig. 15, we show the time evolution of $r_0(t)$, $r_1(t)$, $r_2(t)$ and $r_3(t)$ for simulations performed at $T = 0.05$, with initial conditions reproducing the incoherent state, $r_n = 0$ for all n , obtained by taking the phases independently and uniformly distributed between 0 and 2π . From equation (187), we find that $T = 0.05$ lies between $T_{c,12}$ and $T_{c,13}$. Then, in particular, the observables plotted in Fig. 15 should all increase exponentially in time. The plot shows that the agreement between the numerical and the theoretical growth rates is very good.

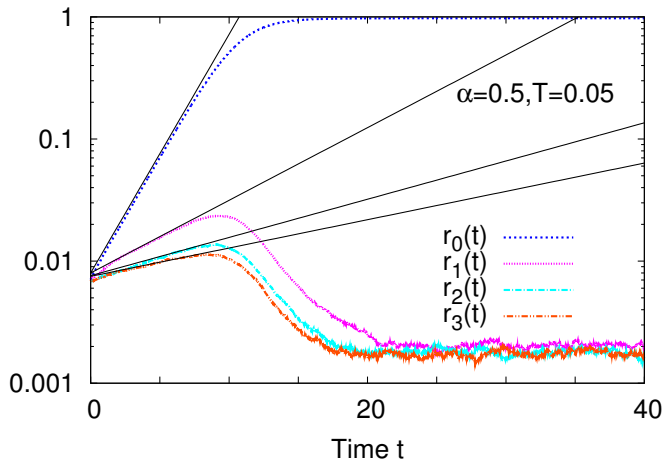


Figure 15. For the model (161), the figure shows the time evolution of the observables $r_0(t), r_1(t), r_2(t)$, and $r_3(t)$ starting from an initial state $\{\theta_i(0); i = 1, 2, \dots, N\}$ that has been obtained by extracting the θ_i 's uniformly in $[-\pi, \pi]$. Therefore the initial state is the incoherent one. In these runs $\alpha = 0.5$ and $T = 0.05$. For these values of α and T , the Fourier modes $n = 0, 1, 2, 3$ are all linearly unstable. In particular, $T_{c,0} = 0.5$, $T_{c,1} \approx 0.18699$, $T_{c,2} \approx 0.12206$, $T_{c,3} \approx 0.10342$. Consequently, $r_0(t), r_1(t), r_2(t)$, and $r_3(t)$ all grow exponentially in time, initially, from their initial values at $t = 0$. The simulations have been performed with $N = 2^{14}$ oscillators, and the plotted data involve and average over 100 independent initial conditions and dynamical realizations. The plots show that after the initial exponential growth, $r_0(t)$ attains a value very close to unity, while $r_1(t), r_2(t), r_3(t)$ all decay to a value very close to zero (and compatible to 0 considering the finite size effects). The straight lines show the theoretical initial exponential growths, with rates given by $(T_{c,m} - T)$. The agreement of the growth rates between theory and simulations is very good.

As is evident from the plot in Fig. 15, the final state reached by the system is the mean-field synchronized one, similar to what was observed for the model (124). One can argue that this is the Gibbs-Boltzmann equilibrium state of our system. For example, it has been proved in Ref. [54] that the equilibrium state of a system of oscillators interacting by long-range interactions on a lattice with periodic boundary conditions is the same as that of the corresponding mean-field system. In the following subsection, we show that indeed such

a state is dynamically stable at temperatures $T < 1/2$.

4.2.3. Linear stability analysis of the mean-field synchronized stationary state Let us then consider the stationary state (169) in which there is only θ and no s dependence:

$$\rho_0(\theta) = A \exp \left[\frac{1}{TB(\alpha)} \int_0^1 ds' \int_{-\pi}^{\pi} d\theta' \frac{\cos(\theta' - \theta)}{|s' - s|_c^\alpha} \rho_0(\theta') \right], \quad (189)$$

where we have put $K = 1$. Using the definitions (129) of $B(\alpha)$ and of the magnetization components (170) and (171), and exploiting the global rotational invariance in θ of the system (161) to put $m_y = 0$, we rewrite this state as

$$\rho_0(\theta) = A \exp \left[\frac{1}{T} m_x \cos \theta \right]. \quad (190)$$

The expression of the normalization constant becomes

$$A = \left[2\pi I_0 \left(\frac{m_x}{T} \right) \right]^{-1}, \quad (191)$$

while the self-consistency relation is

$$m_x = \frac{I_1}{I_0} \left(\frac{m_x}{T} \right). \quad (192)$$

The last equation gives a non-vanishing m_x for $T < 1/2$, as follows from the properties of I_1 and I_0 , see Ref. [28]; for $T \geq 1/2$, the state (190) reduces to the uniform one, equation (177).

As before, the stability of the state (190) is studied by analyzing the linearized equation obtained by inserting in equation (168) the expansion

$$\rho(\theta, s, t) = \rho_0(\theta) + \delta\rho(\theta, s, t); \quad |\delta\rho| \ll 1. \quad (193)$$

In equation (193), both $\rho(\theta, s, t)$ and $\rho_0(\theta)$ are normalized, implying that

$$\int_{-\pi}^{\pi} d\theta \delta\rho(\theta, s, t) = 0. \quad (194)$$

From equation (168), we have at leading order in $\delta\rho$ the linearized equation

$$\begin{aligned} \frac{\partial \delta\rho(\theta, s, t)}{\partial t} &= m_x \frac{\partial}{\partial \theta} (\sin \theta \delta\rho(\theta, s, t)) \\ &- \frac{1}{B(\alpha)} \frac{\partial}{\partial \theta} \left(\left[\int_0^1 ds' \int_{-\pi}^{\pi} d\theta' \frac{\sin(\theta' - \theta)}{|s' - s|_c^\alpha} \delta\rho(\theta', s', t) \right] \rho_0(\theta) \right) + T \frac{\partial^2 \delta\rho(\theta, s, t)}{\partial \theta^2}. \end{aligned} \quad (195)$$

Since the stationary state $\rho_0(\theta)$ is not uniform in θ , a Fourier expansion in θ is not useful. Performing a Fourier expansion in s ,

$$\delta\rho(\theta, s, t) = \sum_{n=-\infty}^{+\infty} \widehat{\delta\rho}_n(\theta, t) e^{2\pi i n s}, \quad (196)$$

we have

$$\begin{aligned} \frac{\partial \widehat{\delta\rho}_n(\theta, t)}{\partial t} &= m_x \frac{\partial}{\partial \theta} \left(\sin \theta \widehat{\delta\rho}_n(\theta, t) \right) \\ -\lambda_n(\alpha) \frac{\partial}{\partial \theta} \left(\left[\int_{-\pi}^{\pi} d\theta' \sin(\theta' - \theta) \widehat{\delta\rho}_n(\theta', t) \right] \rho_0(\theta) \right) &+ T \frac{\partial^2 \widehat{\delta\rho}_n(\theta, t)}{\partial \theta^2}, \end{aligned} \quad (197)$$

where we have used

$$\lambda_n(\alpha) \equiv \frac{\Lambda_n(\alpha)}{B(\alpha)}. \quad (198)$$

From the definitions of $\Lambda_n(\alpha)$ and $B(\alpha)$, we have $0 < \lambda_n(\alpha) \leq 1$.

Let us now look for solutions of equation (197) of the form

$$\widehat{\delta\rho}_n(\theta, t) = \widetilde{\delta\rho}_n(\theta, \mu) e^{\mu t}. \quad (199)$$

Equation (197) then gives

$$\begin{aligned} \mu \widetilde{\delta\rho}_n(\theta, \mu) &= m_x \frac{\partial}{\partial \theta} \left(\sin \theta \widetilde{\delta\rho}_n(\theta, \mu) \right) \\ -\lambda_n(\alpha) \frac{\partial}{\partial \theta} \left(\left[\int_{-\pi}^{\pi} d\theta' \sin(\theta' - \theta) \widetilde{\delta\rho}_n(\theta', \mu) \right] \rho_0(\theta) \right) &+ T \frac{\partial^2 \widetilde{\delta\rho}_n(\theta, \mu)}{\partial \theta^2}. \end{aligned} \quad (200)$$

To solve this equation and to compute the eigenvalues μ , we adopt the following strategy. The function $\widetilde{\delta\rho}_n(\theta, \mu)$ being 2π -periodic in θ , it can be expanded in the basis functions $(\cos p\theta, \sin p\theta)$ with $p = 0, 1, \dots$. Then, we multiply equation (200) in turn by the basis functions, and then integrate over θ from 0 to 2π to obtain a system of algebraic equations. One gets an identity for $p = 0$, while for $p = 1, 2, \dots$, we obtain the system

$$\mu \widetilde{m}_{x,n}^{(p)} = \frac{1}{2} p m_x [\widetilde{m}_{x,n}^{(p-1)} - \widetilde{m}_{x,n}^{(p+1)}] - T p^2 \widetilde{m}_{x,n}^{(p)} + \frac{1}{2} \lambda_n(\alpha) p \widetilde{m}_{x,n}^{(1)} [m_x^{(p-1)} - m_x^{(p+1)}], \quad (201)$$

$$\mu \widetilde{m}_{y,n}^{(p)} = \frac{1}{2} p m_x [\widetilde{m}_{y,n}^{(p-1)} - \widetilde{m}_{y,n}^{(p+1)}] - T p^2 \widetilde{m}_{y,n}^{(p)} + \frac{1}{2} \lambda_n(\alpha) p \widetilde{m}_{y,n}^{(1)} [m_x^{(p-1)} + m_x^{(p+1)}], \quad (202)$$

where we have introduced the notations

$$(\widetilde{m}_{x,n}^{(p)}, \widetilde{m}_{y,n}^{(p)}) \equiv \int_{-\pi}^{\pi} d\theta (\cos p\theta, \sin p\theta) \widetilde{\delta\rho}_n(\theta, \mu), \quad (203)$$

and

$$m_x^{(p)} \equiv \int_{-\pi}^{\pi} d\theta \cos p\theta \rho_0(\theta) = \frac{I_p}{I_0} \left(\frac{m_x}{T} \right). \quad (204)$$

Now, clearly, $\widetilde{m}_{x,n}^{(0)} = \widetilde{m}_{y,n}^{(0)} = 0$, $m_x^{(0)} = 1$ and $m_x^{(1)} \equiv m_x$. There is one system of equation given by equations (201) and (202) for each value of $n = 0, 1, 2, \dots$. These systems are associated with non-Hermitian matrices; therefore, the eigenvalues μ will in general be complex. The stationary state (190) is linearly stable if the eigenvalues of all these systems have negative real parts. We have evaluated numerically the spectrum, and the analysis has put in evidence that this is the case. Actually, there is also a zero eigenvalue, and in general,

the presence of purely imaginary eigenvalues (zero being a particular case) implies that the stationary state is only spectrally stable, while it might be linearly unstable. However, proving that the zero eigenvalue has multiplicity one (see below) ensures that linear stability holds [53].

Before describing the result of the numerical analysis of the systems (201) and (202), we give an argument that points towards the stability of the stationary state (190). Let us define the entropy functional

$$S[\rho(\theta, s, t)] = - \int_0^1 ds \int_{-\pi}^{\pi} d\theta \rho(\theta, s, t) \ln[\rho(\theta, s, t)], \quad (205)$$

and the energy functional

$$E[\rho(\theta, s, t)] = \frac{1}{2} \int_0^1 ds \int_{-\pi}^{\pi} d\theta \rho(\theta, s, t) u(\theta, s, t), \quad (206)$$

where $u(\theta, s, t)$ is the mean-field potential

$$u(\theta, s, t) = - \frac{1}{B(\alpha)} \int_0^1 ds' \int_{-\pi}^{\pi} d\theta' \frac{\cos(\theta' - \theta)}{|s' - s|^\alpha} \rho(\theta', s', t). \quad (207)$$

With the dynamics of $\rho(\theta, s, t)$ governed by the Fokker-Planck equation (168) (with $K = 1$ in the present analysis), it is not difficult to obtain that

$$\begin{aligned} \frac{d}{dt} (E[\rho] - TS[\rho]) &\equiv \frac{d}{dt} F[\rho] \\ &= - \int_0^1 ds \int_{-\pi}^{\pi} d\theta \frac{1}{\rho(\theta, s, t)} \left(\rho(\theta, s, t) \frac{\partial u(\theta, s, t)}{\partial \theta} + T \frac{\partial \rho(\theta, s, t)}{\partial \theta} \right)^2 \leq 0. \end{aligned} \quad (208)$$

We thus see that there is an H -theorem [40, 47] associated with the evolution of $\rho(\theta, s, t)$, with the H -function being the free energy $F[\rho]$; this is in analogy with the mean-field case ($\alpha = 0$) studied in Ref. [25]. The right hand side of the last equation vanishes only for the stationary states given in (169), and in particular, for the state (190). In addition, as proved in [54], the s -independent stationary state (190) realizes the minimum of the free energy. Therefore, equation (208) suggests that if this state is perturbed, the dynamics tends to restore it.

The eigenvalues of the system (201) and (202) have been numerically evaluated by truncating the system at a finite value of p , denoted by p_{max} . As a matter of fact, we have found that the eigenvalues μ of the systems (201) and (202) always have a negative real part for any value of $\lambda_n(\alpha)$ between 0 and 1 and for any temperature in the range $0 < T \leq 1/2$ (except for the zero eigenvalue that we will consider in detail below). We recall that varying n and α , the factor $\lambda_n(\alpha)$ can take any value in that range. Obviously, by truncating the system, one can find only a finite number of eigenvalues, but by increasing the truncation value p_{max} , we have checked that the new eigenvalues have negative real parts with larger absolute values, and the eigenvalues with negative real parts that have smaller absolute values converge extremely fast. We have also found that for T not close to 0, the eigenvalues

are in addition real. This can be understood by considering the systems (201) and (202) for $T \geq \frac{1}{2}$. In that case, since $m_x^{(p)} = 0$ for $p > 0$, they reduce to

$$\mu \tilde{m}_{x,n}^{(p)} = -Tp^2 \tilde{m}_{x,n}^{(p)} + \frac{1}{2} \delta_{p,1} \lambda_n(\alpha) \tilde{m}_{x,n}^{(1)}, \quad (209)$$

$$\mu \tilde{m}_{y,n}^{(p)} = -Tp^2 \tilde{m}_{y,n}^{(p)} + \frac{1}{2} \delta_{p,1} \lambda_n(\alpha) \tilde{m}_{y,n}^{(1)}. \quad (210)$$

The right hand sides give directly the eigenvalues. They are real and all negative, since $T \geq \frac{1}{2}$ and $0 < \lambda_n(\alpha) \leq 1$ (except for T exactly equal to $\frac{1}{2}$ and for $n = 0$, where $\lambda_0(\alpha) = 1$ and then the right hand sides for $p = 1$ are zero). By continuity, the eigenvalues will be real for at least a range of temperatures T smaller than $\frac{1}{2}$.

We conclude the analysis by studying the zero eigenvalue for $0 < T < \frac{1}{2}$. For this, it is not convenient to analyze the systems (201) and (202), but to start directly from equation (200) with $\mu = 0$, i.e.,

$$m_x \frac{\partial}{\partial \theta} \left(\sin \theta \tilde{\delta} \rho_n(\theta, 0) \right) - \lambda_n(\alpha) \frac{\partial}{\partial \theta} \left(\left[\int_{-\pi}^{\pi} d\theta' \sin(\theta' - \theta) \tilde{\delta} \rho_n(\theta', 0) \right] \rho_0(\theta) \right) + T \frac{\partial^2 \tilde{\delta} \rho_n(\theta, 0)}{\partial \theta^2} = 0. \quad (211)$$

The solution of this equation that satisfies the periodicity condition and equation (194) is

$$\tilde{\delta} \rho_n(\theta, 0) = \frac{A}{T} \lambda_n(\alpha) \left[\tilde{m}_{x,n}^{(1)} (\cos \theta - m_x) + \tilde{m}_{y,n}^{(1)} \sin \theta \right] \exp \left[\frac{m_x}{T} \cos \theta \right], \quad (212)$$

where the normalization constant A is given in equation (191), and where we have used the definition (203). This equation shows that in order to have a non-trivial solution, $\tilde{m}_{x,n}^{(1)}$ and $\tilde{m}_{y,n}^{(1)}$ cannot both be equal to 0. We still have to satisfy equation (203) as a self-consistent equation. Multiplying equation (212) by $\cos \theta$ and by $\sin \theta$, we obtain

$$\tilde{m}_{x,n}^{(1)} = \tilde{m}_{x,n}^{(1)} \frac{\lambda_n(\alpha)}{T} (1 - T - m_x^2), \quad (213)$$

$$\tilde{m}_{y,n}^{(1)} = \tilde{m}_{y,n}^{(1)} \lambda_n(\alpha). \quad (214)$$

The first of these equations is satisfied by $\tilde{m}_{x,n}^{(1)} = 0$, or by

$$m_x = \sqrt{1 - T - \frac{T}{\lambda_n(\alpha)}}, \quad (215)$$

that must be satisfied together with the self-consistent relation (192). In Fig. 16, we plot m_x as a function of T as determined by the self-consistent relation (192) and by equation (215) for $\lambda_n(\alpha) = 1$. We see that there is no solution for $0 < T < \frac{1}{2}$. Since the right hand side of equation (215) decreases for decreasing $\lambda_n(\alpha)$, this also proves that there is no solution for any $\lambda_n(\alpha)$. Therefore, the only solution of equation (213) is $\tilde{m}_{x,n}^{(1)} = 0$. This requires that $\tilde{m}_{y,n}^{(1)} \neq 0$, and then equation (214) becomes $\lambda_n(\alpha) = 1$. This is verified only for $n = 0$.

We have finally arrived at the conclusion that equation (211) admits a solution only for $n = 0$, and that this solution is unique and is given by

$$\tilde{\delta}\rho_0(\theta, 0) = \frac{\tilde{m}_{y,n}^{(1)}}{T} \rho_0(\theta) \sin \theta, \quad (216)$$

with $\tilde{m}_{y,n}^{(1)} \neq 0$. This solution represents a global rotation of all oscillators, and is a neutral mode due to the global rotational invariance. The uniqueness of the mode associated with the zero eigenvalue assures that there are no secular terms with a linear growth, thus completing the proof of the linear stability of $\rho_0(\theta)$.

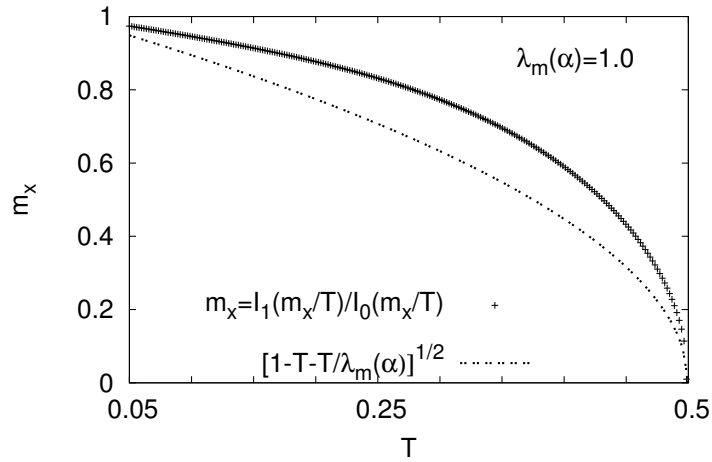


Figure 16. Plot of m_x as a function of T as determined implicitly by the self-consistent relation (192) and by equation (215) with $\lambda_n(\alpha) = 1$. The two curves do not intersect at any T in the range $0 < T < \frac{1}{2}$, showing that there is no solution satisfying both relations.

4.3. The inertial Kuramoto model with a power-law coupling and the same natural frequency for the oscillators

We will now be concerned with the model with inertia, that in the overdamped limit reduced to the model studied in the preceding subsection. The equations of motion are

$$\frac{d\theta_i}{dt} = v_i, \quad (217)$$

$$m \frac{dv_i}{dt} = -\gamma v_i + \frac{\tilde{K}}{\tilde{N}} \sum_{j=1}^N \frac{\sin(\theta_j - \theta_i)}{|x_j - x_i|_c^\alpha} + \tilde{\eta}_i(t),$$

with the same definitions as before of \tilde{N} and of the closest distance convention. We recall the statistical properties of the Gaussian white noise $\tilde{\eta}_i(t)$:

$$\langle \tilde{\eta}_i(t) \rangle = 0, \quad \langle \tilde{\eta}_i(t) \tilde{\eta}_j(t') \rangle = 2\gamma T \delta_{ij} \delta(t - t'). \quad (218)$$

The equations of motion (217) describe the evolution of the α -HMF model [50, 51], within a canonical ensemble.

By performing the reduction to dimensionless quantities as in equations (52)-(57), the equations of motion become

$$\frac{d\theta_i}{dt} = v_i, \quad (219)$$

$$\frac{dv_i}{dt} = -\frac{1}{\sqrt{m}} v_i + \frac{1}{\tilde{N}} \sum_{j=1}^N \frac{\sin(\theta_j - \theta_i)}{|x_j - x_i|_c^\alpha} + \eta_i(t),$$

where we have disregarded the overbars of the dimensionless quantities for notational convenience, and we have

$$\langle \eta_i(t) \rangle = 0, \quad \langle \eta_i(t) \eta_j(t') \rangle = 2 (T/\sqrt{m}) \delta_{ij} \delta(t - t'). \quad (220)$$

The continuum limit of the dynamics is implemented in a manner analogous to that in preceding sections, by introducing the variable $s \in [0, 1]$ as the continuum limit of $s_j = j/N$. The one-particle distribution function $f(\theta, v, s, t)$ is such that $f(\theta, v, s, t) d\theta dv ds$ is the fraction of oscillators located between s and $s + ds$ that at time t has phase between θ and $\theta + d\theta$ and angular velocity between v and $v + dv$. The normalization is

$$\int_{-\pi}^{\pi} d\theta \int_{-\infty}^{\infty} dv f(\theta, v, s, t) = 1 \quad \forall s. \quad (221)$$

The equations of motion in the continuum limit are

$$\frac{d\theta(s, t)}{dt} = v(s, t), \quad (222)$$

$$\frac{\partial v(s, t)}{\partial t} = -\frac{1}{\sqrt{m}} v(s, t) + \frac{1}{B(\alpha)} \int_0^1 ds' \int_{-\pi}^{\pi} d\theta' \int_{-\infty}^{\infty} dv' \frac{\sin(\theta' - \theta)}{|s' - s|_c^\alpha} f(\theta', v', s', t) + \eta(s, t),$$

with $B(\alpha)$ defined previously. The Kramers equation for $f(\theta, v, s, t)$ is

$$\begin{aligned} \frac{\partial f(\theta, v, s, t)}{\partial t} = & -v \frac{\partial f(\theta, v, s, t)}{\partial \theta} + \frac{T}{\sqrt{m}} \frac{\partial^2 f(\theta, v, s, t)}{\partial v^2} \\ & + \frac{\partial}{\partial v} \left[\left(\frac{v}{\sqrt{m}} - \frac{1}{B(\alpha)} \int_0^1 ds' \int_{-\pi}^{\pi} d\theta' \int_{-\infty}^{\infty} dv' \frac{\sin(\theta' - \theta)}{|s' - s|_c^\alpha} f(\theta', v', s', t) \right) f(\theta, v, s, t) \right]. \end{aligned} \quad (223)$$

4.3.1. *Linear stability analysis of the mean-field incoherent stationary state* Below we will present the results of numerical simulations by plotting, as before, the first few of the observables defined in equation (160). Before that, we perform a stability analysis of the s -independent incoherent stationary state of the Kramers equation (223) given by

$$f_0(v) = \frac{1}{2\pi} \frac{1}{\sqrt{2\pi T}} e^{-\frac{v^2}{2T}}. \quad (224)$$

Similarly to equation (92), we linearize the Kramers equation by posing

$$f(\theta, v, s, t) = f_0(v) + e^{\nu t} \delta f(\theta, v, s); \quad |\delta\rho| \ll 1, \quad (225)$$

where normalization of both $f_0(v)$ and $f(\theta, v, s)$ implies that

$$\int_{-\pi}^{\pi} d\theta \int_{-\infty}^{\infty} dv \delta f(\theta, v, s) = 0 \quad \forall s. \quad (226)$$

At leading order, we obtain from equation (223) that

$$\begin{aligned} \nu \delta f(\theta, v, s) = & -v \frac{\partial \delta f(\theta, v, s)}{\partial \theta} + \frac{1}{\sqrt{m}} \frac{\partial}{\partial v} (v \delta f(\theta, v, s)) + \frac{T}{\sqrt{m}} \frac{\partial^2 \delta f(\theta, v, s)}{\partial v^2}, \\ & - \frac{1}{B(\alpha)} \frac{\partial f_0(v)}{\partial v} \int_0^1 ds' \int_{-\pi}^{\pi} d\theta' \int_{-\infty}^{\infty} dv' \frac{\sin(\theta' - \theta)}{|s' - s|_c^\alpha} \delta f(\theta', v', s'). \end{aligned} \quad (227)$$

The analysis of equation (227) is very similar to that followed in section 3.7, and therefore, we do not repeat all the details here. Labelling δf with the eigenvalue ν , we pose

$$\delta f(\theta, v, s, \nu) = \sum_{k=-\infty}^{\infty} b_k(v, s, \nu) e^{ik\theta}, \quad (228)$$

with $b_{-k} = b_k^*$ and $b_0 = 0$. Substituting in equation (227), we have

$$\begin{aligned} & \frac{\partial^2 b_k(v, s, \nu)}{\partial v^2} + \frac{v}{T} \frac{\partial b_k(v, s, \nu)}{\partial v} + \frac{1}{T} (1 - \nu \sqrt{m} - ikv\sqrt{m}) b_k(v, s, \nu) \\ & = \frac{1}{B(\alpha)} \frac{\sqrt{m}}{T} \frac{\partial f_0(v)}{\partial v} i\pi (\delta_{k,1} - \delta_{k,-1}) \int_0^1 ds' \frac{1}{|s' - s|_c^\alpha} \langle 1, b_k \rangle(s', \nu), \end{aligned} \quad (229)$$

where the scalar product is defined by

$$\langle \varphi, \psi \rangle(s'', s') \equiv \int_{-\infty}^{\infty} dv \varphi^*(v, s'') \psi(v, s'). \quad (230)$$

For $k \neq \pm 1$, when the right hand side is equal to 0, equation (229) is identical to equation (96) with $\omega = 0$. Therefore, we can immediately write down the negative eigenvalues as

$$\nu_{p,k} = -\frac{p}{\sqrt{m}} - k^2 T \sqrt{m}; \quad p = 0, 1, 2, \dots \quad (231)$$

For $k = \pm 1$, we proceed as follows. Let us consider only $k = 1$, since $b_{-1} = b_1^*$. We perform the expansion

$$b_1(v, s, \nu) = \sum_{n=-\infty}^{+\infty} b_{1,n}(v, \nu) e^{2\pi i n s}. \quad (232)$$

Substituting in equation (229), we obtain

$$\begin{aligned} & \frac{\partial^2 b_{1,n}(v, \nu)}{\partial v^2} + \frac{v}{T} \frac{\partial b_{1,n}(v, \nu)}{\partial v} + \frac{1}{T} (1 - \nu\sqrt{m} - ikv\sqrt{m}) b_k(v, s, \nu) \\ & = \lambda_n(\alpha) \frac{\sqrt{m}}{T} \frac{\partial f_0(v)}{\partial v} i\pi \langle 1, b_{1,n} \rangle, \end{aligned} \quad (233)$$

where now the scalar product $\langle 1, b_{1,n} \rangle$ does not depend on s , and where $\lambda_n(\alpha)$ is defined in equation (198). Comparing with equation (96), it is evident that on performing the same analysis as in section 3.7, one arrives at the following implicit equation for the eigenvalue ν :

$$\lambda_n(\alpha) \frac{e^{mT}}{2T} \sum_{p=0}^{\infty} \frac{(-mT)^p (1 + \frac{p}{mT})}{p! \left(1 + \frac{p}{mT} + \frac{\nu}{T\sqrt{m}}\right)} - 1 = 0. \quad (234)$$

The stability threshold is again given by the value of the last expression for $\nu = 0$:

$$\frac{\lambda_n(\alpha)}{2T} - 1 = 0. \quad (235)$$

We therefore obtain the same critical temperature for the n th mode as given in equation (187) (where now $K = 1$).

4.3.2. Numerical results In simulations, we monitor as in the previously discussed cases the observables $r_n(t)$ defined in equation (160). In Fig. 17, we show the evolution of $r_0(t)$, $r_1(t)$, $r_2(t)$ and $r_3(t)$, in simulations of the equations of motion (217) with $m = 1$, $\tilde{K} = 1$, $\gamma = 0.5$, at temperature $T = 0.02$ and $\alpha = 0.5$, starting from an initial state uniform in θ and Gaussian in the velocity, equation (224). For these values of T and α , the modes $b_{1,n}$ for $n = 0, 1, 2, 3$ are all unstable (see the critical temperatures in the caption of Fig. 15). The simulation has been performed with $N = 1024$ oscillators.

We see that, as expected, the incoherent state is not stable, since the order parameter r_0 grows exponentially and reaches an asymptotic value that at this temperature is very close to 1. This is similar to what happens in the simulations of the models in the preceding subsections. Also, the long-time decay of r_n with $n > 0$ is similar. However, contrary to the cases in the previous subsections, now the initial exponential growth of these parameters is not visible in Fig. 17. This is probably due to finite-size effects. We stress that these effects for a given number of oscillators N are expected to be more marked for a system with inertia than in an overdamped system, since the former has two dynamical variables per oscillators, and consequently, the distribution f depends on two dynamical variables. In Fig. 18, we plot the results of a simulation run with $N = 2^{17}$ oscillators. For this larger system, the initial exponential growth of all the $r_n(t)$'s is clearly visible. The theoretical rates are also shown with full lines. The agreement with the simulation is satisfactory. The attainment of the asymptotic value of r_0 and the decay to zero of the parameters r_n with $n > 0$ occur at later times with respect to the smaller system, and are not displayed in the figure.

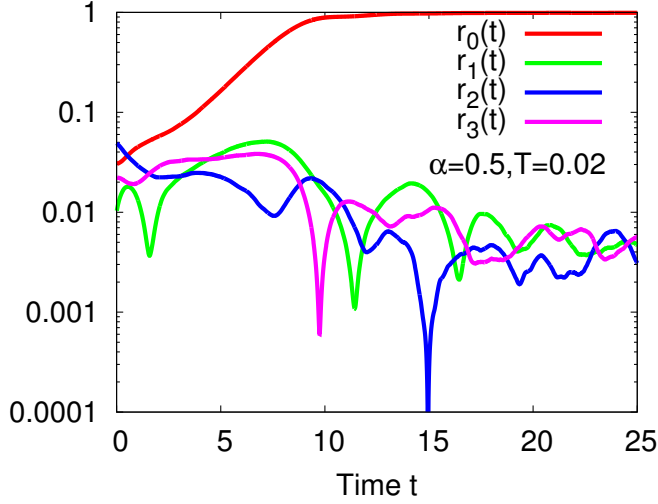


Figure 17. For the model (217), the figure shows the time evolution of the observables $r_0(t), r_1(t), r_2(t), r_3(t)$ for a system of $N = 1024$ oscillators with $m = 1, \tilde{K} = 1, T = 0.02, \alpha = 0.5, \gamma = 0.5$, while starting from an initial state uniform in θ and Gaussian in the velocity, equation (224).

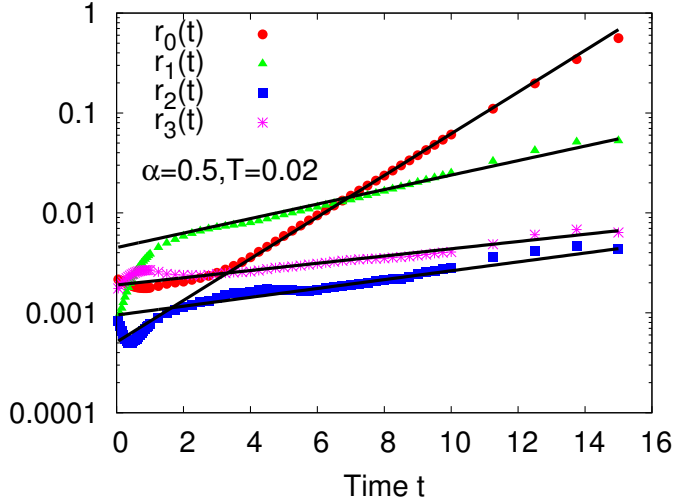


Figure 18. For the model (217), the figure shows the time evolution of the observables $r_0(t), r_1(t), r_2(t), r_3(t)$ for a system of $N = 2^{17}$ oscillators with $m = 1, \tilde{K} = 1, T = 0.02, \alpha = 0.5, \gamma = 0.5$, while starting from an initial state uniform in θ and Gaussian in the velocity, equation (224). The full straight lines show the theoretical growth rates.

5. Conclusions and perspectives

Spontaneous synchronization appears naturally out of a competition between two qualitatively different dynamical regimes in systems that can be described as a set of

interacting oscillators. The main purpose of this work was to show that in addition to this purely dynamical view, introducing noise into the dynamics allows one to study synchronization in the framework of statistical mechanics. This is not only possible, but also very useful, since it paves the way for use of efficient analytical tools commonly employed in the study of the statistical behaviour of many-body systems. One then derives that synchronization is a phase transition, characterized by the appearance of a non-vanishing value of an appropriate order parameter.

We have shown that, interpreted as a system of interacting particles, the Kuramoto model and its various extensions are long-range interacting lattice systems. Furthermore, they are in their original setting mean-field systems, the extreme case of long-range interacting systems, where all pairs of particles interact with equal coupling strengths. We have also considered models where the coupling strengths decay slowly with the distance between the lattice sites. Long-range systems often enjoy peculiar features, both in and out of equilibrium, due to the non-additivity of the interaction energy between subparts of the system. The form of the interaction in the Kuramoto model and its extensions may be used as a prototypical interaction for studying these features.

Statistical dynamics of long-range systems, in the limit of a very large number of particles, can be very well described by equations that involve only the one-particle distribution function. The particular time evolution equation for the one-particle distribution depends on the system at hand: (i) for overdamped systems, it is the continuity equation in the case of noiseless dynamics, and the Fokker-Planck equation for the noisy case; (ii) for underdamped systems, it is the Vlasov equation for the noiseless dynamics, and the Kramers equation for the noisy case. Stable stationary solutions of these equations correspond to stationary states in which the system remains trapped for a time that diverges with the system size (the limit in which the equations for the one-particle distribution function become exact). As exemplified in this review, the phase transitions mentioned above are then a change of the stability properties of the stationary states corresponding to the synchronized and the unsynchronized state.

The presence of distributed natural frequencies in the dynamics of the Kuramoto model leads to a violation of detailed balance in the stationary state, thereby resulting in long-time stationary states which are out of equilibrium. These are the so-called nonequilibrium stationary states (NESSs) characterized by a net non-zero probability current around a closed loop in the configuration phase. As a result, one cannot use the free energy as a thermodynamic potential to determine the nature of the stationary state of the system. However, to this end, we have shown that it is possible to employ successfully at least in numerical simulations probability distributions of the order parameter analogous to those employed in equilibrium statistical mechanics.

In this review, we have restricted our analysis to unimodal distributions for the natural frequencies. Let us comment on this point with respect to the mean-field models. For

such distribution functions, the synchronization transition in the Kuramoto model and in its noisy extension is continuous, i.e., the order parameter of the stable stationary state grows continuously from zero as the coupling strength increases beyond a critical value at a given temperature, or, equivalently, as the temperature is decreased below a critical value for a given coupling strength. On the other hand, in the model with inertia, the transition becomes of first-order type: we have found that in certain ranges of the parameters, both the incoherent and the synchronized state are dynamically stable (this situation is often referred to as bistability), with one of the two states being the globally stable state, depending on the variation of the parameters within the range. This gives rise to the existence of hysteresis loops. The overall picture is probably different with more general frequency distributions. There have been studies of the original Kuramoto model with non-unimodal $g(\omega)$. It has been shown that in the case of a uniform distribution, that can be considered a limiting case (although with a singular derivative) of a unimodal distribution, the transition becomes of a first-order type, since at the threshold value K_c of the coupling parameter given by Eq. (5), there appears a solution of Eq. (16) with $r = r_c = \pi/4$ [55]. Also, continuous bimodal distributions have been studied, and it has been shown that, depending on the structure of the distribution, there can be bistability and states with clusters of oscillators locked at different frequencies (related to the maxima of the bimodal distribution) [56, 57].

Here, we have discussed models in which the mean-field interaction is replaced by coupling strengths between the oscillators that decay as a power law with the distance between the oscillators residing on the sites of a lattice. In particular, we have focussed on one-dimensional lattices, with the parameter α characterizing the decay being smaller than 1, to remain within the framework of long-range interactions. Furthermore, we have imposed periodic boundary conditions. As we have stressed while introducing this class of systems, periodic boundary conditions cause the uniformity on the lattice of the equilibrium or stationary states, but they do not a priori rule out the influence of the lattice structure on the dynamical behavior. However, we have shown that the mean-field Fourier mode of the spatial distribution of oscillator phases dominates the out-of-equilibrium dynamics at long times, since it is this mode that gets destabilized first on increasing the coupling constants or decreasing the temperature. On the other hand, the non-zero Fourier modes destabilize at higher coupling constants or smaller temperatures. This is common to all the lattice models we have analyzed. In particular, the mean-field mode dominates in the underdamped noisy dynamics considered in section 4.3; a similar dominance has been found in the study of the microcanonical ensemble dynamics of this system, i.e., without the noise [58]. Although we do not have analytical or numerical evidences, we feel that it is not unreasonable to adduce the hypothesis that also with more general boundary conditions, the mean-field mode is the one relevant for the dynamics; however, we understand that without a detailed analysis, this statement remains at the level of speculation. Let us remark that there have been earlier works on the Kuramoto model with coupling constants decaying with a power law on one-

dimensional periodic lattices, with the purpose to study the existence of the synchronized phase as a function of the power-law parameter α in the limit $N \rightarrow \infty$. The critical value of α for the existence of the synchronized phase has been numerically evaluated to be (about) 2 [48]; in Ref. [59], a spin wave approximation and simulations performed at larger N values suggest on the other hand that the critical value is $3/2$.

We now point out some important issues that have not been discussed in this review, e.g., details of the dynamical behavior of the system for a large but finite number of oscillators. Among finite-size effects, of particular relevance are slow processes out of equilibrium, and the scaling of the associated timescales with the system size. When the stationary states of the single-particle equations are unstable, we expect that such relaxation does not depend on the size of the system, for large enough system size. On the other hand, stable states could be destabilized by finite-size effects. For example, in Hamiltonian long-range systems, finite systems slowly evolve in time out of the stationary states of the Vlasov equation that governs the dynamics for $N \rightarrow \infty$. The lifetime of these “quasi-stationary” states generally diverges with the system size as a power law [28]. We expect that something similar may happen in the noisy driven systems studied in this review. This could affect, e.g., the rate of hopping between stationary states when there is bistability. Another property that is affected by the finite size of the system is the stability property of the incoherent state of the original Kuramoto model. As a matter of fact, it has been shown that the incoherent state, although neutrally stable in the limit $N \rightarrow \infty$, becomes fully stable for finite N [60], due to a mechanism very similar to that of Landau damping in plasma physics [14].

In conclusion, we would like to stress that the Kuramoto model and its extensions, besides being related to real systems as emphasized in the introduction, provide an interesting benchmark to study and analyze a variety of physical properties. In fact, they offer the possibility to consider synchronization both as a purely dynamical effect and as an emerging phenomenon typical of the statistical behavior of many-body systems. Furthermore, the long-range character of the interaction gives rise to some peculiar properties that are typical for this class of systems. We hope that this review has succeeded in giving a flavor of the aforementioned issues, and will serve as an invitation to indulge in further studies of the Kuramoto model.

Acknowledgments

We acknowledge the hospitality of ENS-Lyon, and support of the CEFIPRA Grant 4604-3 (S.G.) and the grant ANR-10-CEXC-010-01 (S.G. and S.R.). S. G. and A. C. acknowledge the hospitality of the Università di Firenze. We warmly thank F. Bouchet, T. Dauxois, A. Ghosh, M. Komarov, D. Mukamel, C. Nardini, H. Park, A. Patelli, A. Pikovsky, M. G. Potters, and H. Touchette for fruitful discussions over the years on topics reported in this review. We thank the Galileo Galilei Institute for Theoretical Physics (Florence) for the

hospitality and INFN for partial support during the completion of this work.

Appendix A: The noiseless Kuramoto model with inertia: Connection with electrical power distribution models

Here, we briefly discuss, following Refs. [6, 7], how the dynamics (43) arises in connection with electrical power distribution networks.

The essential elements of an electrical power distribution network or grid are synchronous generators located at power plants and motors located with the consumers. While a generator converts mechanical (or other forms of energy) into electrical energy, the reverse is true for a motor. Let P denote the power, which being generated is a positive quantity for a generator and being consumed is negative for a motor. Either unit basically consists of a rotating turbine whose state for the j th unit is represented by its phase

$$\theta_j(t) = \Omega t + \phi_j(t), \quad (\text{A.1})$$

where Ω is the standard supply frequency, $\Omega = 50/60$ Hz typically, while $\phi_j(t)$ is the deviation from uniform rotation. From considerations of energy conservation, the generated or consumed power P_i^{source} of the i th element equals the sum of the power P_i^{trans} exchanged with the grid, the power $P_i^{\text{acc}} = (I/2)(d/dt)(d\theta_i(t)/dt)^2$ accumulated in the turbine, and the amount $P_i^{\text{diss}} = \kappa(d\theta_i(t)/dt)^2$ dissipated in overcoming friction, where I is the moment of inertia of the turbine and κ is the friction constant. The power transmitted between two elements j and i connected by a transmission line depends on the phase difference across the ends of the transmission line, and is given by $P_{\text{max};ji} \sin(\theta_j - \theta_i)$, where $P_{\text{max};ji}$ is the maximum capacity of the transmission line. With $P_i^{\text{trans}} = \sum_j P_{\text{max};ji} \sin(\theta_j - \theta_i)$, we then have

$$P_i^{\text{source}} = \frac{I}{2} \frac{d}{dt} \left(\frac{d\theta_i(t)}{dt} \right)^2 + \kappa \left(\frac{d\theta_i(t)}{dt} \right)^2 + \sum_j P_{\text{max};ji} \sin(\theta_j - \theta_i). \quad (\text{A.2})$$

With the assumption that $|d\phi/dt| \ll \Omega$, one arrives at the equation of motion [6, 7]

$$\frac{d^2 \phi_i(t)}{dt^2} = P_i - \gamma \frac{d\phi_i}{dt} - \sum_j K_{ji} \sin(\phi_j - \phi_i), \quad (\text{A.3})$$

where

$$P_i = \frac{P_i^{\text{source}} - \kappa \Omega^2}{I \Omega}, \quad (\text{A.4})$$

$$\gamma = \frac{2\kappa}{I}, \quad (\text{A.5})$$

$$K_{ji} = \frac{P_{\text{max};ji}}{I \Omega}. \quad (\text{A.6})$$

In the mean-field approximation, where every unit i is connected to every other unit j with equal strength and $K_{ji} = K/N$, where N is the total number of nodes in the network, equation (A.3) reduces to

$$\frac{d^2\phi_i(t)}{dt^2} = P_i - \gamma \frac{d\phi_i}{dt} - \frac{K}{N} \sum_j \sin(\phi_j - \phi_i). \quad (\text{A.7})$$

Note that the P_i 's are intrinsic to the units and in general vary from one unit to another, so that they may be regarded as quenched random variables. The above dynamics is similar to the generalized Kuramoto model dynamics (43) in the absence of noise $\eta_i(t)$.

Appendix B: Simulation details

Here we describe the method to simulate the dynamics (58) for given values of m, T, σ (note that we are dropping overbars for simplicity of notation), and for a given realization of ω_i 's, by employing a numerical integration scheme [61]. To simulate the dynamics over a time interval $[0 : \mathcal{T}]$, we first choose a time step size $\Delta t \ll 1$. Next, we set $t_n = n\Delta t$ as the n -th time step of the dynamics, where $n = 0, 1, 2, \dots, N_t$, and $N_t = \mathcal{T}/\Delta t$. In the numerical scheme, we first discard at every time step the effect of the noise (i.e., consider $1/\sqrt{m} = 0$), and employ a fourth-order symplectic algorithm to integrate the resulting symplectic part of the dynamics [62]. Following this, we add the effect of noise, and implement an Euler-like first-order algorithm to update the dynamical variables. Specifically, one step of the scheme from t_n to $t_{n+1} = t_n + \Delta t$ involves the following updates of the dynamical variables for $i = 1, 2, \dots, N$: For the symplectic part, we have, for $k = 1, \dots, 4$,

$$\begin{aligned} v_i\left(t_n + \frac{k\Delta t}{4}\right) &= v_i\left(t_n + \frac{(k-1)\Delta t}{4}\right) + b(k)\Delta t \left[r\left(t_n + \frac{(k-1)\Delta t}{4}\right) \right. \\ &\quad \left. \sin\left\{ \psi\left(t_n + \frac{(k-1)\Delta t}{4}\right) - \theta_i\left(t_n + \frac{(k-1)\Delta t}{4}\right) \right\} + \sigma\omega_i \right]; \\ r\left(t_n + \frac{(k-1)\Delta t}{4}\right) &= \sqrt{r_x^2 + r_y^2}, \psi\left(t_n + \frac{(k-1)\Delta t}{4}\right) = \tan^{-1} \frac{r_y}{r_x}, \\ r_x &= \frac{1}{N} \sum_{j=1}^N \sin\left[\theta_j\left(t_n + \frac{(k-1)\Delta t}{4}\right)\right], r_y = \frac{1}{N} \sum_{j=1}^N \cos\left[\theta_j\left(t_n + \frac{(k-1)\Delta t}{4}\right)\right], \end{aligned} \quad (\text{B.1})$$

$$\theta_i\left(t_n + \frac{k\Delta t}{4}\right) = \theta_i\left(t_n + \frac{(k-1)\Delta t}{4}\right) + a(k)\Delta t v_i\left(t_n + \frac{k\Delta t}{4}\right), \quad (\text{B.2})$$

where the constants $a(k)$'s and $b(k)$'s are obtained from Ref. [62]. At the end of the updates (B.1) and (B.2), we have the set $\{\theta_i(t_{n+1}), v_i(t_{n+1})\}$. Next, we include the effect of the stochastic noise by keeping $\theta_i(t_{n+1})$'s unchanged, but by updating $v_i(t_{n+1})$'s as

$$v_i(t_{n+1}) \rightarrow v_i(t_{n+1}) \left[1 - \frac{1}{\sqrt{m}}\Delta t \right] + \sqrt{2\Delta t \frac{T}{\sqrt{m}}} \Delta X(t_{n+1}). \quad (\text{B.3})$$

Here ΔX is a Gaussian distributed random number with zero mean and unit variance.

Appendix C: A fast numerical algorithm to compute the interaction expression in models with power-law interactions

For the models discussed in section 4, the interaction term in the equation of motion for each of the N oscillators involves a sum over N terms. This would imply at each time step of numerical simulation of the dynamics a computation time that scales as N^2 . Here we discuss an alternative and efficient numerical algorithm [49] that transforms the interaction term into a convenient form, allowing for its computation by a Fast Fourier Transform (FFT) scheme in a time scaling as $N \ln N$. Use of FFT requires that we choose a power of 2 for N .

Let us denote with J_i the sum appearing in the equations of motion (124), (161) and (219):

$$J_i = \sum_{j=1}^N \frac{\sin(\theta_j - \theta_i)}{(d_{ij})^\alpha}, \quad (\text{C.1})$$

where d_{ij} is the shortest distance between sites i and j on a one-dimensional periodic lattice of N sites. Our simulations results presented in section 4 were obtained by considering the lattice constant a to be unity. Therefore, d_{ij} for $i \neq j$ is given by

$$d_{ij} = \begin{cases} |j - i|; & \text{if } 1 \leq |j - i| \leq N/2, \\ N - |j - i|; & \text{otherwise,} \end{cases} \quad (\text{C.2})$$

while, as explained in the main text, we choose the value of d_{ii} , irrelevant for the equations of motion, equal to 1. Equation (C.1) may be rewritten as

$$J_i = \cos \theta_i \sum_{j=1}^N V_{ij} \sin \theta_j - \sin \theta_i \sum_{j=1}^N V_{ij} \cos \theta_j. \quad (\text{C.3})$$

The first summation may be interpreted as the i th element of the column vector formed by the product of an $N \times N$ matrix $V = [V_{ij}]_{i,j=1,2,\dots,N}$ with the column vector $(\sin \theta_1 \sin \theta_2 \dots, \sin \theta_N)^T$, where $V_{ij} = 1/(d_{ij})^\alpha$. Similarly, the second summation may be interpreted as the i th element of the column vector formed by the product of V with the column vector $(\cos \theta_1 \cos \theta_2 \dots, \cos \theta_N)^T$. The matrix V has the form

$$V = \begin{bmatrix} v_1 & v_N & \dots & v_3 & v_2 \\ v_2 & v_1 & v_N & & v_3 \\ \vdots & v_2 & v_1 & \ddots & \vdots \\ v_{N-1} & & \ddots & \ddots & v_N \\ v_N & v_{N-1} & \dots & v_2 & v_1 \end{bmatrix}, \quad (\text{C.4})$$

with $v_1 = 1$, and

$$v_q = \begin{cases} 1/(q-1)^\alpha & \text{if } 2 \leq q \leq N/2 + 1, \\ 1/(N-q+1)^\alpha & \text{if } N/2 + 2 \leq q \leq N. \end{cases} \quad (\text{C.5})$$

Thus, V is a circulant matrix fully specified by the elements in the first column. The remaining columns of V are cyclic permutations of the elements in the first column, with offset equal to the column index. Note that V can be written as

$$V = v_1 I + v_2 P + v_3 P^2 + \dots + v_N P^{N-1}, \quad (\text{C.6})$$

where P is the cyclic permutation matrix,

$$P = \begin{bmatrix} 0 & 0 & \dots & 0 & 1 \\ 1 & 0 & \dots & 0 & 0 \\ 0 & \ddots & \ddots & \vdots & \vdots \\ \vdots & \ddots & \ddots & 0 & 0 \\ 0 & \dots & 0 & 1 & 0 \end{bmatrix}. \quad (\text{C.7})$$

Since $P^N = I$, the $N \times N$ identity matrix, the eigenvalues of P are given by $w_j = e^{i2\pi(j-1)/N}$, $j = 1, 2, \dots, N$; the w_j s are the N -th root of unity. Equation (C.6) then implies that the eigenvalues of V are given by $\Lambda_j = \sum_{k=1}^N v_k w_j^{k-1}$ for $j = 1, 2, \dots, N$.

It is straightforward to check that the eigenvectors of V are the columns of the $N \times N$ unitary discrete Fourier transform matrix $F = \frac{1}{\sqrt{N}}[f_{jk}]_{j,k=1,2,\dots,N}$, where

$$f_{jk} = e^{-i2\pi(j-1)(k-1)/N} \text{ for } 1 \leq j, k \leq N. \quad (\text{C.8})$$

Then, one has $[F^{-1}VF]_{ij} = \Lambda_j \delta_{ij}$. In terms of the matrices F and F^{-1} , one can rewrite equation (C.3) as

$$J_i = \cos \theta_i \sum_{j=1}^N (F^{-1})_{ij} \Lambda_j (F \sin \theta)_j - \sin \theta_i \sum_{j=1}^N (F^{-1})_{ij} \Lambda_j (F \cos \theta)_j, \quad (\text{C.9})$$

where $(F \sin \theta)_j$ (respectively, $(F \cos \theta)_j$) is the j th element of the column vector formed by multiplying the matrix F with the column vector $(\sin \theta_1 \sin \theta_2 \dots \sin \theta_N)^T$ (respectively, $(\cos \theta_1 \cos \theta_2 \dots \cos \theta_N)^T$). $(F \sin \theta)_j$ and $(F \cos \theta)_j$ are just discrete Fourier transforms, and may be computed very efficiently by standard FFT codes (see, e.g., Ref. [63]). The simulations reported in section 4 were performed by using equation (C.9).

References

- [1] Pikovsky A, Rosenblum M, and Kurths J 2001 *Synchronization: A Universal Concept in Nonlinear Sciences* (Cambridge University Press, Cambridge)
- [2] Bier M, Bakker B M and Westerhoff H V 2000 *Biophys J* **78** 1087
- [3] Winfree A T 1980 *The Geometry of Biological Time* (Springer, New York)
- [4] Buck J 1988 *Quart. Rev. Biol.* **63** 265

- [5] Wiesenfeld K, Colet P and Strogatz S H 1998 *Phys. Rev. E* **57** 1563
- [6] Filatrella G, Nielsen A H and Pedersen N F 2008 *Eur Phys J B* **61** 485
- [7] Rohden M, Sorge A, Timme M and Witthaut D 2012 *Phys. Rev. Lett.* **109** 064101
- [8] Dörfler F, Chertkov M and Bullo F 2013 *Proc. Natl. Acad. Sci. USA.* **110** 2005
- [9] Néda Z, Ravasz E, Vicsek T, Brechet Y and Barabási A L 2000 *Phys. Rev. E* **61** 6987
- [10] Ha S Y, Jeong E and Kang M J 2010 *Nonlinearity* **23** 3139
- [11] Strogatz S H 2003 *Sync: The Emerging Science of Spontaneous Order* (Hyperion, New York)
- [12] Kuramoto Y 1975 *International Symposium on Mathematical Problems in Theoretical Physics, Lecture Notes in Physics, Vol. 39* ed H Arakai (Springer, New York)
- [13] Kuramoto Y 1984 *Chemical oscillations, Waves and Turbulence* (Springer, Berlin)
- [14] Strogatz S H 2000 *Physica D* **143** 1
- [15] Acebrón J A, Bonilla L L, Vicente C J P, Ritort F and Spigler R 2005 *Rev Mod Phys* **77** 137
- [16] Ermentrout B 1991 *J Math Biol* **29** 571
- [17] Sakaguchi H 1988 *Prog Theor Phys* **79** 39
- [18] Acebrón J A and Spigler R 1998 *Phys. Rev. Lett.* **81** 2229
- [19] Hong H, Choi M Y, Yoonk B-G, Park K and Soh K-S 1999 *J. Phys. A: Math. Gen.* **32** L9
- [20] Acebrón J A, Bonilla L L and Spigler R 2000 *Phys. Rev. E* **62** 3437
- [21] Gupta S, Campa A and Ruffo S 2014 *Phys. Rev. E* **89** 022123
- [22] Privman V (ed), 1997 *Nonequilibrium Statistical Mechanics in One Dimension* (Cambridge: Cambridge University Press)
- [23] Derrida B 2005 *Pramana - J. Phys.* **64** 695
- [24] Chavanis P H 2011 *Physica* **390** 1546
- [25] Chavanis P H 2014 *Eur. Phys. J. B* **87** 120
- [26] Inagaki S 1993 *Prog. Theor. Phys.* **90** 577
- [27] Antoni M and Ruffo S 1995 *Phys. Rev. E* **52** 2361
- [28] Campa A, Dauxois T and Ruffo S 2009 *Phys. Rep.* **480** 57
- [29] Bouchet F, Gupta S and Mukamel D 2010 *Physica A* **389** 4389
- [30] Chavanis P H 2006 *Int. J. Mod. Phys* **20** 3113.
- [31] Escande D F 2010 *Long-Range Interacting Systems*, ed T Dauxois, S Ruffo, and L F Cugliandolo (Oxford University Press, New York)
- [32] Bouchet F and Venaille A 2012 *Phys. Rep.* **515** 227
- [33] Bramwell S T 2010 *Long-Range Interacting Systems*, ed T Dauxois, S Ruffo, and L F Cugliandolo (Oxford University Press, New York)
- [34] Tanaka H, Lichtenberg A J and Oishi S 1997 *Phys. Rev. Lett.* **78** 2104
- [35] Gupta S and Mukamel D 2011 *J. Stat. Mech.: Theory Exp.* P03015
- [36] Tsuchiya T, Konishi T and Gouda N 1994 *Phys. Rev. E* **50** 2607
- [37] Barré J, Dauxois T, De Ninno G, Fanelli D and Ruffo S 2004 *Phys. Rev. E* **69** 045501(R)
- [38] Touchette H 2009 *Phys. Rep.* **478** 1
- [39] Gardiner C W 1983 *Handbook of Stochastic Methods for Physics, Chemistry and the Natural Sciences* (Springer, Berlin)
- [40] Huang K 1987 *Statistical mechanics* (Wiley, New York)
- [41] Chavanis P H 2013 *Eur. Phys. J. Plus* **128** 106
- [42] Gradshteyn I S and Ryzhik I M 1980 *Table of Integrals, Series, and Products* (Academic, London)
- [43] Smirnov V I 1964 *A course of higher mathematics. Vol. 3. Part. 2, Complex variables special functions* (Pergamon Press, Oxford)
- [44] Binder K 1987 *Rep. Prog. Phys.* **50** 783
- [45] Kramers H A 1940 *Physica* **7** 284
- [46] Griffiths R B, Weng C Y and Langer J S 1966 *Phys. Rev.* **149** 301

- [47] Balescu R, 1987 *Statistical Dynamics: Matter Out of Equilibrium* (London: Imperial College Press)
- [48] Rogers J L and Wille L T 1996 *Phys. Rev. E* **54** R2193
- [49] Gupta S, Potters M and Ruffo S 2012 *Phys. Rev. E* **85** 066201
- [50] Anteneodo C and Tsallis C 1998 *Phys. Rev. Lett.* **80** 5313
- [51] Tamarit F and Anteneodo C 2000 *Phys. Rev. Lett.* **84** 208
- [52] Gupta S, Campa A and Ruffo S 2012 *Phys. Rev. E* **86** 061130
- [53] Holm D D, Marsden J E, Ratiu T and Weinstein A 1985 *Phys. Rep.* **123** 1
- [54] Campa A, Giansanti A and Moroni D 2003 *J. Phys. A: Math. Gen.* **36** 6897
- [55] Pazó D 2005 *Phys. Rev. E* **72** 046211
- [56] Martens E A, Barreto E, Strogatz S H, Ott E, So P and Antonsen T M 2009 *Phys. Rev. E* **79** 026204
- [57] Pazó D and Montbrió E 2009 *Phys. Rev. E* **80** 046215
- [58] Bachelard R, Dauxois T, De Ninno G, Ruffo S and Staniscia F 2011 *Phys. Rev. E* **83** 061132
- [59] Chowdhury D and Cross M C 2010 *Phys. Rev. E* **82** 016205
- [60] Buice M A and Chow C C 2007 *Phys. Rev. E* **76** 031118
- [61] Nardini C, Gupta S, Ruffo S, Dauxois T and Bouchet F 2012 *J. Stat. Mech.: Theory Exp.* P12010
- [62] McLachlan R I and Atela P 1992 *Nonlinearity* **5** 541
- [63] Antia H M 2002 *Numerical Methods for Scientists and Engineers, 2nd Edition* (Birkhauser, Basel)